(2)

UNIVERSITY OF NEVADA RENO

Seismological Laboratory
Mackay School of Mines
University of Nevada Reno
Reno, Nevada 89557-0047
(702) 784-4975

11 Feburary, 1986

Air Force Office of Scientific Research
Attn: NP
Bolling Air Force Base
Washington, D.C. 20330

FINAL TECHNICAL REPORT

ARPA Order	No. 4397
Program Code	3D60
Grantee:	University of Nevada Regents
Effective Date:	1 Oct 1982
Grant Termination Date:	30 June 1985
Amount of Grant:	$203,692
Grant No.	49620-83-C-0012
Principal Investigators:	Alan S. Ryall Keith F. Priestley (702) 784-4259
Program Manager:	Keith F. Priestley
Short Title of Work:	Attenuation in the western Great Basin

Approved for public release; distribution unlimited.

Sponsored by
Advanced Research Projects Agency (DOD)
ARPA Order No. 4397
Monitored by AFOSR Under Grant No. 49620-83-C-0012

UNCLASSIFIED

SECURITY CLASSIFICATION OF THIS PAGE (When Data Entered)

REPORT DOCUMENTATION PAGE

READ INSTRUCTIONS BEFORE COMPLETING FORM

1. REPORT NUMBER	2. GOVT ACCESSION NO. / 3. RECIPIENT'S CATALOG NUMBER
4. TITLE (and Subtitle): Attentuation in the Western Great Basin	5. TYPE OF REPORT & PERIOD COVERED: Final Report 10/1/84 - 6/30/85
	AFOSR-TR- 86-0375
7. AUTHOR(s): Keith Priestley	F49620-83-C-0012
9. PERFORMING ORGANIZATION NAME AND ADDRESS: Seismological Laboratory, Mackay School of Mines, University of Nevada, Reno, Nevada 89557	10. PROGRAM ELEMENT, PROJECT, TASK AREA & WORK UNIT NUMBERS: 61101F
11. CONTROLLING OFFICE NAME AND ADDRESS: Defense Advanced Research Projects Agency, 1400 Wilson Blvd., Arlington, Va. 22209	12. REPORT DATE: 2/11/86 13. NUMBER OF PAGES: 114
14. MONITORING AGENCY NAME & ADDRESS (if different from Controlling Office): Air Force Office of Scientific Research, Bolling AFB/Bldg 410, Washington, D.C. 20332	15. SECURITY CLASS. (of this report): unclassified 15a. DECLASSIFICATION/DOWNGRADING SCHEDULE

16. DISTRIBUTION STATEMENT (of this Report)

Unlimited

Approved for public release; distribution unlimited.

17. DISTRIBUTION STATEMENT (of the abstract entered in Block 20, if different from Report)

Unlimited

18. SUPPLEMENTARY NOTES

19. KEY WORDS (Continue on reverse side if necessary and identify by block number)

m_b-M_S-M_l, attenuation, L_g, magnitude bias, crustal structure, source spectra, extremal bounds, Q

20. ABSTRACT

In a comparison of teleseismic P-wave delays in the vicinity of the Central Nevada Test Site in Hot Creek Valley, Nevada, with P-delay data over a wider region in the Great Basin, we found that upper mantle speeds under Hot Creek Valley stations are higher than the average for the Great Basin as a whole, but lower than those beneath Pahute Mesa. These observations indicate that the caldera complex in Hot Creek Valley may have a high speed root similar to that proposed to exist beneath the Silent Canyon caldera at Pahute Mesa. In contrast, the Hot Creek Valley anomaly is not as strong as the Pahute Mesa anomaly. The shadow zone caused by the Pahute Mesa structure is much more pronounced and consequently magnitudes of Pahute Mesa explosions can be underestimated relative to the magnitude of Hot Creek Valley explosions of similar yield.

DD FORM 1 JAN 73 1473 EDITION OF 1 NOV 65 IS OBSOLETE

UNCLASSIFIED

(cont)

SECURITY CLASSIFICATION OF THIS PAGE(When Data Entered)

Spectral amplitudes for 24 events of the Mammoth Lakes earthquakes sequence have been determined for the frequency range 0.1-10.0 Hz, including the M_L 6 earthquake at 1450 UT on May 27, 1980, which is of particular interest as a result of the controversy surrounding its mechanism. We have found nothing in the spectra of this event nor in the spectra of the aftershocks to distinguish them from spectra of "tectonic" earthquakes. However, the spectra themselves do not distinguish between various possible explanations for the non-double-couple source mechanism observed in moment tensor inversion and first motion data for the largest events of the Mammoth Lakes earthquake sequence.

The attenuation of Great Basin crustal phases in the Wood-Anderson bandpass is examined. The shape of the $\log A_o(\Delta)$ curve which results suggests more attenuation of energy in the Wood-Anderson passband than in southern California. For Great Basin paths we find, for events with $M_L \leq 5.5$, that

$$\log A_o(\Delta) = \begin{cases} \log_{10}\left[\dfrac{e^{-0.016R}}{R}\right] - 0.31 & 0 \leq \Delta \leq 90 \text{ km} \\ \log_{10}\left[\dfrac{e^{-0.006R}}{R^{0.83}}\right] - 1.08 & 90 \leq \Delta \leq 600 \text{ km} \end{cases}$$

where Δ is epicentral distance, $R = \sqrt{\Delta^2 + h^2}$ is hypocentral distance, and h is focal depth. Our data also suggest a magnitude bias in the correction term. Using the revised magnitude scale and seismic moments, M_o, estimated from spectral analysis, the data are well fit by the straight line

$$\log M_o = (1.20 \pm 0.05) M_L + (17.49 \pm 0.19)$$

for $1 \leq M_L \leq 6$.

The relative excitation of low frequency (0.05 to 0.125 Hz) and high frequency (0.5 to 10.0 Hz) energy is compared for several moderate earthquakes (M_L 4 - 5.5) in the 1980 Mammoth Lakes, California sequence. Comparison of m_b and M_s for the Mammoth Lakes earthquake sequence and Nevada Test Site explosions show that all of the earthquakes analyzed discriminate from explosions. Seismic moment (M_o) is related to M_s by

$$\log M_o = M_s + 19.4(\pm 0.06)$$

We have empirically related the gross logarithmic amplitude parameters M_L, m_b, and M_s, and the seismic spectrum observed at near epicentral distance.

We have determined an average, frequency dependent, apparent L_g $Q(f)$ function for Great Basin paths, by measuring the spatial decay of spectral amplitudes. Spectra of the L_g phase were inverted to simultaneously recover the source spectrum and frequency dependent Q. Averaging the results for all the paths yields

$$Q(f) = 212 f^{0.53} \quad (0.2\ Hz \leq f \leq 4.0\ Hz).$$

This result is in excellent agreement with Singh and Herrmann's Q model for this same area, based on observations of coda decay.

Observations of m_b bias at selected sites within the Soviet Union are looked at. Magnitude m_b is determined for five earthquakes on 25 and 27 May 1980, from recordings at eight Soviet seismic stations on a 4300 km-long profile from eastern Kazakh to eastern Siberia. A comparison of tabulated magnitude residuals for Soviet seismic stations from previous work of Ringdal (1985), North (1976) and Vanek et al. (1978, 1980) shows excellent agreement between these studies.

Finally, we interpret data from two seismic refraction profiles recorded by the U.S. Geological Survey in the vicinity of the proposed Nuclear Waste Repository at Yucca Mountain in southern Nevada. Gravity and well log data are used to correct the refraction travel-time data for delays due to lateral variations in near-surface structure. The travel-times for the two profiles were combined, reparameterized in terms of delay time and ray parameter, and inverted for average, extermal velocity-depth bounds for the region. These show a steep gradient in the shallow crust (depth less than 5 km) with speeds increasing from $\approx 4.5\ ks^{-1}$ to $6.2\ ks^{-1}$ and a shallow gradient below 5 km where speeds increase from $\approx 6.2\ ks^{-1}$ to $6.5\ ks^{-1}$ at 25 km.

M sub L

single quote

Journal reprints are included as appendices.

TECHNICAL SUMMARY

Keith Priestley and David Chavez

Here we summarize the seven projects completed during the time period October 1, 1982 and June 30, 1985. Detailed discussion of each project is covered in the appendicies.

Appendix A discusses a comparison of teleseismic P-wave delays in the vicinity of the Central Nevada Test Site in Hot Creek Valley, Nevada, with P-delay data over a wider region in the Great Basin. This shows that upper mantle speeds under Hot Creek Valley stations are higher than the average for the Great Basin as a whole, but lower than those beneath Pahute Mesa. These observations indicate that the caldera complex in Hot Creek Valley may have a high speed root similar to that proposed to exist beneath the Silent Canyon caldera at Pahute Mesa, however the Hot Creek Valley anomaly is not as strong as the Pahute Mesa anomaly. These high-speed upper mantle structures cause defocusing for outgoing rays resulting in a shadow zone at the distance range corresponding to many European stations. The shadow zone caused by the Pahute Mesa structure is much more pronounced and consequently magnitudes of Pahute Mesa explosions can be underestimated relative to the magnitude of Hot Creek Valley explosions of similar yield. When magnitude versus yield relationships developed using Pahute Mesa data are applied to other areas, such as Hot Creek Valley, they can result in a biased estimate of yield.

In Appendix B, spectral amplitudes for 24 events of the Mammoth Lakes earthquakes sequence have been determined for the frequency range 0.1-10.0 Hz. The M_L 6 earthquake at 1450 UT on May 27, 1980 is of particular interest because of the controversy surrounding its mechanism. A comparison of spectral levels determined from analysis of locally recorded strong motion and broadband digital data and spectral levels from regionally recorded surface waves extrapolated back to the source yields consistent results, indicating flat spectra in the band 0.1-1.0 Hz. The spectra observed in this study do not show pronounced spectral peaks predicted by theoretical studies of ground motion due to the jerky extension of a fluid-driven tensile crack containing a low-viscosity fluid. We have found nothing in the spectra of the M_L 6 event that occurred at 1450 UT, on May 27, 1980, nor in the spectra of the aftershocks to distinguish them from spectra of "tectonic" earthquakes. However, the spectra themselves do not distinguish between various possible explanation for the non-double-couple source mechanism observed in moment tensor inversion and first motion data for the largest events of the Mammoth Lakes earthquake sequence.

In Appendix C, we examine attenuation of Great Basin crustal phases in the Wood-Anderson bandpass. The local magnitude distance correction term, $\log A_o(\Delta)$, has been estimated for paths within the Great Basin by converting

seismograms of earthquakes in the vicinity of Mammoth Lakes, California into equivalent Wood-Anderson seismograms and measuring the decay of peak amplitude with distance. The shape of the $\log A_o(\Delta)$ curve which results suggests more attenuation of energy in the Wood-Anderson passband than in southern California. For Great Basin paths we find, for events with $M_L \leq 5.5$, that

$$\log A_o(\Delta) = \begin{cases} \log_{10}\left[\dfrac{e^{-0.016R}}{R}\right] - 0.31 & 0 \leq \Delta \leq 90 \text{ km} \\ \log_{10}\left[\dfrac{e^{-0.006R}}{R^{0.83}}\right] - 1.08 & 90 \leq \Delta \leq 600 \text{ km} \end{cases}$$

where Δ is epicentral distance, $R = \sqrt{\Delta^2 + h^2}$ is hypocentral distance, and h is focal depth. Our data also suggest a magnitude bias in the correction term, in that for events above $M_L \approx 5.5$, peak amplitudes recorded at epicentral distances below 20 km decay less rapidly than those for smaller events recorded at the same sites. This observation is consistent with the hypothesis that there is a near source saturation of M_L due to the effects of a finite source size for large earthquakes. Using the revised magnitude scale and seismic moments, M_o, estimated from spectral analysis, the data are well fit by the straight line

$$\log M_o = (1.20 \pm 0.05) M_L + (17.49 \pm 0.19)$$

for $1 \leq M_L \leq 6$. M_o versus M_L values from model calculations which assume constant stress drop predict curved moment-magnitude plots over this magnitude range. The fact that we observe a linear relationship suggests that the stress drop of these events is not constant but rather increases with M_L, in particular for events above $M_L \approx 5.5$.

Appendix D compares the relative excitation of low frequency (0.05 to 0.125 Hz) and high frequency (0.5 to 10.0 Hz) energy for several moderate earthquakes (M_L 4 - 5.5) in the 1980 Mammoth Lakes, California sequence. Such studies have importance for both source mechanism and seismic decrimination studies. We have determined local magnitude (M_L), teleseismic body wave magnitude (m_b), and surface wave magnitude (M_s) for a large number of events in the magnitude range 1 to 6.2. Comparison of long-period spectral amplitude, Ω_o, derived from body waves recorded at near epicentral distances with that derived from surfaces waves recorded at regional distances are not significantly different, indicating that the low frequency and high frequency radiation are consistent with a simple source. Comparison of m_b and M_s for the Mammoth Lakes earthquake sequence and Nevada Test Site explosions show that all of the earthquakes analyzed discriminate from explosions. Seismic moment (M_o) is related to M_s by

$$\log M_o = M_s + 19.4(\pm 0.06)$$

We have empirically related the gross logarithmic amplitude parameters M_L, m_b, and M_s, and the seismic spectrum observed at near epicentral distance. One representative event of this group was selected as a standard and M_L, m_b and M_s for that event were scaled (at their observed frequencies) to the observed seismic spectrum. Corresponding magnitudes for three other events were then scaled to the seismic spectrum using the derived relationships. For events of similar depth, the local spectral values can be predicted from the distant magnitude measurements to within 10%. For a deeper event, spectral values were predicted to within about 25%. This confirms that the spectral shape inferred from distant measurements of magnitude is congruent with the spectral shape observed directly in the near field. The majority of Mammoth Lakes events examined can be interpretated as simple events while, in comparison, several of the San Fernando aftershocks in the same magnitude range studied by Tucker and Brune (1977) could be interpreted as partial stress drop events. The near equality of high and low frequency radiation for Mammoth Lakes aftershocks suggests that, for each event, the seismic radiation over the frequency band studied is coming from a simple source, possibly the breaking of a single asperity. The differences suggested between Mammoth Lakes aftershocks and the San Fernando earthquakes may arise because most of the events studied for Mammoth Lakes are occurring in the more competent (ie. higher static stress), granitic block above a deeper, through-going fault plane. The data suggest that partial stress drop events are more common on developed fault systems, whereas full stress drop events are more common in the surrounding country rock as it adjust to the stress field generated by movement on the developed fault plane.

In appendix E we have determined an average, frequency dependent, apparent L_g $Q(f)$ function for Great Basin paths, by measuring the spatial decay of spectral amplitudes. We examined seismograms for several earthquakes occurring around the periphery of the Great Basin recorded by wide-band digital seismographs. Spectra of the L_g phase were inverted to simultaneously recover the source spectrum and frequency dependent Q. Averaging the results for all the paths yields

$$Q(f) = 212 f^{0.53} \quad (0.2\ Hz \leq f \leq 4.0\ Hz).$$

This result is in excellent agreement with Singh and Herrmann's Q model for this same area, based on observations of coda decay.

Appendix F discusses observations of m_b bias at selected sites within the Soviet Union. Magnitude m_b is determined for five earthquakes on 25 and 27 May 1980, from recordings at eight Soviet seismic stations on a 4300 km-long

profile from eastern Kazakh to eastern Siberia. The records were hand-digitized, and magnitudes were determined from traces corrected for instrument response as well as the uncorrected traces. Four of the five earthquakes were at Mammoth Lakes, California, in the western Great Basin; the fifth was at Tonga in the south Pacific. Magnitude residuals with respect to network-averaged m_b's listed in the ISC Bulletin were high for stations at Yakutsk and Seymchan in Siberia, low for raypaths through the Baikal rift zone, and intermediate for a station at Semipalatinsk, about 100 km from the East Kazakh test site. A comparison of tabulated magnitude residuals for Soviet seismic stations from previous work of Ringdal (1985), North (1976) and Vanek et al. (1978, 1980) shows excellent agreement between these studies. Our results are slightly more scattered but in good agreement with previous work. Recalculation of m_b for 83 events recorded on granite at the Nevada Test Site provided a determination of magnitude bias (δm_b = -0.10 +- 0.35) for the NTS granite site with respect to ISC magnitude. Comparison of this value with δm_b's for the Soviet stations provides a direct measure of the magnitude bias of the NTS area relative to areas in the USSR in which the stations are located. This bias reflects only differences in attenuation, and does not account for other effects such as differences in coupling, focussing, and tectonic release. The magnitude bias due to attenuation differences between the NTS granite site and the station at Semipalatinsk is -0.20.

Finally, in Appendix G, we interpret data from two seismic refraction profiles recorded by the U.S. Geological Survey in the vicinity of the proposed Nuclear Waste Repository at Yucca Mountain in southern Nevada. The first profile consists of 33 recordings of a nuclear explosion at the Nevada Test Site and extends from 45 to 110 km. The second consists of 71 recordings of a chemical explosion near Beatty, Nevada, and extends from 0 to 65 km. Gravity and well log data are used to correct the refraction travel-time data for delays due to lateral variations in near-surface structure.

The travel-times for the two profiles were combined, reparameterized in terms of delay time and ray parameter, and inverted for average, extermal velocity-depth bounds for the region. These show a steep gradient in the shallow crust (depth less than 5 km) with speeds increasing from $\approx 4.5\, ks^{-1}$ to 6.2 ks^{-1} and a shallow gradient below 5 km where speeds increase from $\approx 6.2\, ks^{-1}$ to 6.5 ks^{-1} at 25 km.

A specific velocity-depth model consistent with the extremal bounds has been found by two-dimensional ray tracing. The structure of the upper crust is highly variable with the Paleozoic basement varying between the surface and 3.5 km depth. A thick, low-speed section is indicated by large delays across the Crater Flat-Prospector Pass caldera complex. A prominent arrival 1.5 to 2.0

seconds after the initial P-wave time, observed in the distance range 40 to 75 km, is interpreted as a mid-crustal boundary at 12 to 16 km depth. The profiles are of insufficient length to see P_n, however a prominent arrival 3 to 4 seconds after P_g, observed at distances greater than 80 km, is interpreted as P_mP from the Moho at approximately 35 km depth.

GEOPHYSICAL RESEARCH LETTERS, VOL. 12, NO. 9, PAGES 573-576, SEPTEMBER 1985

Appendix A

MAGNITUDE BIAS IN THE GREAT BASIN AND ITS IMPLICATIONS FOR EXPLOSION MAGNITUDE VERSUS YIELD ESTIMATES

Keith F. Priestley and David E. Chávez

Seismological Laboratory, University of Nevada

Abstract. Comparison of teleseismic P-wave delays in the vicinity of the Central Nevada Test Site in Hot Creek Valley, Nevada, with P-delay data over a wider region in the Great Basin, shows that upper mantle speeds under Hot Creek Valley stations are higher than the average for the Great Basin as a whole, but lower than those beneath Pahute Mesa. These observations indicate that the caldera complex in Hot Creek Valley may have a high speed root similar to that proposed to exist beneath the Silent Canyon caldera at Pahute Mesa, however the Hot Creek Valley anomaly is not as strong as the Pahute Mesa anomaly. These high-speed upper mantle structures cause defocusing for outgoing rays resulting in a shadow zone at the distance range corresponding to many European stations. The shadow zone caused by the Pahute Mesa structure is much more pronounced and consequently magnitudes of Pahute Mesa explosions can be underestimated relative to the magnitude of Hot Creek Valley explosions of similar yield. When magnitude versus yield relationships developed using Pahute Mesa data are applied to other areas, such as Hot Creek Valley, they can result in a biased estimate of yield.

Introduction

The acceptance of a Threshold Test Ban Treaty requires the ability to accurately estimate the yield of nuclear explosions. Such estimates are based primarily on seismic measurements, and the bulk of the data for relating seismic amplitudes (or magnitudes) to yield comes from the Nevada Test Site (NTS). The near surface structure at NTS is complicated by extensive Cenozoic volcanism, and it is possible that this has affected structures as deep as the upper mantle low velocity zone beneath NTS. Thus, it is important to evaluate how well the empirical magnitude versus yield curves derived for NTS can predict the yield of explosions at other sites.

The underground nuclear explosion Faultless was detonated at the Central Nevada Test Site (CNTS) in Hot Creek Valley, Nevada, approximately 150 km north of NTS. The International Seismological Centre (ISC) body wave magnitude, m_b, of 6.3 is more than 0.3 units (a factor of two in amplitude) greater than that predicted from empirical magnitude-yield curves for NTS explosions [Everden, 1970], given the maximum yield of 1000 kilotons [Springer and Kinnaman, 1971]. CNTS is physiographically similar to Pahute Mesa at NTS, and in view of the close proximity of the two sites it might be expected that the magnitude-yield curves for NTS sould apply to CNTS. Here we provide evidence that this is not the case.

Spence [1974] used travel-time residuals for NTS explosions recorded at teleseismic distances to infer the presence of a high speed structure in the mantle beneath the 14 m.y. old Silent Canyon caldera at Pahute Mesa. Hedge and Noble [1971] argue that Silent Canyon, and in fact most of the basalts of the southern Great Basin region, originate in the upper mantle. Thus, the high speed material proposed by Spence [1974] may represent upper mantle material largely depleted of its partial melt component by differentiation and associated eruption of the partial melt phase. Differences in upper mantle structure between Hot Creek Valley and Pahute Mesa may be the cause of the Faultless magnitude anomaly.

Inferences on Upper Mantle Structure

Chávez and Priestley [in preparation] have studied teleseismic P-delays for the Great Basin. Among the data used in this study are recordings from seven seismographs operated by the U. S. Geological Survey in and around Hot Creek Valley (Fig. 1). Here, we summarize the results for the Hot Creek Valley data.

Figure 1 shows the generalized geology in the vicinity of Hot Creek Valley. The area is dominated by a series of nested calderas which range in age from 25 to 35 m.y., i.e., 10 to 20 m.y. older than Silent Canyon caldera at Pahute Mesa. To the southeast of Hot Creek Valley is the Lunar Craters volcanic field, a site of Quaternary volcanism [Stewart, 1980].

We first searched for lateral variations in structure under Hot Creek Valley by computing teleseismic P-wave residuals at each station relative to the average residual across the CNTS network. Figure 2 shows relative residual as a function of azimuth. Station locations are indicated by circles centered at each site. The circles have a radius of 1.0 second, and the circumference represents a zero residual. Lines drawn from the circle are scaled according to the size of the residual. Those inside the circle are negative residuals (early arrivals) and lines outside the circle are positive residuals (late arrivals). The azimuth of each line corresponds to the azimuth of approach of the wavefront. Figure 2a shows the residuals at each of the CNTS stations, after the data have been corrected for known variations in sediment thickness and for

Paper number 5L6529.
0094-8276/85/005L-6529$03.00

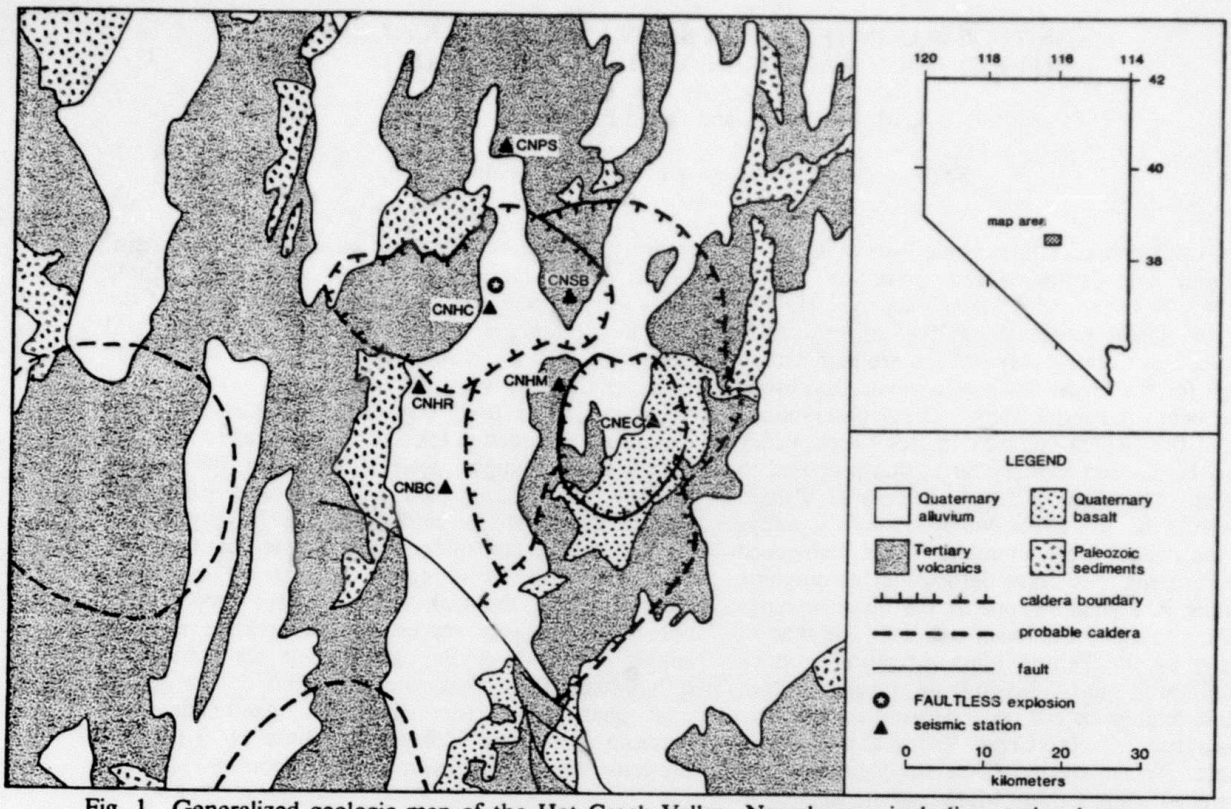

Fig. 1. Generalized geologic map of the Hot Creek Valley, Nevada area including station locations and the Faultless shot point.

inferred Moho dip. The data show that the residuals across the Hot Creek Valley network are small, indicating no strong small-scale lateral variations in structure.

Residuals relative to event average will not reveal any large-scale anomalies under Hot Creek Valley which affect the entire network. We therefore computed P-wave residuals relative to a regional event average using stations throughout the Great Basin. The results, shown in Figure 2b, indicate that Hot Creek Valley is relatively fast compared to the Great

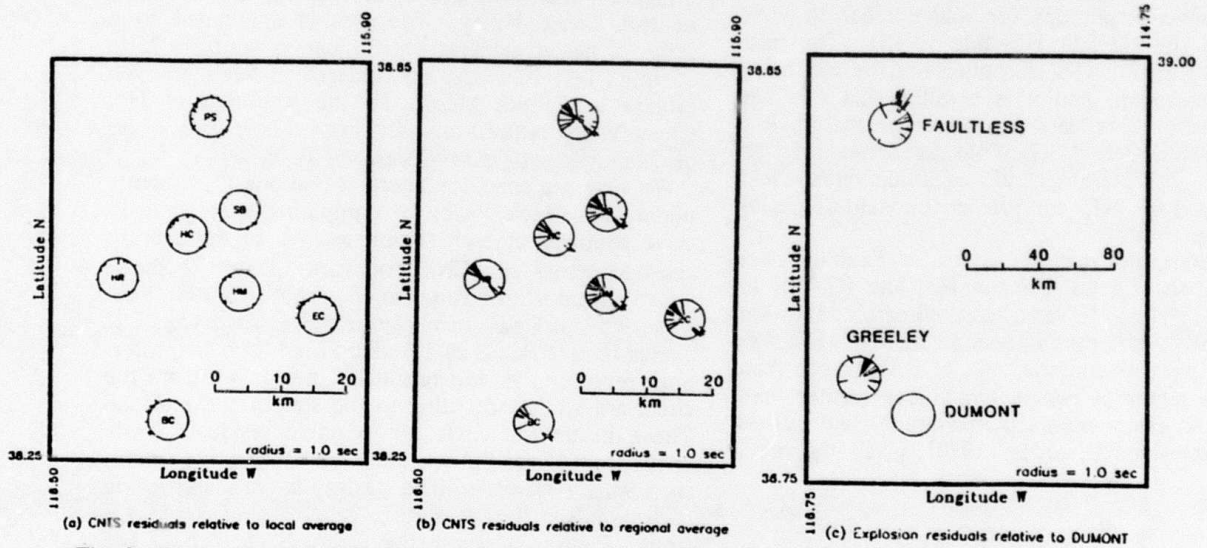

Fig. 2. Maps of travel time residuals versus azimuth (format described in the text): a) relative to the event average for Hot Creek Valley stations after corrections for surface geology and inferred Moho dip; b) relative to event average for Great Basin seismic stations; c) for Faultless and Greeley relative to Dumont at Hot Creek Valley, Pahute Mesa, and Yucca Flat, respectively.

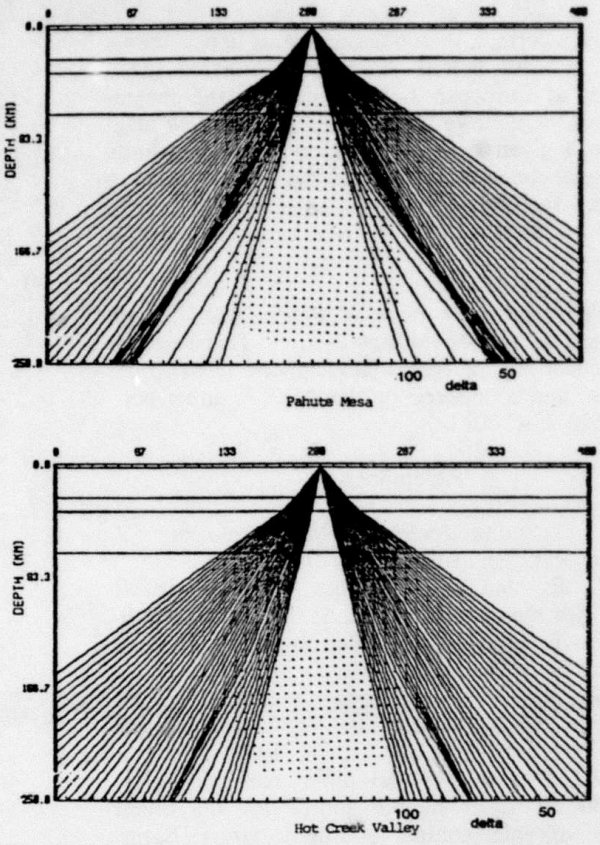

Fig. 3. a) Ray paths through a hypothetical high speed body beneath Pahute Mesa as postulated by Spence [1974]. b) Ray paths through a hypothetical high speed body beneath Hot Creek Valley postulated by Chávez and Priestley [in preparation]

Basin as a whole, suggesting that, as beneath Silent Canyon, a high speed vestige of a root to the Hot Creek Valley caldera complex exits at depth.

In Figure 2c we compare travel time residuals for Faultless in Hot Creek Valley, and Greeley at Pahute Mesa, to the Dumont explosion at Yucca Flat. Compared to Dumont, speeds under Faultless are slow while those under Greeley are fast. This suggests that Yucca Flat travel times are also being affected by the high speed material beneath Pahute Mesa, or prehaps by another, similar structure. A plausible explanation for these observations is that high speed mantle material exists under both Pahute Mesa [as proposed by Spence, 1974] as well as Hot Creek Valley. The Hot Creek Valley caldera complex is considerably older than that at Pahute Mesa however, and consequently the anomalous structure under Hot Creek Valley has had more time to equilibrate with the surrounding mantle. As a result, the magnitude of the Hot Creek Valley anomaly is less.

Effects of Upper Mantle Structure on Teleseismic Amplitudes

Figure 3 compares ray paths from hypothetical explosions above the proposed upper mantle structures beneath Pahute Mesa (Fig. 3a) and Hot Creek Valley (Fig. 3b). The models shown are qualitative and are only intended to illustrate a possible mechanism for the amplitude anomaly observed for Faultless. In our calculations, the high speed upper mantle bodies shown by the stippled regions were defined by a gradation from a speed of 7.7 km/sec in the "unperturbed" upper mantle to 8.2 km/sec in the interior of the high speed zone. The location of the high speed material under Pahute Mesa is taken from Spence [1974], and that under Hot Creek Valley is from Chávez and Priestley [in preparation]. The density of rays shown in Figure 3 is proportional to the expected amplitude. In both Figures 3a and 3b, there is a smooth variation in ray density (and hence amplitude) from 20^o to approximately 45^o. At distances greater than 60^o, there is a substantial defocusing of the rays leaving Pahute Mesa, resulting in a shadow zone. The shadow zone resulting from the structure at Hot Creek Valley is weak in comparison. Based on this figure, we would expect that at distances beyond 60^o, the amplitudes for events in Hot Creek Valley would be greater than those for similar sized events at Pahute Mesa.

Most m_b measurements for Nevada explosions reported by the ISC are heavily biased by amplitude measurements made at European stations. For Pahute Mesa explosions (Fig. 3a), these stations fall in the shadow zone while Figure 3b suggests that events detonated in Hot Creek Valley will be affected to a much smaller extent. Figure 4 is a comparison of the variation in amplitudes of Faultless and Greeley with distance along a north-east azimuth towards Europe. The values plotted are ratios of the Faultless or Greeley P-wave amplitude, to the amplitude of Dumont at Yucca Flat. (Spence [1974] used Dumont as a reference in his travel time study, assuming that it occurred above more normal Great Basin mantle. Our P-delay studies indicate that, compared to the average Great Basin, Yucca Flat is also affected by high speed material, however here we are only concerned with differences between NTS and CNTS.) The amplitudes for Faultless and Greeley are similar at distances less than 40^o. Beyond that, the Faultless amplitude ratios remain close to a constant level with increasing distance, while those for Greeley decrease. At distances between 60^o to 80^o (ie., European stations), Faultless clearly has larger relative amplitudes than Greeley , the

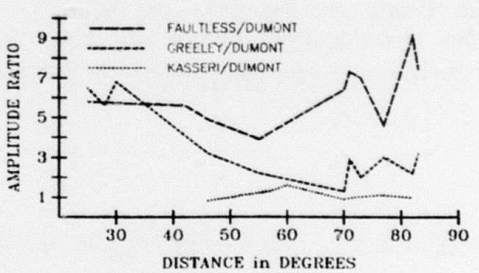

Fig. 4. Comparison of Faultless, Greeley and Kasseri P-wave amplitudes relative to Dumont as a function of distance along a northeast azimuth.

Greeley amplitude ratio having decreased by a factor of 2 to 3.

Discussion

The variation in amplitude with distance shown in Figure 4 supports our hypothesis proposed here that low amplitudes observed at European stations result from defocusing of waves due to anomalous upper mantle structure beneath Pahute Mesa. Lynnes and Lay [1984] have also noted low amplitudes for Pahute Mesa explosions along northeast azimuths. However the amplitude variation shown in Figure 4 for Greeley could be the result of tectonic release. Wallace, et al. [1983] studied wave forms for a large number of explosions at Pahute Mesa and found that a number of the early, large explosions (and Greeley in particular) show waveform distortion which they attribute to a significant component of tectonic release. In comparison to the 1966 Greeley explosion, Wallace, et al. [1983] found that the 1975 Kasseri explosion located 2 km from Greeley but with similar yield, showed simple waveforms indicating only a small component of tectonic release. In Figure 4 we also compare the short-period P-wave amplitudes of Greeley and Kasseri at common stations along a northeast azimuth and find that the amplitude versus distance relationship for Kasseri is identic ' to that shown for Greeley, indicating that the Greeley amplitude variation is not solely the result of tectonic release.

The yield of nuclear explosions can also be estimated from surface waves. L_g waves are a superposition of higher mode crustal surface waves, and as such they are free from the effects of anomalous upper mantle structure beneath the site of the explosion. We have compared L_g amplitudes for Greeley and Faultless at two short period World Wide Standard Seismograph Network stations in the eastern United States, and find no significant difference in the L_g amplitudes between the two events. Based on these measurements, Faultless was no larger (and possibly somewhat smaller) than Greeley.

These results have important implications for the estimation of yields of explosions based on teleseismic body-wave magnitudes. The majority of magnitude versus yield data are derived from explosions at NTS, where most of the large explosions have been detonated on Pahute Mesa. The ISC body wave magnitudes for these events are biased by the large number of stations reporting from Europe. If our hypothesis is correct, then the anomalous upper mantle structure beneath Pahute Mesa will result in lower amplitudes at European stations, causing the magnitude versus yield curve to be biased towards low magnitudes for a given yield. Application of the magnitude versus yield curve derived from NTS explosions to other areas, such as the CNTS, can result in an overestimate of yield, as appears to have been the case for Faultless.

Acknowledgments. We thank W. Peppin and J. Brune for a critical review of the manuscript. This research was funded in part by the DARPA of the Department of Defense and monitored by the AFOSR under contract F49620-83-C-0012.

References

Everden, J., Magnitude versus yield of explosions, *J. Geophys. Res., 75,* 1028–1032, 1971.

Hedge, C. E., and D. C. Noble, Upper Cenozoic basalts with high Sr^{87}/Sr^{86} and Sr/Rb ratios, southern Great Basin, western United States, *Bull. Geol. Soc. Am., 82,* 3503–3510, 1971.

Lynnes, C., and T. Lay, Defocusing of short period P–waves by a high velocity anomaly beneath Pahute Mesa, *Trans. AGU, EOS, 65,* , 994, 1984.

Spence, W., P–wave residual differences and inferences on an upper mantle source for the Silent Canyon volcanic centre, southern Great Basin, Nevada, *Geophy. J. R. Astron. Soc., 38,* 505–523, 1974.

Springer, D., and R. Kinnaman, Seismic source summary for U.S. under ground explosions, 1961–1970, *Bull. Seismol. Soc. Am., 61,* 1073–1098, 1971.

Stewart, J. H., 1980, Geology of Nevada, *Nevada Bureau of Mines and Geology, Special Publication 4.*

Wallace, T. C., D. V Helmberger, and G. R. Engen, Evidence of tectonic release from underground nuclear explosions in long–period P–waves, *Bull. Seismol. Soc Am., 73,* 593–613, 1983.

Keith F. Priestley and David E. Chávez, Seismological Laboratory, Mackay School of Mines, University of Nevada - Reno, Reno, Nevada 89557

(Received April 4, 1985;
revised June 17, 1985;
accepted June 18, 1985.)

JOURNAL OF GEOPHYSICAL RESEARCH, VOL. 90, NO. B13, PAGES 11,177–11,185, NOVEMBER 10, 1985

Surface Wave Excitation and Source Mechanisms of the Mammoth Lakes Earthquake Sequence

KEITH F. PRIESTLEY

Seismological Laboratory, University of Nevada, Reno

JAMES N. BRUNE AND JOHN G. ANDERSON

Institute of Geophysics and Planetary Physics, Scripps Institution of Oceanography, University of California, San Diego, La Jolla

Spectral amplitudes for 24 events of the Mammoth Lakes earthquake sequence have been determined for the frequency range 0.1–10.0 Hz. The M_L 6 earthquake that occurred at 1450 UT on May 27, 1980, is of particular interest because of the controversy surrounding its mechanism. A comparison of spectral levels determined from analysis of locally recorded strong motion and broadband digital data and spectral levels from regionally recorded surface waves extrapolated back to the source yields consistent results, indicating flat spectra in the band 0.1–1.0 Hz. The spectra observed in this study do not show pronounced spectral peaks predicted by theoretical studies of ground motion due to the jerky extension of a fluid-driven tensile crack containing a low-viscosity fluid. We have found nothing in the spectra of the M_L 6 event that occurred at 1450 UT, on May 27, 1980, nor in the spectra of the aftershocks to distinguish them from spectra of "tectonic" earthquakes. However, the spectra themselves do not distinguish between various possible explanations for the non-double-couple source mechanism observed in moment tensor inversion and first motion data for the largest events of the Mammoth Lakes earthquake sequence.

INTRODUCTION

The Mammoth Lakes earthquakes are located at the intersection of the Sierra Nevada frontal fault system and the Long Valley caldera. The caldera was formed 0.7 m.y. ago by collapse and subsidence associated with the eruption of the Bishop tuff [*Bailey et al.*, 1976], and volcanism has continued on a reduced scale into the Holocene. The dominant fault in the area south of the caldera is the Hilton Creek fault along which several hundred meters of pure normal fault displacement has occurred since the formation of the caldera [*Bailey et al.*, 1976]. Extension of the Hilton Creek fault into the caldera appears to have occurred as recently as 0.3 m.y. ago, possibly indicating that the caldera had cooled sufficiently by that time to support stresses large enough to generate earthquakes.

The Mammoth Lakes earthquake sequence clearly began with an M_L 5.8 event on October 4, 1978, located beneath the Wheeler Crest, 30 km northwest of Bishop, California. Following this event, activity gradually spread to the north and west. The main energy release, which began on May 25, 1980, was preceded for over a year by M_L 3.5–4.5 earthquake swarms in the region of the M_L 6 events. These swarms generally clustered near the southern boundary of the caldera and migrated eastward toward the eventual epicenter of the first M_L 6 event [*Cramer and Toppozada*, 1980]. The main episode of strain release commenced with an M_L 6.1 (all local magnitude estimates for the main events are from *Uhrhammer and Ferguson* [1980]) event at 1633 UT on May 25 (hereafter referred to as May 25, 1980—1633) and was followed by a second M_L 6.0 event at 1649 UT. These initial events occurred along an east-west trend near the southern boundary of the caldera. Seismicity then migrated southward from the caldera boundary. *Cramer and Toppozada* [1980] note that no events at the magnitude 5 level occurred south of the southern boundary of the caldera until after the M_L 6.1 event at 1944 UT, which occurred 6–7 km south of the first M_L 6 event. The last of the large events (M_L 6.2) occurred about 9 km south of the 1944 event, at 1450 UT on May 27 (hereafter referred to as May 27, 1980—1450). *Lide and Ryall* [1984] have found that in the 2 months following the main events, aftershocks and continuing swarms occurred along the southern boundary of the caldera and along several NNE-SSW trends nearly orthogonal to the caldera boundary. The first and second M_L 6 events occurred along the first of these trends, and the first, third, and last of the M_L 6 events occurred along the latter trend. The epicenters of nearly all of the aftershocks and all of the M_L 6 events are well to the west of the projection of the Hilton Creek fault at depth, indicating that this is not the causative fault for the earthquake sequence.

Considerable controversy has arisen regarding the source mechanisms of the larger events of the Mammoth Lakes sequence. Focal mechanisms derived from local and regional first motion data indicate strike-slip motion with a NE-SW T axis and NW-SE P axis [*Cramer and Toppozada*, 1980; *Ryall and Ryall*, 1980]. This implies right-lateral motion on east-west trending faults or left-lateral motion on north-south trending faults. Unconstrained moment tensor inversion of long-period teleseismic body and surface wave data result in a large, non-double-couple component for the first and last of the M_L 6 events, and the inversion of the teleseismic waveform data plus teleseismic first motion data indicate mechanisms for the first, third, and fourth of the M_L 6 events which differ significantly from strike slip [*Given et al.*, 1982; *Barker and Langston*, 1983].

The observed non-double-couple mechanism may arise in a number of ways. *Given et al.* [1982] have constrained the moment tensor to be a double couple and interpreted the results in terms of left-lateral oblique slip on NNE trending planes dipping eastward. They suggest that the discrepancy between the regional and teleseismic mechanisms could arise from either structural effects which distort the teleseismically

Paper number 4B5306.
0148-0227/85/004B-5306$05.00

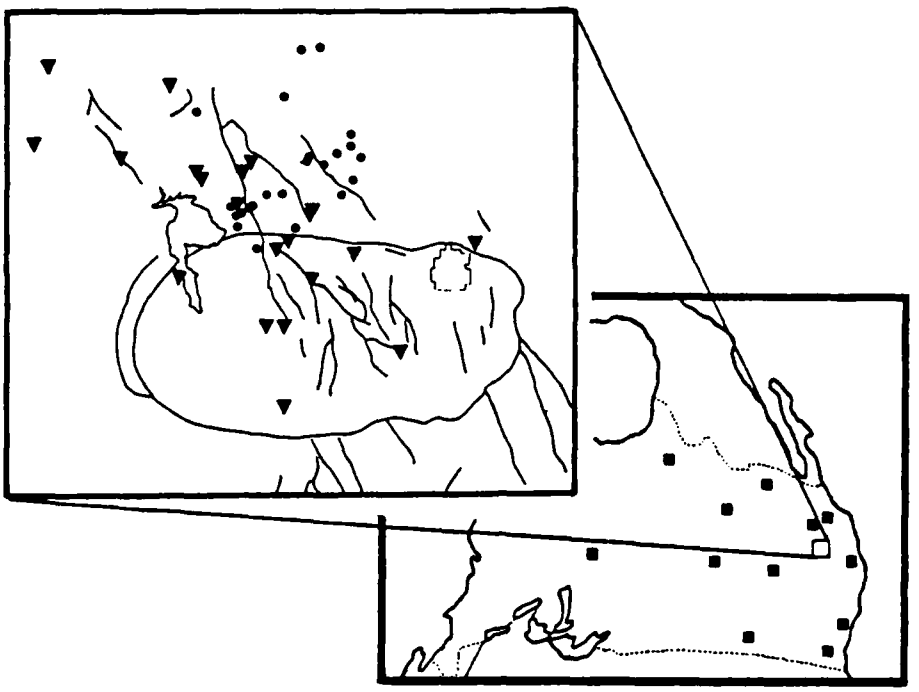

Fig. 1. Location maps showing the events studied and the stations from which seismograms were analyzed. In the lower right-hand map the solid circles denote locations of events, triangles denote location of strong motion accelerographs, and squares denote location of digital seismographs. The upper left-hand map shows the locations of the long-period ...smographs used for the surface wave analysis.

observed radiation pattern or complex rupture during the event. Distortion of the outgoing rays may result from complex structure beneath the Long Valley caldera, for example the presence of magma chambers, which were first proposed by *Bailey et al.* [1976] using geological evidence and *Hill* [1976] using seismological evidence. Similar anomalies in focal mechanisms have been reported for mid-oceanic ridge earthquakes, and these have been attributed to defocusing of the ray paths due to magma beneath the rise crest [*Solomon and Julian*, 1974]. *Wallace* [1984] and *Lide and Ryall* [1984] have interpreted the non-double-couple mechanism as arising from a multiple source. Reversal of polarity observed on short-period and long-period instruments at the same site [*Wallace et al.*, 1982] suggest a complex source time function with the short-period arrivals representing the failure of an asperity (possibly with a strike-slip mechanism) and the long-period arrivals due to the overall response of the faulting episode. Similar non-double-couple mechanisms for events in Greece have been shown to be the result of events with rupture on multiple planes (D. MacKenzie, personal communications, 1984).

On the other hand, *Julian* [1983] has suggested that the results of inverting the surface wave and long-period body wave data and taking the regional and teleseismic first motion data as a whole are better fit by a compensated linear vector dipole (CLVD) mechanism [*Knopoff and Randall*, 1970] than they are by a double-couple mechanism. Julian has noted that the CLVD mechanism is consistent with all but four and two of the first-motion data, respectively, for the May 25, 1980—1633 and May 27, 1980—1450 M_L 6 events, as opposed to 32 and 16 inconsistent data for the double-couple mechanism, and has suggested that the May 25, 1980—1633 and May 27, 1980—1450 events are due to injection of a fluid into an expanding crack, i.e., dike formation. *Aki* [1984], utilizing the calculations of *Chouet* [1981], has suggested that the non-double-couple mechanism results from the rapid opening of a channel between two preexisting cracks filled with magma.

In this study we compare spectral amplitudes of 24 Mammoth Lakes earthquakes ranging in magnitude from M_L 3.5 to M_L 6.2, over the frequency band $\approx$0.05–20 Hz. Spectral amplitudes from approximately 0.5 to 20 Hz are derived from spectral analysis of locally recorded body wave data. Spectral amplitudes from approximately 0.05 to 0.125 Hz are derived from analysis of regionally recorded surface wave data. The wide bandwidth of the spectral amplitude measurements allows us to compare the observed spectral shapes with theoretical spectral shapes for ground motion resulting from "tectonic" earthquakes and ground motion predicted for a propagating tensile crack.

DATA

This study is based on seismograms of the Mammoth Lakes earthquakes recorded on the seismic stations shown in Figure 1. The events, shown as solid circles, comprise only a small fraction of the total number of events which have occurred in the Mammoth Lakes area since October 1978. Locations after May 27, 1980, are largely from C. S. Lide (written communication, 1984). Locations for some of the earlier events are from the University of Nevada or University of California, Berkeley bulletins. The events selected for analysis were those recorded on at least one local strong motion or digital seismograph and one long-period regional seismograph. The SMA-1 strong motion accelerographs, shown as triangles in Figure 1, were installed by the California Division of Mines and Geology [*Turpin*, 1980] or by the University of Southern California (USC) [*Moslem et al.*, 1983]. We also used shear wave spectra supplied by R. Archuleta from data recorded by the U.S. Geological Survey. Digital stations, shown by squares in Figure 1 and described by *Archuleta et al.* [1982], consist of either force balance accelerometer or velocity transducers and Sprengne-

ther DR-100 recorders. For events along the southern boundary of the caldera the SMA-1 and digital seismographs cover a large fraction of the focal sphere compared with many previous studies of a similar nature. The radiation pattern of events south of the caldera are not as well sampled.

The inset map in Figure 1 shows the locations of the regional long-period stations from which seismograms were used to determine surface wave magnitude. These stations completely surround the Mammoth Lakes region and are all World-Wide Standard Seismograph Network (WWSSN) stations, with the exception of the California Institute of Technology (CIT) station at Pasadena (PAS).

ANALYSIS

Determination of Body Wave Moment

Displacement amplitude spectra were computed by Fourier transforming the S wave arrival on the strong motion accelerograms and then dividing the acceleration spectra by ω^{-2} to give the displacement spectra. The time window was chosen to be long enough to include the entire S wave arrival but short enough to minimize the inclusion of surface wave energy. The spectra have been normalized to a distance of 10 km. Since the precise locations of the foci of the events are not known, we have not used the epicenter and seismograph coordinates to determine the distance but have estimated the epicentral distance R from the S-P times assuming an average S wave velocity of 3.4 km s^{-1} and an average P wave velocity of 5.8 km s^{-1}. In addition, we have not rotated the data into transverse and radial components but have computed the spectra for both horizontal components and computed the vector sum of these two values.

The spectra were interpreted in terms of a flat, low-frequency asymptote Ω_0, a high-frequency ω^{-2} falloff, and the corner frequency f_c at which the two trends intersect. The far-field spectral parameters were then related to the source parameter seismic moment M_0 using the relationship given by *Brune* [1970].

$$M_0 = \frac{4\pi\rho\beta^3\Omega_0 R}{kR_{\theta\varphi}} \tag{1}$$

where ρ is the density ($\rho = 2.8$ g cm^{-3}), β is the shear wave velocity ($\beta = 3.5$ km s^{-1}), $R_{\theta\varphi}$ is the rms average of the radiation pattern (taken here as 0.6), and k is a correction factor for the amplification of SH waves at the free surface (taken as 2). The correction of the amplitude of the S wave on being reflected at the free surface assumes that the waves are horizontally polarized (SH). Since we have not rotated the data into transverse and radial components, the data are in general some mixture of SH and SV motion. *Abe* [1974] discusses experimental studies of amplification on reflection and concludes that using $k = 2$ applies approximately to SH wave signals containing some SV motion. *Helmberger and Malone* [1975] discuss problems due to multiple arrivals caused by reflections in deducing source parameters from S waves recorded at epicentral distances much greater than the source depth. The station-source configuration shown in Figure 1 indicates that this should not be a problem in this study.

A source of error inherent in the estimate of Ω_0 and consequently in the estimates of M_0 comes from the assumption of a single, average correction for radiation pattern. If sufficient instruments were available or if the source parameters including direction and velocity of rupture were known, this source of error could be reduced. A value of 0.6 was used for $R_{\theta\varphi}$ [*Thatcher and Hanks*, 1973]. At some azimuths the amplitude could be 1.67 times larger than the amplitude determined assuming this correction, while near a node in the radiation pattern the amplitude could be quite small. Furthermore, if the source dimension is comparable to the wavelength involved, source propagation might distort the radiation pattern by focusing or defocusing energy, thereby changing the apparent corner frequency for different directions and possibly reducing the calculated moment.

No Q correction was made in determining the spectra. *Archuleta et al.* [1982] found that whole path Q had a small effect on the measurement of Ω_0 for Mammoth Lakes events.

Determination of Surface Wave Moment

Tucker and Brune [1977] determined the seismic moment of seven aftershocks of the San Fernando earthquake from the surface wave spectra. This gave an estimate of seismic moment independent of that obtained from S wave spectra and one based on lower frequencies (0.03–0.10 Hz in their case). They made a careful estimate of the errors involved in estimating the seismic moment from the surface wave spectra. The errors included procedural errors, path structure and attenuation, lateral refraction (multipathing), source finiteness, and uncertainties in fault parameters (depth, dip, strike, and slip vector) in correcting for radiation pattern. They concluded that these effects could lead to a maximum error in the final result of no more than a factor of 4.

In this study we also determined the seismic moment from surface waves for comparison with seismic moments determined from the S wave spectra. However, we used a different procedure which allowed us to determine the seismic moment from a large number of events without the time-consuming digitization of the surface wave seismograms.

Surface wave magnitude (M_S) defined by the formula [*Marshall and Basham*, 1972]

$$M_S = \log A + B'(\Delta) + P(T) \tag{2}$$

was determined from seismograms of long-period seismograph stations, primarily in the western United States. In equation (2), A is one half the peak-to-peak ground amplitude of the maximum amplitude Rayleigh wave with period T at distance Δ. $B'(\Delta)$ corrects for average attenuation, scattering, geometrical spreading, and refraction, and $P(T)$ is a correction factor for dispersion and allows measurement of the surface wave amplitude at any period. *Marshall and Basham* [1972] have tabulated $P(T)$ for continental North America for periods ranging from 10 to 40 s. In some cases the maximum surface wave amplitude observed for the Mammoth Lakes earthquakes was in the 8- to 10-s range. Since $P(T)$ is a smoothly varying function, we have extrapolated $P(T)$ to 8-s period. The surface wave magnitudes for the Mammoth Lakes events studied here are tabulated in Table 1.

The surface wave moment is linearly related to the surface wave amplitude and thus to the surface wave magnitude. We have determined a relationship between the surface wave magnitude and the seismic moment in the following manner. Surface wave synthetics were generated by a computer routine (written by G. Masters) for an earthquake with $M_0 = 10^{21}$ dyn cm at a number of regional seismographs from which data were used to determine the surface wave magnitudes. From the synthetic surface wave seismograms we determined the surface wave magnitude in the same manner as discussed above for the Mammoth Lakes earthquakes and thus deter-

TABLE 1. Summary of Earthquake Source Parameters and Comparison of Short-Period and Long-Period Estimates of Seismic Moment

Focal Parameters					Body Wave			Surface Wave		
Date	Time	Latitude	Longitude	Depth	M_L	M_o, dyn cm	EM_o	M_s	M_o, dyn cm	EM_o
Dec. 8, 1979	2138	37.58	118.88	6.9	4.2	1.94×10^{21}		2.23	4.2×10^{21}	1.66
May 17, 1980	0114	37.62	118.80	1.3	4.3	5.18×10^{21}		3.01	2.6×10^{22}	
May 26, 1980	0436	37.58	118.80	0.8	4.2	2.01×10^{21}		2.83	1.7×10^{22}	2.62
May 26, 1980	1020	37.60	118.78	4.6	4.5	9.77×10^{22}		3.25	4.5×10^{22}	1.24
May 26, 1980	1224	37.53	118.87	12.4	5.1	2.68×10^{23}	1.22	4.18	3.8×10^{23}	1.37
May 26, 1980	1857	37.56	118.83	0.2	5.7	4.93×10^{23}	1.17	4.35	5.6×10^{23}	1.33
May 27, 1980	0201	37.50	118.90	6.0	3.6	1.13×10^{22}		2.31	5.1×10^{21}	
May 27, 1980	1450	37.45	118.79	11.7	6.2	7.24×10^{24}	1.81	5.45	7.2×10^{24}	1.18
May 27, 1980	1901	37.58	118 77	0.1	4.8	1.12×10^{23}	2.05	3.43	6.8×10^{22}	1.86
May 27, 1980	2341	37.60	118.90	9.0	3.8	9.01×10^{21}	1.59	2.30	5.0×10^{21}	1.63
May 27, 1980	2357	37.53	118.88	0.1	4.0	2.15×10^{22}		2.41	6.5×10^{21}	
May 28, 1980	0402	37.60	118.79	3.0	3.9	1.16×10^{22}	1.75	2.64	1.1×10^{22}	
May 28, 1980	0516	37.58	118.89	2.5	4.9	1.71×10^{23}	4.78	3.69	1.2×10^{23}	1.86
May 31, 1980	0058	37.54	118.81	0.4	4.5	4.29×10^{22}	2.30	2.72	1.3×10^{22}	1.50
May 31, 1980	1011	37.58	118.82	3.3	4.2	2.63×10^{22}	2.14	2.95	2.2×10^{22}	
May 31, 1980	1516	37.60	118.78	5.8	4.9	1.34×10^{23}	1.74	3.65	1.1×10^{23}	1.50
May 31, 1980	1520	37.60	118.78	6.1	4.0	1.41×10^{22}	1.86	2.86	1.8×10^{23}	
May 31, 1980	1535	37.60	118.78	4.6	3.8	2.62×10^{21}	2.53	2.00	2.5×10^{21}	
May 31, 1980	2315	37.61	118.83	12.9	3.8	8.09×10^{21}	1.98	2.52	8.3×10^{21}	1.81
June 1, 1980	0647	37.47	118.83	7.4	4.7	9.45×10^{22}	1.36	2.86	1.8×10^{22}	1.23
June 5, 1980	1941	37.56	118.87	7.4	4.3	1.33×10^{22}		2.44	7.0×10^{21}	2.24
June 11, 1980	0440	37.55	118.88	6.4	3.8	2.45×10^{22}	4.17	3.05	2.8×10^{22}	1.99
June 28, 1980	0057	37.58	118.82	2.6	3.8	3.05×10^{22}		2.31	5.1×10^{21}	
June 28, 1980	0058	37.58	118.81	1.3	4.2	1.09×10^{23}	1.06	2.83	1.7×10^{22}	1.29

mined a relationship between the surface wave magnitude and seismic moment.

Factors affecting the calculation of the synthetic surface wave seismograms are the earth velocity and attenuation structure and the fault parameters of the individual earthquakes. Since the events are located at the western edge of the Great Basin, while most of the seismograph stations are located in western North America, we have used the velocity structure determined for the Great Basin from surface wave dispersion measurements [*Priestley and Brune*, 1978]. The attenuation structure for the Great Basin by *Patton and Taylor* [1984] was used, with a slight lowering of Q_β from that of Patton and Taylor in the surficial layer. Since we do not have fault plane solutions nor do we know the focal depth for the majority of events we have studied, we determined in average relationship for the Mammoth Lakes area in the following manner. *Vetter and Ryall* [1983] have determined fault plane solutions for a large number of events in the Mammoth Lakes area and found that the mechanisms can generally be divided into two groups. The first group consists of earthquakes with strike-slip mechanisms (average plane of strike N14°E, dip 80°ESE, slip N16°E or strike N73°W, dip 80°SSW, slip N76°E) which are most commonly at depths less than 9 km. The second group consists of earthquakes with oblique or normal mechanisms (average planes of strike N03°E, dip 64°E, slip N40°E or strike N50°W, dip 38°SW, and slip N86°W) usually at depths greater than 9 km. Synthetic surface wave seismograms were calculated for both mechanisms for 2, 5, 8, 11, and 14 km depth. Surface wave magnitudes were determined from the 10 records at each station and an average conversion factor determined for both focal mechanisms and all focal depths. The resulting relationship between surface wave magnitude M_S and seismic moment M_0 for the Mammoth Lakes area is given by

$$\log M_0 = M_S + 19.40\ (\pm 0.06) \qquad (3)$$

To verify the validity of our moment–surface wave magnitude relationship, we can compare equation (3) with other moment magnitude relations established for the western United States. *Wyss and Brune* [1968] originally established a moment–local magnitude relationship for events less than magnitude 6 in the western United States. Seismic moments were determined for 272 events which averaged over a wide range of tectonic regions (California, Nevada, Arizona, Utah, and Baja California). These were found to be best fit by the curve given by

$$\log M_0 = 1.7M_L + 15.1 \qquad 3 < M_L < 6$$

Using the $M_S - M_L$ relationship given by *Wyss and Brune* [1968], this becomes in terms of $M_S(G)$ (the surface wave magnitude defined by *Gutenberg* [1945]):

$$\log M_0 = M_S(G) + 19.2 \qquad 3 < M_S < 6$$

This definition cam be compared with the relationship derived directly from *Gutenberg*'s [1945] definition of surface wave magnitude. According to that definition, a magnitude 6 earthquake produces a far-field displacement of 100 μm at distance 22° for surface waves of period 20 s. In terms of moment Gutenburg's relationship becomes

$$\log M_0 = M_S(G) + 19.3$$

This point thus represents average of the numerous observations on which the surface wave magnitude was based. As pointed out by *Richter* [1958], the scale was adjusted to agree with the local magnitude values of 6–7. *Tucker and Brune* [1977] did not explicitly give a relationship between surface wave magnitude and seismic moment. However, from the values given in their Tables 1 and 3, the average relationship is

$$\log M_0 = M_S + 19.3$$

This relationship, determined using a Gutenburg continental

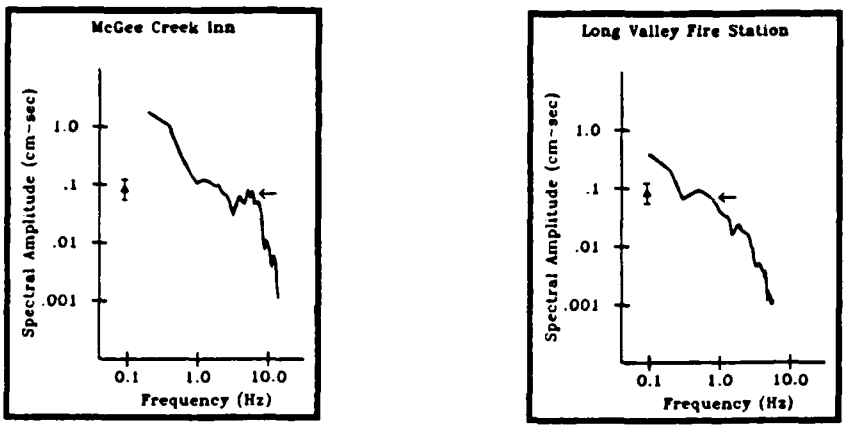

Fig. 2. Spectra from strong motion recordings at the sites "McGee Creek Inn" and "Long Valley Fire Station" for the M_L 4.9 event occurring at 1516 UT on May 31, 1980. Spectra are the vectorial sum of the two orthogonal components and have been normalized to 10 km. The long-period spectral levels picked from these spectra are denoted by the arrow, and the long-period spectral levels determined from the surface wave observations are denoted by the triangle with error bars.

earth model and the Marshall-Basham definition of surface wave magnitude, is in good agreement with the relationship based on the Gutenburg definition of surface wave magnitude. Comparing these various relationships between M_S and M_0, we conclude that the use of the Great Basin velocity [*Priestley and Brune*, 1978] and attenuation [*Patton and Taylor*, 1984] model has increased the estimated moment of the events by 26% over that determined for the Gutenburg continental model.

Equation (3) allows us to rapidly determine the seismic moment M_0 from the surface wave magnitude observation in Table 1. The resulting values of seismic moment (see Table 1) were converted to an equivalent value of Ω_0 by solving equation (1) for Ω_0 and substituting the seismic moment derived from the surface wave observations. This gives values of Ω_0 at frequencies of the surface waves for comparison with the spectra obtained from the body wave record on the accelerometers.

Error Analysis

Errors in Ω_0 (and consequently in M_0) were estimated by calculating an average spectral value and a standard deviation where more than one recording was available for an event. The average values of Ω_0 was determined by

$$\langle \Omega_0 \rangle = \text{antilog} \left\{ \frac{1}{NS} \sum_{i=1}^{NS} \log [\Omega_{0_i} R_i / 10] \right\}$$

where Ω_{0_i} is the long-period spectral level at the ith station, R_i is the distance to the ith station, and NS is the number of stations recording the event. The standard deviation of the log average value of Ω_0 was determined by

$$\text{s.d.}(\log \langle \Omega_0 \rangle) = \left\{ \frac{1}{NS - 1} \sum_{i=1}^{NS} [\log (\Omega_0) - \log \langle \Omega_0 \rangle]^2 \right\}^{1/2}$$

A multiplicative error factor is then determined from

$$E\Omega_0 = \text{antilog} \{\text{s.d.}(\log \langle \Omega_0 \rangle)\}$$

As pointed out by *Archuleta et al.* [1982], when calculating average values of Ω_0 or its derivative M_0, it is necessary to compute the averages using the equations in the above forms to give equal weight to each observation. If a simple arithmetical average value is determined, it will be biased toward larger values, since the errors associated with Ω_0 are lognormally distributed.

Observed Spectra

Figures 2 and 3 are displacement spectra for two events of the 24 Mammoth Lakes earthquakes we studied. All spectra are computed from strong motion accelerograms of the USC–CIT data set. The plotted spectra are the vectorial average of the two orthogonal components and have been normalized to a hypocentral distance of 10 km. The arrows indicate our picks of the corner frequency and long-period spectral level.

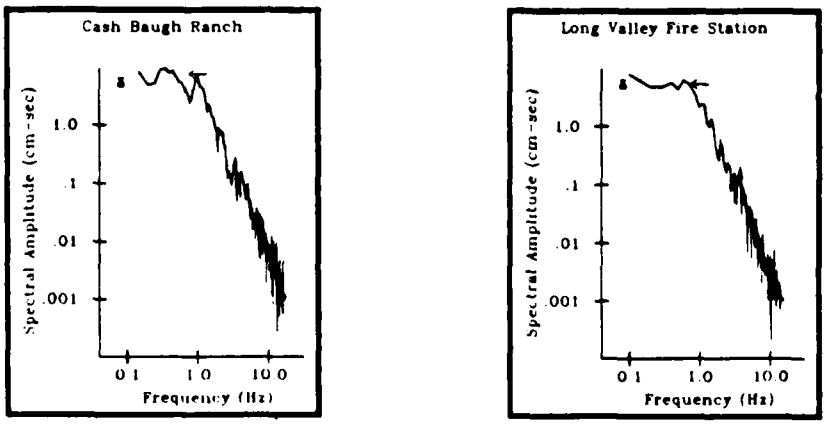

Fig. 3. Spectra from strong motion recordings at the sites "Cash Baugh Ranch" and "Long Valley Fire Station" for the M_L 6.2 event occurring at 1450 UT on May 27, 1980. The notation is the same as for Figure 2.

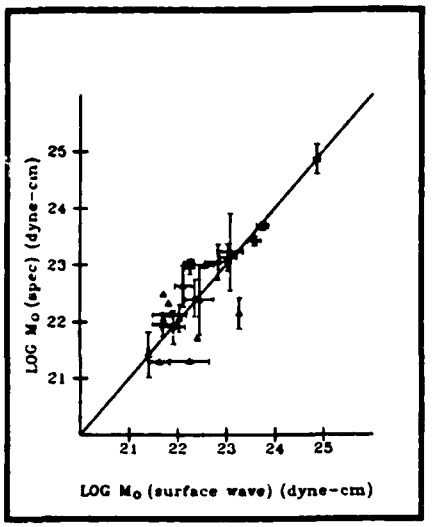

Fig. 4. Comparison of the body wave and surface wave determined moments for the 24 events studied. The line is for reference and is of unit slope and zero intercept.

The triangle with error bars denotes the average spectral level determined from the surface wave measurements.

Figure 2 is two of 14 spectra for an M_L 4.9 event occurring at 1516 UT on May 31, 1980 (hereafter referred to as May 31, 1980—1516). The focus of this event is nearly identical to that of the May 25, 1980—1633 event. The average value of the long-period spectral level $\langle\Omega_0\rangle$ measured from the 14 spectra is 1.03×10^{-1} cm s, corresponding to $M_0 = 1.34 \times 10^{23}$ dyn cm. Our values include estimates of Ω_0 from the data of *Archuleta et al.* [1982] (six observations) plus eight additional spectra from the USC–CIT strong motion data. Our value of $\langle\Omega_0\rangle$ does not differ significantly from their. The seismic moment from the surface wave observation is 1.1×10^{23} dyn cm which is not significantly different from the body wave value.

Spectra of the largest earthquake we studied, the May 27, 1980—1450 M_L 6 shock, are shown in Figure 3. This event is of particular interest because of the controversy concerning its mechanism. Four values of moment have been published for this event. *Archuleta et al.* [1982] determined a moment of 2.33×10^{24} dyn cm from the spectral analysis of two locally recorded seismograms. *Uhrhammer and Ferguson* [1980] estimated a moment of 5.0×10^{24} dyn cm from the spectra of 51.2 s of the broadband displacement record of the vertical component seismogram at Jamestown, California, 140 km west of Mammoth Lakes. *Barker and Langston* [1983] inverted seven long-period teleseismic *P* waveforms and five long-period teleseismic *SH* waveforms to obtain the moment tensor for this event. They found a moment of 1.03×10^{25} dyn cm and 36% CLVD. *Given et al.* [1982] inverted long-period surface wave from this event and used this result to model the long-period body waves. They found a moment of 1.10×10^{25} dyn cm. Our values of 7.26×10^{24} and 7.20×10^{24} dyn cm for the body and surface wave observations, respectively, are somewhat higher than the values reported by *Archuleta et al.* [1982] but in reasonable agreement with the other reported values of moment.

DISCUSSION

Figure 4 is a plot comparing the surface waves moments and body wave moments of the Mammoth Lakes earthquakes from Table 1. The reference line through the points has unit slope and intercept zero. Those points lying above the line have larger body wave moments compared to the observed surface wave moment, while those below the line have larger surface wave moments compared to the observed body wave moment. Vertical error bars denote the spread in the observed body wave moment, while horizontal error bars denote the spread in the observed surface wave moment. It is clear from this figure that there are no significant differences between the moments determined at 8–20 s from surface waves and the moments determined at periods near 1-s from body waves. Where we have analyzed events in common, our results from the surface wave measurements support the moment estimates of *Archuleta et al.* [1982] and thus their findings of nearly constant stress drop ($\Delta\sigma \sim 50$ bars) for events with seismic moments greater than approximately 1×10^{21} dyn cm. All of the events we have studied are larger than 1×10^{21} dyn cm, and therefore we cannot substantiate the dependence of stress drop on seismic moment which *Archuleta et al.* [1982] observed for smaller events. However, the wider bandwidth of our spectra permit us to address the problem of the source mechanism controversy surrounding the Mammoth Lakes events.

Aki et al. [1977] and *Chouet* [1981] derive theoretical ground motion in the far and near-feld, respectively, due to the extension of a fluid-driven tensile crack embedded in a layered half-space. In both studies the source was a jerky opening of a channel ahead of the crack tip due to excess pressure of the fluid in the crack. Seismic waves are generated by the vibrations of the newly created crack walls due to the rapid application of excess fluid pressure. Both the far-field and near-field studies show a peaked character to the ground motion spectra, in contrast to "tectonic" earthquake spectra, which are flat to some corner frequency and then fall off at higher frequencies. *Chouet* [1981] varied the model parameters to analyze the effects of fluid compressibility, source depth, and structure of the medium on the ground motion. He found that the spectral peaks depend on the source geometry, the medium characteristics, the receiver position, the component of ground motion being studied, and critically on the crack stiffness factor C defined as $C = bL/d\mu$, where b is the bulk modules of the fluid, L is the full length of the crack, d is the crack width, and μ is the rigidity of the solid. The crack vibrates most easily when the crack is empty ($C = 0$) [see *Aki et al.*, 1977, Figures 6–9]. The spectral peak becomes broadened, however, when the crack stiffness factor is about 5, implying that the bulk modulus of the magma is low enough to contain bubbles [*Aki*, 1984]. *Chouet*'s [1981] model calculations show a pattern similar to the non-double-couple mechanism observed for the largest Mammoth Lakes earthquakes (May 25, 1980—1633, May 25, 1980—1450). Utilizing *Chouet*'s [1981] calculations, *Aki* [1984] has proposed that these events result from the sudden opening of a channel between two preexisting fluid-filled cracks due to the higher fluid pressure in one of the cracks. The pressure in the magma drops due to the increased total crack volume, and the crack tip closes as a result.

However, as shown in Figure 4, none of the events we have studied show significant differences in level in the frequency band 0.1–1.0 Hz and therefore do not show the spectral peaking predicted by the *Aki* [1984] model for a low-viscosity fluid. Most of the strong motion and digital recording seismographs for the May 27, 1980—1450 event were located to the north of this event thus sampling only a portion of the focal sphere; hence it may be argued that we have sampled that

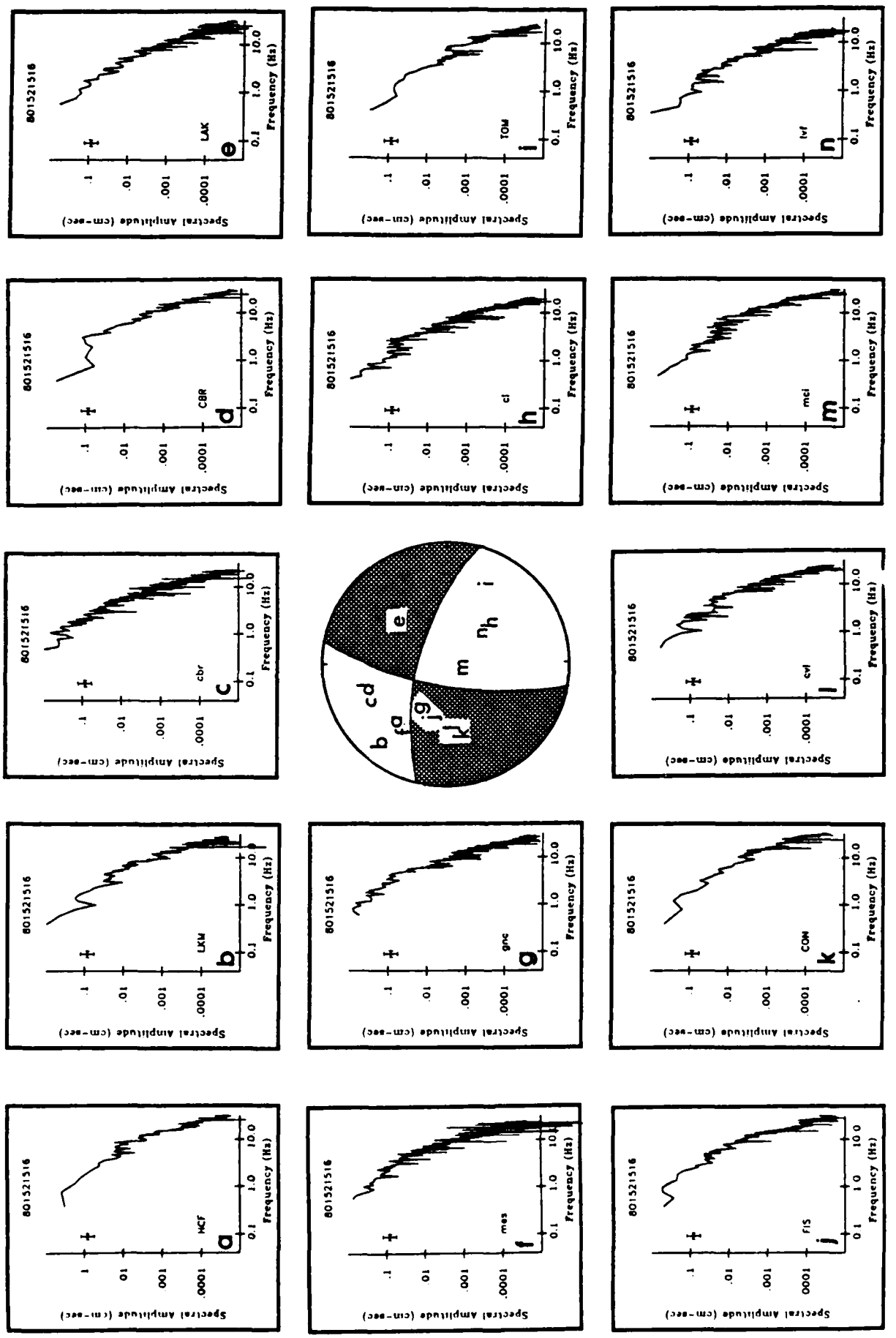

Fig. 5. Variation of the spectra for the event occurring at 1516 UT on May 31, 1980, as a function of position on the focal sphere. The focal mechanism is from U. R. Vetter (written communication, 1984).

part of the radiation pattern where the peaked nature of the spectrum is least prominent. Figure 5 shows the distribution of spectra for the M_L 4.9 May 31, 1980—1516 aftershock which occurred in almost the same location as the May 25, 1980—1633 M_L 6 event which also had a non-double-couple mechanism [*Given et al.*, 1982; *Julian*, 1983]. The focal mechanism from local and regional first-motion data for the May 31, 1980—1516 event is from U. R. Vetter (written communication, 1984) and is very similar to the solution independently determined by *Archuleta et al.* [1982]. Figure 5 shows an upper hemisphere plot with the northwest and southeast being the compression quadrants. This solution is similar to the focal mechanism given by *Cramer and Toppozada* [1980] and *Ryall and Ryall* [1980] from local and regional first motion data for the May 25, 1980—1633 event. The location of the stations from which the spectra were computed are indicated on the focal sphere. Some of the individual spectra show a suggestion of peaking near 1 Hz but not of the magnitude predicted by *Aki et al.* [1977] and *Chouet* [1981]. We find nothing in the spectra of the Mammoth Lakes events we have studied which distinguish them from spectra of "tectonic" events observed in numerous previous studies. The flat nature of the spectra does not rule out the opening of a tensile crack as the source of the elastic waves for these earthquakes. It does preclude the opening of a tensile crack with the subsequent injection of a fluid of low viscosity.

SUMMARY

Spectra for 24 Mammoth Lakes earthquakes greater than 1×10^{21} dyn cm, including the M_L 6 event occurring at 1450 UT on May 27, 1980, have been determined. The short-period portion of the spectra (0.5–10.0 Hz) have been determined from spectral analysis of the locally recorded strong motion and broadband digital data. A relationship has been derived between the Marshall-Basham surface wave magnitude and seismic moment, allowing us to determine the seismic moment directly from time domain amplitude measurements of the surface waves recorded at regional stations. This gives an estimate of the seismic moment independent of that obtained from the S wave spectra and one based on lower frequencies (0.05–0.125 Hz). A comparison of the seismic moments indicate that for any one event, no significant difference in the spectral level exist between the values determined at surface wave frequencies (0.05–0.125 Hz) and the S wave corner frequency (1–5 Hz). The events studied, and in particular the May 27, 1980—1450 M_L 6 event, do not show peaked spectra predicted from theoretical analysis of the ground motion resulting from a fluid-driven, propagating tensile crack. We have found nothing in the spectra of these events to distinguish them from "tectonic" earthquakes. The absence of a peaked spectrum does not rule out dike injection as the source of these earthquakes, but it does rule out a particular model of magmatic intrusion, namely, that of *Chouet* [1981] and *Aki* [1984], for a low-viscosity fluid. As *Aki* [1984] has pointed out, the opening of a channel between two preexisting fluid filled cracks would largely alleviate this problem by involving the movement of only minor amounts of viscous material, which could be accomplished in an adequately small time.

Note added in proof. *Barker* [1985] has shown, using theoretical seismograms, that low-speed, near-surface material can cause significant amplification of near-source ground motion. If this has occurred in the data discussed here, it would tend to strengthen the conclusions of the paper.

Acknowledgments. This research was partly supported by the Defense Advanced Research Projects Agency of the Department of Defense and monitored by the Air Force Office of Scientific Research under contract F49620-83-C-0012 (K.P.) and by the National Science Foundation under grant CEE-8319620 (J.B. and J.A.). R. J. Archuleta supplied spectra from the U.S. Geological Survey data, and A. F. Shakal and B. E. Tucker supplied strong motion records from the California Strong Motion Instrumentation Program. The authors wish to thank D. E. Chavez and A. S. Ryall for a careful review of the manuscript.

REFERENCES

Abe, K., Seismic displacement and ground motion near a fault: The Saitama earthquake of September 21, 1931, *J. Geophys. Res.*, *79*, 4393–4399, 1974.

Aki, K., Evidence for magma intrusion during the Mammoth Lakes earthquakes of May 1980 and implications of the absence of volcanic (harmonic) tremor, *J. Geophys. Res.*, *89*, 7689–7696, 1984.

Aki, K., M. Fehler, and S. Das, Source mechanism of volcanic tremor: Fluid-driven crack models and their applications to the 1963 Kilauea eruption, *J. Volcanol. Geotherm. Res.*, *2*, 259–287, 1977.

Archuleta, R. J., E. Cranswick, C. Mueller, and P. Spudich, Source parameters of the 1980 Mammoth Lakes, California, earthquake sequence, *J. Geophys. Res.*, *87*, 4595–4607, 1982.

Bailey, R. A., G. B. Dalymple, and M. A. Lanphere, Volcanism, structure and geochronology of Long Valley caldera, Mono County, California, *J. Geophys. Res.*, *81*, 725–744, 1976.

Barker, J. S., Modeling local structure using aftershocks of the May 1980 Mammoth Lakes earthquakes (abstract), *Earthquake Notes*, *55*, 31, 1985.

Barker, J. S., and C. A. Langston, A teleseismic body wave analysis of the May 1980 Mammoth Lakes, California, earthquakes, *Bull. Seismol. Soc. Am.*, *73*, 419–434, 1983.

Brune, J. N., Tectonic stress and the spectra of seismic shear waves from earthquakes, *J. Geophys. Res.*, *75*, 4997–5009, 1970. (Correction, *J. Geophys. Res.*, *76*, 5002, 1971.)

Chouet, B., Ground motion in the near field of a fluid-driven crack and its interpretation in the study of shallow volcanic tremor, *J. Geophys. Res.*, *86*, 5985–6016, 1981.

Cramer, C. H., and T. R. Toppozada, A seismological study of the May 1980 and earlier earthquake activity near Mammoth Lakes, California, *Spec. Rep. Calif. Div. Mines Geol.*, *150*, 91–130, 1980.

Given, J. W., T. C. Wallace, and H. Kanamori, Teleseismic analysis of the 1980 Mammoth Lakes earthquake sequence, *Bull. Seismol. Soc. Am.*, *72*, 1093–1109, 1982.

Gutenburg, B., Amplitudes of surface waves and the magnitudes of shallow earthquakes, *Bull. Seismol. Soc. Am.*, *35*, 3–12, 1945.

Helmberger, D. V., and S. D. Malone, Modeling local earthquakes as shear dislocations in a layered half space, *J. Geophys. Res.*, *80*, 4881–4888, 1975.

Hill, D. P., Structure of Long Valley caldera from a seismic refraction experiment, *J. Geophys. Res.*, *81*, 745–753, 1976.

Julian, B. R., Evidence for dyke intrusion earthquake mechanisms near Long Valley caldera, California, *Nature*, *303*, 323–325, 1983.

Knopoff, L., and M. Randall, The compensated linear-vector dipole: A possible mechanism for deep earthquakes, *J. Geophys. Res.*, *75*, 4957–4963, 1970.

Lide, C. S., and A. S. Ryall, Relationship of aftershocks locations and mechanisms of the May, 1980 Mammoth Lakes earthquakes, Active Tectonic and Magmatic Processes in Long Valley Caldera, *U.S. Geol. Surv. Open File Rep.*, *84-939*, 440–452, 1984.

Marshall, P. D., and P. W. Basham, Discrimination between earthquakes and underground explosions employing an improved M_S scale, *Geophys. J. R. Astron. Soc.*, *28*, 431–458, 1972.

Moslem, K., A. Amini, B. Kontic, J. Anderson, and T. Heaton, Accelerograms from the Mammoth Lakes, California earthquake sequence of May–July, 1980 recorded on a temporary array, *Rep. CE 83-01*, Univ. of South. Calif., Los Angeles, 1983.

Patton, H. J., and S. R. Taylor, Q structure of the Basin and Range from surface waves, *J. Geophys. Res.*, *89*, 6929–6940, 1984.

Priestley, K. F., and J. N. Brune, Surface waves and the structure of the Great Basin of Nevada and western Utah, *J. Geophys. Res.*, *83*, 2265–2272, 1978.

Richter, C. F., *Elementary Seismology*, 768 pp., W. H. Freeman, San Francisco, Calif., 1958.

Ryall, A., and F. Ryall, Spatial–temporal variations in the seismicity preceding the May, 1980, Mammoth Lakes, California, earthquakes, *Spec. Rep. Calif. Div. Mines Geol.*, *150*, 27–39, 1980.

Solomon, S., and B. Julian, Seismic constraints on ocean-ridge mantle structure: Anomalous fault plane solutions from first motions, *Geophys. J. R. Astron. Soc.*, *38*, 265–285, 1974.

Thatcher, W., and T. C. Hanks, Source parameters of southern California earthquakes, *J. Geophys. Res.*, *78*, 8547–8576, 1973.

Tucker, B. E., and J. N. Brune, Source mechanism and m_b-M_s analysis of aftershocks of the San Fernando earthquake, *Geophys. J. R. Astron. Soc.*, *49*, 371–426, 1977.

Turpin, C. D., Strong-motion instrumentation program results from the May, 1980, Mammoth Lakes, California earthquake sequence, *Spec. Rep. Calif. Div. Mines Geol.*, *150*, 75–90, 1980.

Uhrhammer, R. A., and R. W. Ferguson, The 1980 Mammoth Lakes earthquake sequence, *Spec. Rep. Calif. Div. Mines Geol.*, *150*, 131–136, 1980.

Vetter, U. R., and A. S. Ryall, Systematic change of focal mechanisms with depth in the western Great Basin, *J. Geophys. Res.*, *88*, 8237–8250, 1983.

Wallace, T. C., A re-examination of the moment tensor solutions of the 1980 Mammoth Lakes earthquakes, Active Tectonic and Magmatic Processes in Long Valley Caldera, *U.S. Geol. Surv. Open File Rep.*, *84-939*, 409–439, 1984.

Wallace, T., J. Given, and H. Kanamori, A discrepancy between long- and short-period mechanisms of earthquakes near the Long Valley caldera, *Geophys. Res. Lett.*, *9*, 1131–1134, 1982.

Wyss, M., and J. N. Brune, Seismic moment, stress, and source dimensions for earthquakes in the California–Nevada region, *J. Geophys. Res.*, *73*, 4681–4694, 1968.

J. G. Anderson and J. N. Brune, Institute of Geophysics and Planetary Physics, Scripps Institution of Oceanography, University of California, San Diego, La Jolla, CA 92093.

K. F. Priestley, Mackay School of Mines, Seismological Laboratory, University of Nevada, Reno, NV 89557.

(Received October 12, 1984;
revised January 9, 1985;
accepted January 25, 1985.)

Bulletin of the Seismological Society of America, Vol. 75, No. 6, pp. 1583-1598, December 1985

M_L OBSERVATIONS IN THE GREAT BASIN AND M_0 VERSUS M_L RELATIONSHIPS FOR THE 1980 MAMMOTH LAKES, CALIFORNIA, EARTHQUAKE SEQUENCE

BY DAVID E. CHÁVEZ AND KEITH F. PRIESTLEY

ABSTRACT

The local magnitude distance correction term, log $A_0(\Delta)$, has been estimated for paths within the Great Basin by converting seismograms of earthquakes in the vicinity of Mammoth Lakes, California, into equivalent Wood-Anderson seismograms and measuring the decay of peak amplitude with distance. The shape of the log $A_0(\Delta)$ curve which results suggests more attenuation of energy in the Wood-Anderson passband than in southern California. For Great Basin paths we find, for events with $M_L \leqq 5.5$, that

$$\log A_0(\Delta) = \begin{cases} \log_{10}\left[\dfrac{e^{-0.016R}}{R}\right] - 0.31 & 0 \leqq \Delta \leqq 90 \text{ km} \\ \log_{10}\left[\dfrac{e^{-0.006R}}{R^{0.83}}\right] - 1.08 & 90 \leqq \Delta \leqq 600 \text{ km} \end{cases}$$

where Δ is epicentral distance, $R = \sqrt{\Delta^2 + h^2}$ is hypocentral distance, and h is focal depth. Our data also suggest a magnitude bias in the correction term, in that for events above $M_L \approx 5.5$, peak amplitudes recorded at epicentral distances below 20 km decay less rapidly than those for smaller events recorded at the same sites. This observation is consistent with the hypothesis that there is a near-source saturation of M_L due to the effects of a finite source size for large earthquakes. Using the revised magnitude scale and seismic moments, M_0, estimated from spectral analysis, the data are well fit by the straight line

$$\log M_0 = (1.20 \pm 0.05)M_L + (17.49 \pm 0.19)$$

for $1 \leqq M_L \leqq 6$. M_0 versus M_L values from model calculations which assume constant stress drop predict curved moment-magnitude plots over this magnitude range. The fact that we observe a linear relationship suggests that the stress drop of these events is not constant but rather increases with M_L, in particular for events above $M_L \approx 5.5$.

INTRODUCTION

Local magnitude, M_L, was defined by Richter (1935) to be

$$M_L = \log A - \log A_0(\Delta)$$

where A is the maximum zero to peak trace amplitude in millimeters recorded on a standard Wood-Anderson torsion seismograph (static magnification = 2800, natural period = 0.8 sec, and damping factor = 0.8) at an epicentral distance Δ. The log $A_0(\Delta)$ function removes the distance dependence from the amplitude, incorporating geometrical spreading, change in wave type, scattering, and anelastic attenuation. The nature of these last three will depend on the structure between the source and receiver and in general will vary between regions. Richter empirically determined

the shape of the log $A_0(\Delta)$ curve for southern California and calibrated it so that log $A_0(100) = -3$, i.e., a M_L zero earthquake would have a peak Wood-Anderson trace amplitude of 1 μm at an epicentral distance of 100 km. Initially, the curve was defined for the range $25 < \Delta < 600$ km, however Gutenburg and Richter (1942) later extended it to zero distance using data from low-gain torsion seismographs. Values for log $A_0(\Delta)$ from 0 to 600 km are published in Richter (1958, p. 342).

The Richter (1958) log $A_0(\Delta)$ values have been used in estimating M_L outside of the southern California region for which they were developed. As pointed out in a number of studies, this invokes the tacit assumption that the attenuation function is the same as in southern California. This will not always be the case however, and consequently equal numerical M_L values for earthquakes in different regions will not necessarily imply the same seismic energy release at the source. This is of interest in engineering seismology because M_L [and hence log $A_0(\Delta)$] plays an important role in the analysis and prediction of strong ground motion.

In this paper, we use events in the vicinity of Mammoth Lakes, California, recorded both near the source and at regional distances to develop a log $A_0(\Delta)$ curve for the Great Basin. We are fortunate in that ray paths from Mammoth Lakes eastward travel exclusively in the Great Basin while paths westward travel through or near areas where the log $A_0(\Delta)$ function is known. This allows us to directly calibrate the attenuation curve to that for which M_L is defined.

For many applications, the seismic moment, M_0, is often a preferable measure of earthquake size since moment is directly related to specific source properties, namely the fault area and amount of slip. Moreover, M_L will saturate for events sufficiently large that the corner frequency is below the Wood-Anderson passband while M_0 will not. Theoretical source models and the widespread use of digital recordings have made possible the routine estimation of M_0 for a large range of sizes. Here, we develop a M_0 versus M_L relationship for events in the 1980 Mammoth Lakes sequence and compare it to those for other areas.

Previous Work

Few Wood-Anderson attenuation functions have been determined for areas outside of southern California primarily because of the lack of a sufficient number of standard seismographs with which to constrain the curve. The increasing availability of digital seismograms for calibrated stations now offers the possibility of doing so by creating "synthetic" Wood-Anderson seismograms. Bakun and Joyner (1984) used such data to develop a log $A_0(\Delta)$ curve for central California. They found that the original southern California curve was appropriate except for some modification at near distances, where their data indicated that Richter's (1958) curve did not completely remove the distance dependence.

The original log $A_0(\Delta)$ curve has also been reevaluated for southern California. For instance, Luco (1982), Jennings and Kanamori (1983), and Munguia and Brune (1984) have used strong motion and/or digital recordings to determine M_L at distances from 0 to 100 km for events with $M_L > 6$. Similar to the results of Bakun and Joyner (1984), all found that M_L is systematically underestimated at distances less than 50 km, relative to that determined at more distant stations. Luco (1982) and Jennings and Kanamori (1983) interpreted this as a result of deficiencies in the original log $A_0(\Delta)$ function, and each developed revised attenuation curves to remove the bias. Munguia and Brune (1984) however, hypothesize that the underestimation of M_L for large events is a consequence of finite source effects. They describe a numerical experiment which suggests that at large epicentral distances,

arrivals from various portions of the causative fault constructively interfere to produce larger amplitude arrivals and hence yield a greater magnitude. At near distances, the arrivals interfere destructively, leading to smaller amplitudes and a lower estimate of M_L.

Munguia and Brune noted the opposite trend when considering smaller earthquakes ($3.0 \leqq M_L \leqq 5.5$). Recordings within an epicentral distance of 10 km or less yielded magnitudes which were up to one unit greater than those at larger distances. They suggested that this was due to site amplifications as well as high-frequency source spectra not adequately accounted for by Richter's (1958) $\log A_0(\Delta)$ curve.

Boore and Hutton (1984) used regression analysis on several thousand actual and simulated Wood-Anderson data to determine a revised southern California $\log A_0(\Delta)$ curve for the distance range $10 \leqq \Delta \leqq 560$ km. They, as well as Bakun and Joyner (1984), modeled the decay in peak Wood-Anderson amplitude as a combination of material attenuation and geometrical spreading using

$$A_0 = C \frac{e^{-\gamma R}}{R^{\eta}} \tag{1}$$

where γ and η are the material attenuation and geometrical spreading coefficients, respectively, $R = \sqrt{\Delta^2 + h^2}$ is hypocentral distance, h is focal depth, and C is a constant. [Although Richter (1935) defined $\log A_0(\Delta)$ in terms of epicentral distance, he did so assuming that the events he studied had similar focal depths. It becomes necessary to use hypocentral distance in order to eliminate the distance bias from near source M_L estimates if one considers earthquakes at a variety of depths (Jennings and Kanamori, 1983)]. Boore and Hutton (1984) found that $\gamma = 0.0046$ km^{-1} for $\eta = 1$. A more recent solution (Boore, personal communication, 1985) has $\gamma = 0.0035$ km^{-1} and $\eta = 1.09$. In this paper, all reference to Boore and Hutton (1984) should be taken to mean their more recent results, given above. Their results suggest less attenuation for distances beyond 200 km than what is indicated by Richter's (1958) curve. At distances closer than 50 km, they obtain a curve similar to those proposed by Luco (1982) and Jennings and Kanamori (1983). Thus, Boore and Hutton (1984) and Bakun and Joyner (1984) find a similar near-source bias for both large and small earthquakes, a result which differs from that of Munguia and Brune (1984).

Data and Analysis

The data analyzed in this study consist of seismograms of earthquakes in the vicinity of Mammoth Lakes, California, primarily events in the 1980 sequence. The data at distances less than 30 km include velocity and acceleration records obtained by the U.S. Geological Survey (Archuleta *et al.*, 1982), and strong motion accelerograms from instruments installed by the California Divisions of Mines and Geology (Turpen, 1980) and by the University of Southern California and the California Institute of Technology (Moslem *et al.*, 1983). For distances from 90 to 600 km, we have data from broadband stations operated by the Lawrence Livermore National Laboratory. Similar broadband instruments installed by the University of Nevada recorded aftershocks of the 23 November 1984 $M_L = 5.7$ earthquake near Bishop, California. We have also used seismograms from the Wood-Anderson seismograph at Dugway, Utah. In all, 479 seismograms for 88 earthquakes in the range $2.5 \leqq M_L \leqq 6$ were studied. Figure 1 is a map showing the source regions and station locations for the data analyzed.

Following Bakun *et al.* (1978), we synthesized Wood-Anderson seismograms by transforming the original, horizontal component time series into the frequency domain and dividing by the instrument response, thus converting the data to ground displacement. This was then multiplied by a Wood-Anderson response, and the result was transformed back into the time domain to give a "synthetic" Wood-Anderson seismogram, i.e., that which would have been recorded at the site had the original instrument been replaced with a Wood-Anderson torsion seismograph with

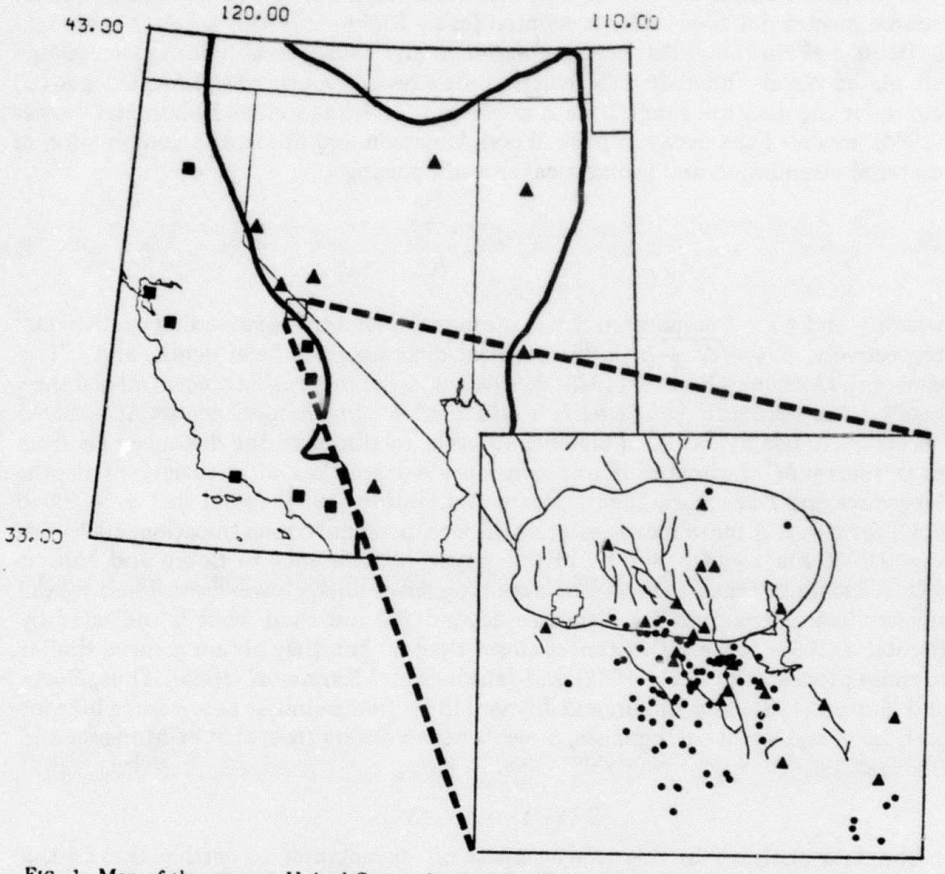

FIG. 1. Map of the western United States showing the Mammoth Lakes, California, source region (enlargement, epicenters plotted as dots), and seismic stations used in this study. The triangles indicate seismic stations used to determine the Great Basin attenuation curve, and the squares give the locations of the California Wood-Anderson seismographs used in determining the reference magnitudes (UCB to the north, CIT to the south). The heavy line delineates the border of the Basin and Range.

sufficient dynamic range. We determined the average of the maximum zero to peak amplitudes of the two horizontal components at each station, and these average amplitudes and their associated epicentral distances constitute our data set. These data, after normalization described below, are plotted in Figure 2. Figure 2a displays the entire data set while, for clarity, Figure 2b shows the data at close distances. The shape of the curve implied by the data points describes the Great Basin log $A_0(\Delta)$ function.

Station corrections. The amplitudes at close distances ($\Delta < 30$ km) are from a variety of stations with differing site geology and presumably different site responses (enlargement, Figure 1). We attempted to remove any apparent trends from the amplitude versus distance plot which may be a consequence of the combination of station distribution and site amplification by applying corrections determined in the following manner. Since the raw amplitude data include both site and distance effects, we first reduced the distance dependence by correcting the data using Boore and Hutton's (1984) log $A_0(\Delta)$ curve with the assumption that the shape of the

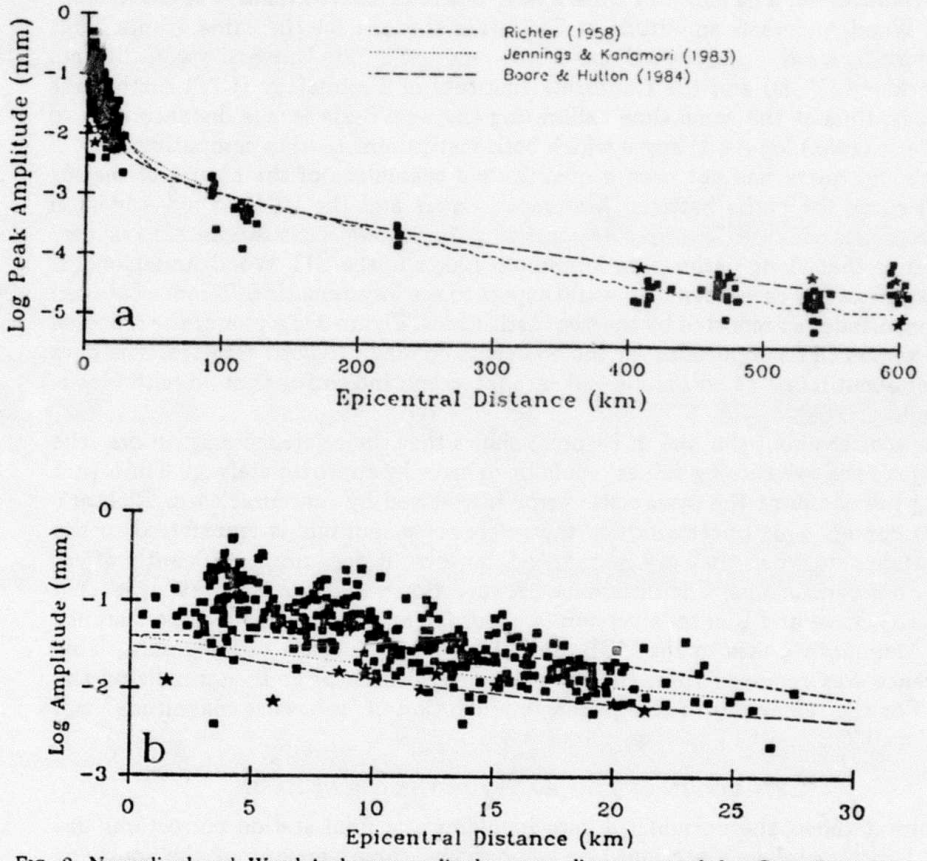

FIG. 2. Normalized peak Wood-Anderson amplitudes versus distance recorded at Great Basin sites. The squares indicate amplitudes for events with reference magnitudes below 5.5, the stars are for magnitude 5.5 and above events. Lines give the indicated southern California log $A_0(\Delta)$ functions.

actual log $A_0(\Delta)$ curve resembles theirs at that distance range. Then, assuming that a station on granite required no correction, the stations were grouped by site geology (granite, rhyolite, rhyodacite, glacial till, lake deposits, or alluvium), and the average magnitude bias was determined relative to the granite site. These corrections were applied to the raw data, and a log $A_0(\Delta)$ function was determined for the corrected data using the method described in the next section. The above procedure was repeated, this time using the new log $A_0(\Delta)$ curve and removing the constraint that the granite correction was zero. The resulting geology-based corrections ranged

from −0.16 for the granite site to approximately −0.50 for alluvium and other unconsolidated sediments. These corrections are included in all data presented here.

As it turns out, the shape of the corrected amplitude versus distance curve is not significantly different from the uncorrected, implying that distance dependence is responsible for the major trend of the curve. At distances beyond 90 km, the data from each station plot as a group, isolated from the others, causing individual station biases to be easily recognized. For this reason, we decided it was not necessary to estimate station corrections for the more distant sites at this point in the analysis.

Normalization. The data in Figure 2 have been normalized relative to the average peak Wood-Anderson amplitude at California stations for the same events. This was done by subtracting the average M_L as reported by the University of California at Berkeley (UCB) and the California Institute of Technology (CIT) earthquake catalogs, thus at the same time calibrating the amplitude versus distance data to Richter's (1958) log $A_0(\Delta)$ curve which both institutions used in computing M_L.

Although there has not been a quantitative evaluation of the nature of the log $A_0(\Delta)$ curve for paths between Mammoth Lakes and the UCB Wood-Anderson seismographs (Figure 1), our data suggest that the apparent attenuation is very similar to that along paths from Mammoth Lakes to the CIT Wood-Andersons. If this were not the case, then one would expect to see a systematic difference between the magnitudes as reported by the two institutions. Figure 3 is a plot of the reported UCB versus CIT magnitudes for the 55 events common to both catalogs. The data scatter about a line of unit slope and zero intercept, indicating that no path bias is present.

The scatter about the line in Figure 3 shows that the reference magnitudes (the average of the two catalog values) could be in error by approximately ±0.3 unit [not taking into account the systematic error introduced by inaccuracies in Richter's (1958) curve]. This uncertainty in the reference magnitude is transferred to the amplitude data when they are normalized, however it does not significantly affect any of our conclusions. The difference between Boore and Hutton's (1984) revised log $A_0(\Delta)$ curve and Richter's version is about 0.3 at 350 km, the average distance from Mammoth Lakes to the UCB and CIT Wood-Anderson seismographs. This difference was removed from the reference magnitudes prior to normalizing the data. For the remainder of this paper, any mention of "reference magnitude" will mean the UCB and CIT average minus 0.3.

Estimation of Log $A_0(\Delta)$ for the Great Basin

Figure 2 shows the normalized data including the final station corrections described in the previous section. For comparison, three versions of the southern California log $A_0(\Delta)$ curve are included in the plot. These are Richter's (1958) original curve, Jennings and Kanamori's (1983) modifications to it, and Boore and Hutton's (1984) revised curve. In Figure 2 (as well as in Figures 4 and 5), stars are used to indicate data from events with a reference magnitude above 5.5 while squares denote those data from smaller earthquakes.

Figure 2 reveals that there exists a difference beween the southern California and Great Basin log $A_0(\Delta)$ functions. At distances beyond 200 km (Figure 2a), peak Wood-Anderson amplitudes decay more rapidly than Boore and Hutton's (1984) curve predicts. The data at that distance range are better fit by Richter's (1958) curve. At near distances (Figure 2b), the data points at distances below 10 km fall above the various southern California curves, but merge with them for $10 \leqq \Delta \leqq 30$

km. The trend of the data is oblique to the curves, indicating more rapid attenuation of energy than predicted by the southern California log $A_0(\Delta)$ functions.

The data also suggest that the amplitude decay at close distances is a function of magnitude. The points in Figure 2b for $M_L \geqq 5.5$ events (stars) plot below the main population (squares) and show little variation in amplitude with distance over the interval $0 \leqq \Delta \leqq 30$ km. These points tend to scatter about the attenuation curve proposed by Jennings and Kanamori (1983). This observation cannot be a consequence of site effects, since the same stations recorded both large and small earthquakes. This is consistent with the hypothesis of Munguia and Brune (1984) that there is a near-source M_L saturation due to finite source effects for large events. In view of this apparent magnitude bias in the log $4_0(\Delta)$ curve, only those data from events with $M_L < 5.5$ were considered when developing the Great Basin Wood-Anderson attenuation curve.

Figure 2a shows that the data at 100 km scatter about −3, the point through

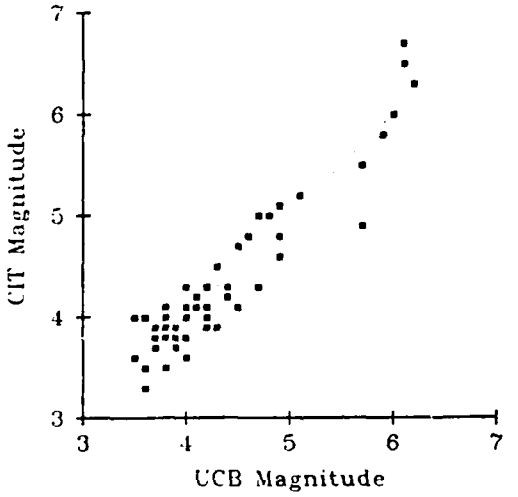

FIG. 3. Plot of M_L as reported by UCB versus that reported by CIT. The dashed line has unit slope and zero intercept.

which the southern California curves were constrained to pass. Because of this, we decided to also constrain the Great Basin log $A_0(\Delta)$ curve in a like manner. (There is no *a priori* reason to assume that this would be the case. Energy from a magnitude zero earthquake propagating through a medium whose attenuation properties differ substantially from those of southern California will require log $A_0(100)$ to have a value other than −3.)

We used the model given by equation (1) to describe the observed spatial attenuation. There is a trade-off between γ and η, so we assumed that $\eta = 1$ for $0 \leqq \Delta \leqq 90$ km and $\eta = 0.83$ for $90 \leqq \Delta \leqq 600$ km. The value of $\eta = 1$ represents body wave geometrical spreading for sources buried in a homogeneous medium, while $\eta = 0.83$ is the theoretical time domain geometrical spreading coefficient of a dispersed Airy phase which Campillo *et al.* (1984) have numerically verified to be applicable for the *Lg* phase. *Lg* is commonly the largest amplitude phase on our simulated Wood-Anderson seismograms at regional distances.

In Figure 4 are the same data as in Figure 2, superimposed on curves given by (1) for a variety of γ, and constrained to equal -3 at 100 km. These curves indicate the range in γ which is possible, given the scatter in the data. At distances beyond 90 km (Figure 4a), γ can vary between 0.004 and 0.009 km^{-1} with a (visually) preferred value of 0.006 km^{-1}.

At the closer distances (Figure 4b), the data lie within lines corresponding to $0.005 \leqq \gamma \leqq 0.025$ km^{-1}, and are best fit by a γ of 0.016 km^{-1}. These curves assume

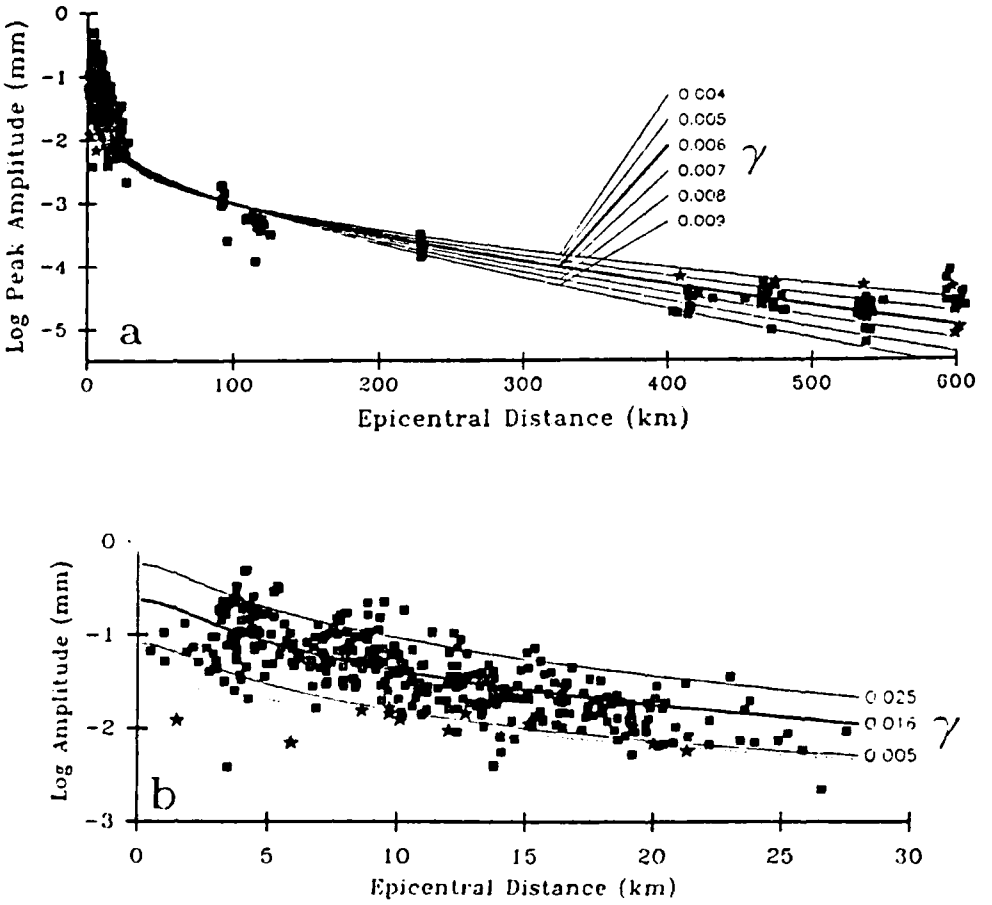

FIG. 4. The same data as in Figure 2, superimposed on curves given by equation (1). (a) Assuming a geometrical spreading coefficient of $\eta = 0.83$. (b) Assuming $\eta = 1$ and a 2-km focal depth. The material attenuation coefficients, γ, are shown for each curve; the preferred fits to the data are indicated by a heavy line. The dotted line in (b) is Boore and Hutton's (1984) curve assuming a 5-km focal depth.

a focal depth of 2 km, chosen since the trends which result more closely match that of the data than what was obtained using other reasonable focal depths. The median depth which was actually computed in the earthquake locations was 5 km, however attenuation curves computed using that depth are flatter than required by the data for epicentral distances below 10 km. This is illustrated by the dotted line in Figure 4b which assumes a 5 km focal depth (Boore and Hutton's, 1984, curve). The implications of this is that either our model for describing the attenuation [equation

(1)] is inadequate at very near distances or that the actual focal depths are shallower than obtained. The former being the case would preclude our ascribing any physical interpretation to the constants in the attenuation function. The curve empirically describes the spatial attenuation however, and can be used in computing M_L without regard to the validity of equation (1). Based on Figure 4, our estimate of the Great Basin log $A_0(\Delta)$ function is

$$\log A_0(\Delta) = \begin{cases} \log_{10}\left[\dfrac{e^{-0.016R}}{R}\right] - 0.31 & 0 \leqq \Delta \leqq 90 \text{ km} \\ \log_{10}\left[\dfrac{e^{-0.006R}}{R^{0.83}}\right] - 1.08 & 90 \leqq \Delta \leqq 600 \text{ km}. \end{cases} \quad (2)$$

Discussion

We computed a $M_L(syn)$ by applying equation (2) to the data, and Figure 5 shows the differences between $M_L(syn)$ and the reference magnitudes, called $M_L(wa)$, as a function of distance. Jennings and Kanamori's (1983) curve was used for the data from events with reference magnitude above 5.5 and $\Delta < 30$ km. The points scatter about the zero reference line showing that, on the average, the distance dependence has been removed from the data. The figure has a suggestion of a systematic overestimation of M_L at distances beyond 500 km, however, we feel this is an illusory consequence of the need for a station correction at 600 km (Dugway). Dugway is the only station beyond 90 km which is situated on sediments; all the others are installed on competent bedrock. Although we cannot exclude the possibility that these other stations require some correction (Tucker *et al.*, 1984), they should be small relative to that at Dugway. Figure 5 indicates a correction for Dugway of −0.41.

Applying Jennings and Kanamori's (1983) attenuation curve to the data for events above reference magnitude 5.5 causes them to fall within the main population of data points. Use of equation (2) instead of Jennings and Kanamori's log $A_0(\Delta)$ values would have preserved the difference between the large and small events evident in Figures 2b and 4b. We have considerably less data for the larger events and so are unable to unequivocally state the need for a magnitude dependent attenuation curve. Our data do, however, indicate that extra care must be taken when determining M_L at close distances. Given the data currently available, we recommend that for Great Basin paths and epicentral distances under 30 km, the log $A_0(\Delta)$ function given by equation (2) be used only for events below $M_L \approx 5.5$. Jennings and Kanamori's (1983) curve appears more appropriate for larger events at that distance range.

Figure 6 compares the attenuation curve found for Great Basin paths to Richter's (1958) southern California curve, Jennings and Kanamori's (1983) modifications to it, and Boore and Hutton's (1984) revised curve. Based on the results of Bakun and Joyner (1984), Richter's (1958) curve at distances beyond 100 km can also be viewed as representing attenuation in central California. We find that in the Great Basin, the attenuation of energy with frequencies in the Wood-Anderson passband is greater than in southern California but slightly less than that in central California. The scatter in the data allow for equal attenuation in the Great Basin and central California, however. The trend of the data at close distances also suggests stronger

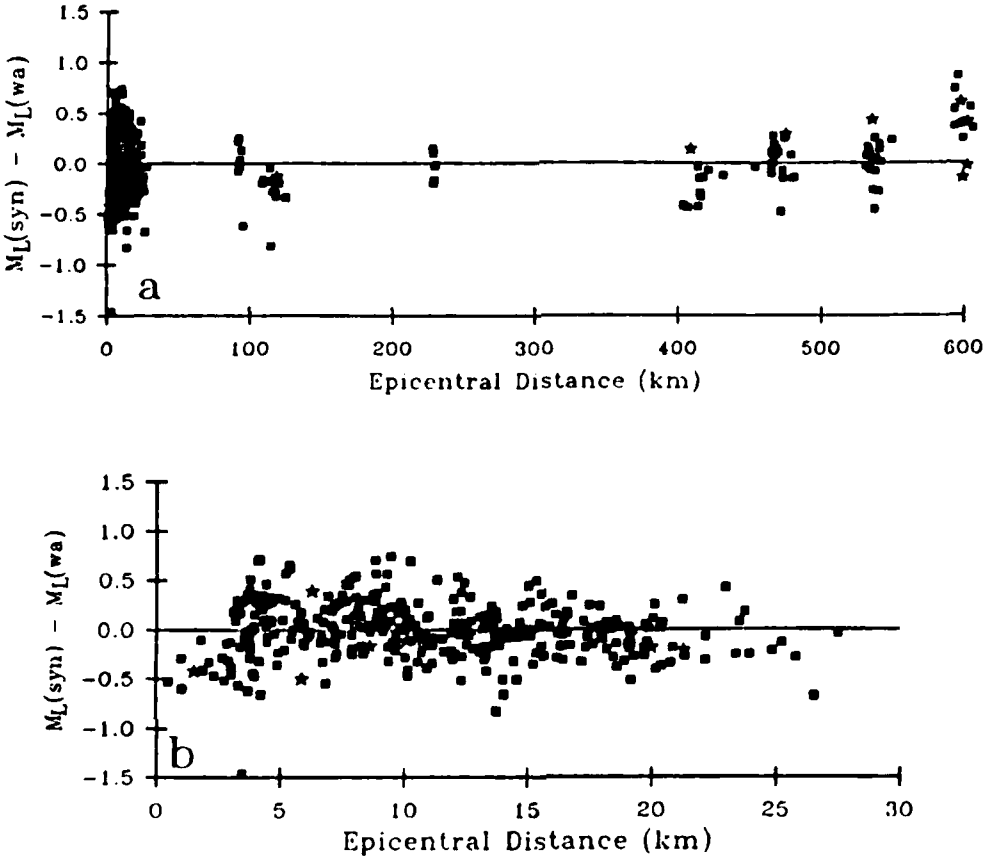

FIG. 5. The difference between estimates of M_L made from Great Basin equivalent Wood-Andersons, $M_L(syn)$, and the California reference magnitudes, $M_L(wa)$. The amplitudes from events below 5.5 (squares) were corrected using equation (2); those from larger events (stars) were corrected using Jennings and Kanamori's curve for epicentral distances below 30 km, and equation (2) for greater distances.

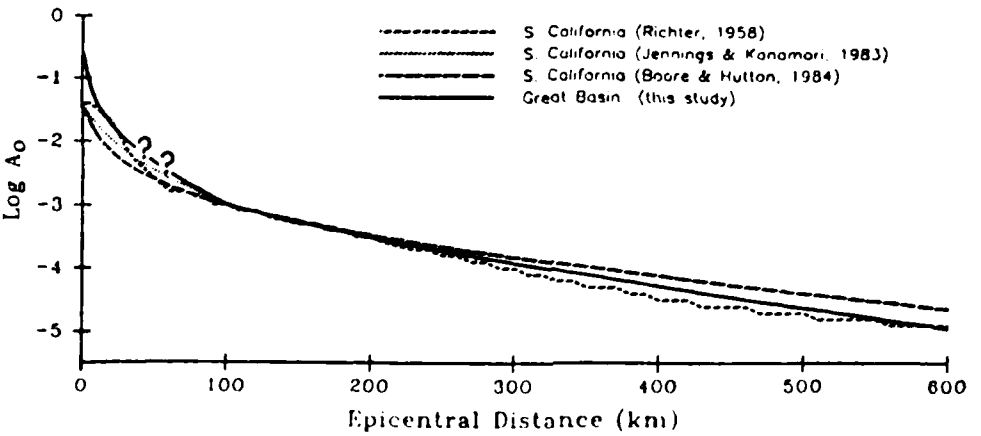

FIG. 6. Comparison of the log $A_0(\Delta)$ curve obtained for the Great Basin with Richter's (1958) southern California curve, Jennings and Kanamori's (1983) modification to it, and Boore and Hutton's (1984) revised curve. The question marks indicate the distance range for which no Great Basin data were available.

attenuation than given by any of the southern California curves. We have no data for the distance range $30 \leqq \Delta \leqq 90$ km; the curve shown is a continuation of that found for $\Delta \leqq 30$ km.

The material attenuation coefficients are related to the seismic quality factor, Q, through

$$Q = \frac{\pi f}{U\gamma}$$

where f is the frequency of the wave, and U is its group velocity. Thus, we can estimate the Q for Lg in the Great Basin by assuming $U = 3.5$ km/sec (the typical Lg group velocity) and $f = 1.25$ Hz (the Wood-Anderson natural frequency). Given the range in γ indicated in Figure 4a, we find that the Great Basin LgQ at frequencies near 1 Hz is between 125 and 280, with a preferred value of 190. Boore and Hutton's (1984) curve suggests that LgQ in southern California is closer to our upper limit. For comparison, Patton and Taylor (1984) examined surface waves to conclude that the shear wave Q in the Great Basin was about 100 in the lower crust and 30 in the upper mantle, while Singh and Herrmann (1983) found a coda Q of 200 for California. The value of $\gamma = 0.016$ km^{-1} obtained at close distances implies a 1-Hz shear wave Q of 75, assuming $U = 3.3$ km/sec.

Our conclusion that attenuation in the Great Basin is less than in southern California is in conflict with Evernden's (1975) study of intensities in the Great Basin which concluded that it has slightly less attenuation than California. Part of this discrepancy could be explained by the fact that central California attenuation does appear to be greater than that in the Great Basin. Whatever the case, the data require a systematic increase in attenuation relative to southern California, in order to bring our M_L estimates into agreement with those made using the UCB and CIT Wood-Anderson recordings of the same earthquakes and Boore and Hutton's (1984) $\log A_0(\Delta)$ function.

A recent development which affects studies of this type is the suggestion that there has been a systematic miscalibration of California Wood-Anderson seismographs (e.g., Bakun and Joyner, 1984). It appears possible that these instruments operate at a gain of 2100 rather than 2800, as is required by the definition of M_L. This presumably was also the case for the instruments used by Richter (1935) which would indicate that the "standard" Wood-Anderson gain is actually 2100. Since it has not yet been firmly established in the literature that this problem exits, we have used a gain of 2800 when converting the data. Thus, there is the possibility of a systematic error of approximately 0.12 in the constants in equation (2). We also point out that the attenuation curve developed for the Great Basin is tied to the southern California curve through our normalization procedure. Future modifications to the southern California $\log A_0(\Delta)$ function will necessitate similar modifications to the Great Basin curve.

M_0 Versus M_L Relationships for the 1980 Mammoth Lakes Sequence

Using the $\log A_0(\Delta)$ curve developed here for the smaller events ($M_L \leqq 5.5$) and Jennings and Kanamori's (1983) curve (at close distances) for the larger events, we recomputed M_L for 65 earthquakes of the 1980 Mammoth Lakes, California, sequence for which estimates of the seismic moment were available. The data include events used to determine the revised attenuation curve plus 17 others with

$0.5 \leqq M_L \leqq 2.8$ which were not used above since no reference magnitudes were available. Figure 7 is a plot of these revised magnitudes versus the seismic moments taken from Archuleta *et al.* (1982) and Priestley *et al.* (1985). These moments are based on spectral analysis of the same local digital and strong-motion recordings from which the synthetic Wood-Anderson seismograms were derived. Priestley *et al.* (1985) also determined the moments of the larger ($M_L \geqq 4.0$) events from regional surface wave recordings and found them to be in agreement with those determined from spectral analysis of the local recordings.

Two straight lines were fit to the data. For events in the magnitude range $1 \leqq$

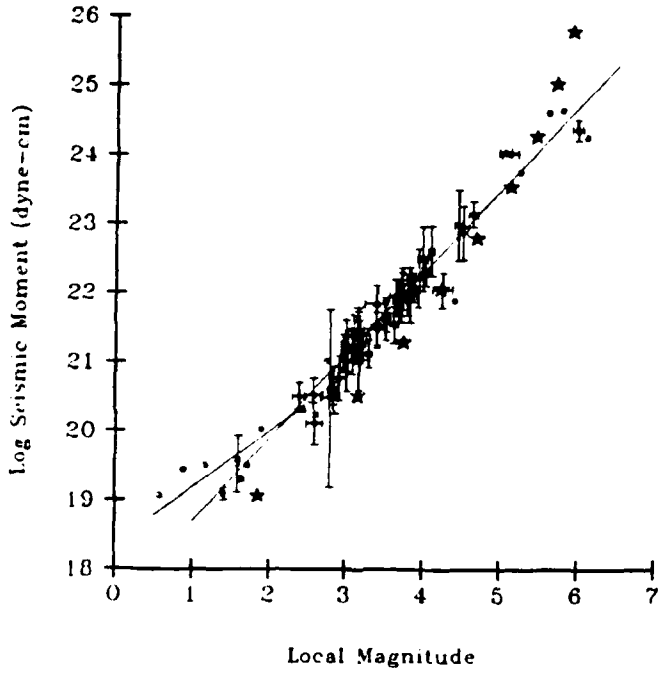

FIG. 7. Log M_0 versus M_L for earthquakes in the 1980 Mammoth Lakes, California, sequence. One standard deviation of the mean error bars are given for events with multiple recordings. The lines are least-squares fits to the data, and the stars are theoretical values taken from Hanks and Boore (1984).

$M_L \leqq 6$, the data are fit by the line

$$\log M_0 = (1.20 \pm 0.05)M_L + (17.49 \pm 0.19). \quad (3)$$

A few of the smaller events ($M_L \leqq 1.5$) deviate from this line. For events in the magnitude range $0.5 \leqq M_L \leqq 3$, the moments scatter about the line

$$\log M_0 = (0.81 \pm 0.08)M_L + (18.37 \pm 0.18),$$

however, it is strongly affected by the three smallest events. There are very few recordings for these three events, and it could be easily argued that neither their

moments nor their magnitudes are well determined. Furthermore, they were recorded at very close epicentral distances, and it is possible that variations in focal depth are affecting the results. Hanks (personal communication, 1985) has also pointed out that a f_{max} (Hanks, 1982) of 10 Hz would cause the magnitude of those events to be underestimated by about 0.3 magnitude unit, which is enough to bring the points close the line given by equation (3). For these reasons, we feel that the deviation of those data from the rest is not particularly significant. If we neglect those points, then the moment-magnitude data are linearly related over the entire magnitude range $1 \leqq M_L \leqq 6$, and do not exhibit any curvature of the type noted by Bakun (1984) or Hanks and Boore (1984) for other California earthquakes.

The M_0 versus M_L relationship given in equation (3) can be compared to that given by Archuleta *et al.* (1982) who used data primarily in the range $3 \leqq M_L \leqq 5$ with only one event above $M_L = 5$. Our data, on the other hand, span the range $0.5 \leqq M_L \leqq 6$ with seven events above $M_L = 5$. Archuleta *et al.* (1982) found that the M_0 versus M_L relationship for the 40 events for which they had UCB M_L determinations was, for the range $2.9 \leqq M_L \leqq 6.2$,

$$\log M_0 = (0.96 \pm 0.06)M_L + (18.14 \pm 0.23)$$

but for the larger events with more reliable M_L estimates ($3.5 \leqq M_L \leqq 6.2$), it was

$$\log M_0 = (1.05 \pm 0.08)M_L + (17.76 \pm 0.33).$$

The greater slope in equation (3) is due to the fact that we used larger moments for events with $M_L > 5.0$ than did Archuleta *et al.* (1982). For example, for the 27 May 1980 event at 14:50, Archuleta *et al.* (1982) found a seismic moment of 2.33×10^{24} dyne-cm based on two recordings whereas Priestley *et al.* (1985) obtained a value of 7.24×10^{24} dyne-cm when using nine recordings.

In comparing this result with other regions of California, the slope in equation (3) is less than the least-squares fit Archuleta *et al.* (1982) made to the data in Thatcher and Hanks (1973), but is very similar to the relation found by Bakun and Lindh (1977)

$$\log M_0 = (1.21 \pm 0.03)M_L + (17.02 \pm 0.07)$$

for the Oroville, California, earthquake sequence. Oroville, in the western Sierra Nevada, is located in a structural environment which is more similar to that of Mammoth Lakes than the southern California region studied by Thatcher and Hanks (1973).

In a recent study of five different source regions (Parkfield, San Juan Bautista, the Sargent fault, Coyote Lake, and the Livermore Valley), Bakun (1984) detected an inflection in the log M_0 versus M_L plot at about $M_L = 3$. For the events in the range $1.5 \leqq M_L \leqq 3.5$, he found the relationship to be

$$\log M_0 = 1.2M_L + 17$$

which is essentially the same as the relationship given in equation (3) based on data in the range $1 \leqq M_L \leqq 6$. However, for events in the similar range $3.5 \leqq M_L \leqq 6.25$,

Bakun (1984) found the relationship to be

$$\log M_0 = 1.5 M_L + 16.$$

Bakun (1984) and Hanks and Boore (1984) have noted that moment versus magnitude plots for California earthquakes exhibit positive curvature when the range of magnitudes considered is sufficiently large. Hanks and Boore were able to model this curvature using the method described by Boore (1983). In Boore (1983), seismograms of hypothetical earthquakes are generated which have an amplitude spectrum equal to that predicted by the Brune (1970, 1971) source model, given specified source parameters. Boore assumed a constant "stress parameter" of 100 bars, thus restricting the spectrum scaling law to be a function of seismic moment alone. The stress parameter controls the strength of the high-frequency radiation, and Hanks and Boore (1984) have referred to it as the a_{rms} stress drop.

Hanks and Boore (1984) computed M_0 and M_L from these "seismograms" and found that their assumption of constant stress drop allowed them to reproduce the observed curvature in the moment versus magnitude plot for $0 \leqq M_L \leqq 6$. Their theoretical values are included in Figure 7. They show only slight curvature for magnitudes below $M_L \approx 5$, but beyond that the seismic moment increases ever more rapidly with increasing M_L. This phenomenon is not present in the observed data, indicating that the assumption of constant stress drop independent of magnitude is not valid for the 1980 Mammoth Lakes earthquakes, over the range $1 \leqq M_L \leqq 6$. However, given the small curvature in the theoretical values below $M_L \approx 5$, together with the scatter in the observations, the data are consistent with constant stress drop for the smaller events. The data fall to the left of the theoretical values for $M_L < 5$. This fact suggests that the stress drops for these events are less than the 100 bars assumed by Hanks and Boore (1984) in their computations. Likewise, Figure 7 suggests that events larger than $M_L \approx 5.5$ had stress drops above 100 bars. This is in agreement with results from spectral analysis of Archuleta *et al.* (1982) and Priestley *et al.* (1985) who found that the largest events had stress drops on the order of 1000 bars.

Teleseismically determined estimates of seismic moment for the three largest events are 0.5 to one order of magnitude greater than the locally determined estimates shown in Figure 7 (Given *et al.*, 1982; Barker and Langston, 1983). While this discrepancy has yet to be explained, it does indicate the possibility that the actual moments of the larger events are greater than what we used. If this is the case, then the moment-magnitude plot would exhibit curvature at larger magnitudes.

SUMMARY

We have developed a $\log A_0(\Delta)$ function which removes the distance dependence from local magnitude estimates using Great Basin recordings of $M_L \leqq 5.5$ earthquakes. The data indicate greater attenuation of energy in the Wood-Anderson passband than in southern California, but equal or slightly less attenuation than in central California. Peak Wood-Anderson amplitudes of events larger than $M_L \approx 5.5$ decay less rapidly than those for smaller events at close distances, consistent with near-source saturation of M_L due to the finite source size of the larger earthquakes. A revised moment-magnitude relationship for the 1980 Mammoth Lakes earthquakes is similar to other Sierra Nevada (Oroville) earthquakes. Comparison of the moment-magnitude data to theoretical values suggests that events below $M_L \approx 5$

had constant stress drop while larger events had increasingly greater stress drops, if we use locally determined estimates of seismic moment.

ACKNOWLEDGMENTS

We thank J. Anderson, R. Archuleta, H. Patton, W. Richins, and A. Shakal for providing us with the bulk of the data used in this study. W. Peppin assisted in the development of the Wood-Anderson conversion program. W. Bakun and T. Hanks made several helpful comments on an earlier version of this report. This work benefited significantly from a critical review of the manuscript by D. Boore. This research was funded in part by the Defense Advanced Research Projects Agency of the Department of Defense and monitored by the Air Force Office of Scientific Research under Contract F49620-83-C-0012, and by the U.S. Geological Survey under Contract 14-08-001-21863.

REFERENCES

Archuleta, R. J., E. C. Cranswick, C. Mueller, and P. Spudich (1982). Source parameters of the 1980 Mammoth Lakes, California, earthquake sequence, *J. Geophys. Res.* **87,** 4595–4607.

Bakun, W. H. (1984). Magnitudes and moments of duration, *Bull. Seism. Soc. Am.* **74,** 2335–2356.

Bakun, W. H. and W. B. Joyner (1984). The M_L scale in central California, *Bull. Seism. Soc. Am.* **74,** 1827–1844.

Bakun, W. H., S. T. Houck, and W. H. K. Lee (1978). A direct comparison of "synthetic" and actual Wood-Anderson seismograms, *Bull. Seism. Soc. Am.* **68,** 1199–1202.

Barker, J. S. and C. A. Langston (1983). A teleseismic body-wave analysis of the May 1980 Mammoth Lakes, California, earthquakes, *Bull. Seism. Soc. Am.* **73,** 419–434.

Boore, D. M. (1983). Stochastic simulation of high-frequency ground motions based on seismological models of the radiated spectra, *Bull. Seism. Soc. Am.* **73,** 1865–1902.

Boore, D. M. and K. Hutton (1984). Attenuation of peak motions from Wood-Anderson seismographs in southern California, *Earthquake Notes* **54,** 25.

Brune, J. N. (1970). Tectonic stress and the spectra of seismic shear waves from earthquakes, *J. Geophys. Res.* **75,** 4997–5009.

Brune, J. N. (1971). Correction, *J. Geophys. Res.* **76,** 5002.

Campillo, M., M. Bouchon, and B. Massinon (1984). Theoretical study of the excitation, spectral characteristics, and geometrical attenuation of regional seismic phases, *Bull. Seism. Soc. Am.* **74,** 79–99.

Evernden, J. F. (1975). Seismic intensities, "size" of earthquakes and related parameters, *Bull. Seism. Soc. Am.* **65,** 1287–1313.

Given, J. W., T. C. Wallace, and H. Kanamori (1982). Teleseismic analysis of the 1980 Mammoth Lakes earthquake sequence, *Bull. Seism. Soc. Am.* **72,** 1093–1109.

Gutenberg, B. and C. F. Richter (1942). Earthquake magnitude, intensity, energy, and acceleration, *Bull. Seism. Soc. Am.* **32,** 163–191.

Hanks, T. C. (1982). f_{max}, *Bull. Seism. Soc. Am.* **72,** 1867–1879.

Hanks, T. C. and D. M. Boore (1984). Moment-magnitude relations in theory and practice, *J. Geophys. Res.* **89,** 6229–6235.

Jennings, P. C. and H. Kanamori (1983). Effect of distance on local magnitudes found from strong-motion records, *Bull. Seism. Soc. Am.* **73,** 265–280.

Luco, J. E. (1982). A note on near-field estimates of local magnitude, *Bull. Seism. Soc. Am.* **72,** 941–958.

Moslem, K., A. Amini, B. Kontic, J. Anderson, and T. Heaton (1983). Accelerograms from the Mammoth Lakes, California earthquake sequence of May–July, 1980 recorded on a temporary array, Report No. CE 83-01, University of Southern California.

Munguia, L. and J. N. Brune (1984). Local magnitude and sediment amplification observations from earthquakes in the northern Baja California-southern California region, *Bull. Seism. Soc. Am.* **74,** 107–119.

Patton, H. J. and S. R. Taylor (1984). Q structure of the Basin and Range from surface waves, *J. Geophys. Res.* **89,** 6929–6940.

Priestley, K. F., J. N. Brune, and J. G. Anderson (1985). Surface wave excitation and source mechanisms of the Mammoth Lakes earthquake sequence, *J. Geophys. Res.* (in press).

Richter, C. F. (1935). An instrumental earthquake magnitude scale, *Bull. Seism. Soc. Am.* **25,** 1–32.

Richter, C. F. (1958). *Elementary Seismology*, W. H. Freeman and Co., San Francisco, California, 758 pp.

Singh, S. and R. B. Herrmann (1983). Regionalization of crustal coda Q in the continental United States, *J. Geophys. Res.* **88**, 527–538.

Thatcher, W. and T. C. Hanks (1973). Source parameters of southern California earthquakes, *J. Geophys. Res.* **78**, 8547–8576.

Tucker, B. E., J. L. King, D. Hatzfeld, and I. L. Nersesov (1984). Observations of hard-rock site effects, *Bull. Seism. Soc. Am.* **74**, 121–136.

Turpen, C. D. (1980). Strong-motion records from the Mammoth Lakes earthquakes of May 1980, *Calif. Div. Mines Geol. Preliminary Report 27.*

SEISMOLOGICAL LABORATORY
MACKAY SCHOOL OF MINES
UNIVERSITY OF NEVADA
RENO, NEVADA 89557

Manuscript received 11 April 1985

SCALING OF M_L, m_b AND M_s TO THE SEISMIC SPECTRUM FOR THE MAMMOTH LAKES, CALIFORNIA EARTHQUAKES

Keith F. Priestley

Seismological Laboratory, University of Nevada, Reno, NV 89557

James N. Brune

Institute of Geophysics and Planetary Physics
Scripps Institution of Oceanography
University of California, San Diego
La Jolla, California 92093

SUMMARY : In this paper we compare the relative excitation of low frequency (0.05 to 0.125 Hz) and high frequency (0.5 to 10.0 Hz) for several moderate earthquakes (M_L 4 - 5.5) in the 1980 Mammoth Lakes, California sequence. Such studies have importance for both source mechanism and seismic decrimination studies. We have determined local magnitude (M_L), teleseismic body wave magnitude (m_b), and surface wave magnitude (M_s) for a large number of events in the magnitude range 1 to 6.2. Comparison of spectral amplitude Ω_o derived from body waves recorded at near epicentral distances and derived from surfaces waves recorded at regional distances, are, within the errors,the same indicating that the low frequency and high frequency radiation are consistent with a simple source. Comparison of m_b and M_s for the Mammoth Lakes earthquake sequence and Nevada Test Site explosions show that all of the earthquakes analyzed discriminate from explosions. Seismic moment (M_o) is related to M_L and M_s by the following relationships:

$$\log M_o = (1.20 \pm 0.05) M_L + (17.49 \pm 0.19) \ ,$$

$$\log M_o = M_s + 19.4\,(\pm 0.06) \ .$$

We have empirically related the gross logarithmic amplitude parameters M_L, m_b, and M_s, and the seismic spectrum observed at near epicentral distance. One representative event of this group was selected as a standard and M_L, m_b and M_s (at their observed frequencies) for that event were scaled to the observed seismic spectrum. Corresponding magnitudes for three other events were scaled to the observed seismic spectrum using the derived relationships. For events of similar depth, the local spectral values can be predicted from the distant magnitude measurements to within 10%. For a deeper event spectral values were predicted to within about 25%. This confirms that the spectral shape inferred from distant measurements of magnitude is congruent with the spectral shape observed directly in the near field. The majority of Mammoth Lakes events examined can be interpretated as simple events. In comparison,

several of the San Fernando aftershocks in the same magnitude range studied by Tucker and Brune (1977) could be interpreted as partial stress drop events. The near equality in the high and low frequency radiation for Mammoth Lakes aftershocks suggest that for each event the seismic radiation over the frequency band studied is coming from 1 simple same source, possibly the breaking of a single asperity. The suggested differences between Mammoth Lakes aftershocks and the San Fernando earthquakes may arise because most of the events studied for Mammoth Lakes are occurring in the more competent, higher stress, granitic block above a deeper through-going fault plane. The data suggest the idea that partial stress drop events are more common on developed fault systems, whereas full stress drop events are more common in the surrounding country rock as it adjust to the stress field generated by movement on the developed fault plane.

1.0 Introduction

Earthquakes with similar local magnitude, M_L, presumably have similar short-period amplitudes, and yet they can show large differences in their long-period amplitudes. Regional variations in the relative excitation of high and low frequency seismic waves have been noted in a number of studies in western North America. Brune, Espinosa and Oliver (1963) found a wide range in the surface wave excitation, for a given M_L, of earthquakes in the California-Nevada region. Wyss and Brune (1968) found that earthquakes in Nevada often generated smaller amplitude surface waves for a given M_L, than do earthquakes along the San Andreas fault or along the northern California coast. In a later study, Wyss and Brune (1971) noted large differences in the ratio of Gutenburg energy, E_G, determined from M_L, with seismic moment, M_o, determined from surface waves, for earthquakes in the California region. In particular, they found that earthquakes along the Sierran front to the north of Bishop, California had small ratios of M_s to M_L when compared to other areas in California. However at that time it was not possible to assess the effects of variations in source depth and source mechanism. In contrast, Tucker and Brune (1977) found that some of the larger aftershocks ($M_L > 4$) of the San Fernando earthquake sequence had spectral amplitudes at 0.1 Hz (based on surface waves) which were as much as an order of magnitude larger than the spectral amplitude at 1 Hz (based on body waves), i.e. the spectrum was not flat between 0.1 and 1.0 Hz.

These differences can arise due to the effects of the path, focal depth, radiation factor, and source parameters. Previous studies (Wyss and Brune, 1971; Thatcher, 1972) suggest that the observed differences between low and high frequency radiation result primarily from variations in the source spectrum. Brune *et al* (1985) have speculated that three classes of earthquakes exist: "partial stress drop" events ($\Delta\sigma << 100$ bars); "full stress drop" events ($\Delta\sigma \approx 100$ bars); and "overstress" events ($\Delta\sigma > 300$ bars), where the relative excitation of high and low frequency radiation varies depending on the type of event. Full stress drop events are those with a stress drop comparable to the effective stress, i.e., on the order of a hundred bars. This value of stress agrees with estimates of the upper limit of shear stress across the San Andreas fault based on

the lack of an observable frictional heat flow anomaly (Brune *et al.*, 1969; Lachenbruck and Sass, 1980). Partial stress drop events may occur when the fault locks soon after the rupture passes so that the average slip over the fault cannot reach a value corresponding to the initial dynamic stress drop over the whole fault. Alternatively, they may occur when the stress release is not uniform and coherent over the whole fault plane, but rather is more like a series of multiple events with part of the fault remaining locked. Such complexities could occur as a result of asperities on the fault, or due to a complex fault plane geometry. Overstress events may result possibly from a high quasi-static stress buildup due to strength inhomogeneities (barriers or asperities) which are stressed during an earthquake, or directly from the failure process, i.e., fault slip could cause a rapid, quasi-static stress buildup to much higher levels than could be maintained by the rocks on the time scale of long-term tectonic processes. In the latter case, the very high stress drop events are not necessarily indicative of regions which were under high stress before the earthquake.

Understanding the differences in the relative excitation of high frequency (0.5-10.0 Hz) and low frequency (0.05-0.125 Hz) seismic waves, and the propagation of this energy to regional distances, is important for understanding source mechanisms. It is particularly relavant to the problem of discriminating small explosions from earthquakes at regional distance. The $m_b - M_s$ discriminant, which compares the relative excitation of body versus surface waves, is presently one of the primary techniques for distinguishing explosions from earthquakes.

This study examines the relative excitation of high and low frequency seismic energy from earthquakes of the 1980 Mammoth Lakes, California, sequence. These earthquakes have been studied more thoroughly than perhaps any other earthquake sequence in the western United States. A dense network of high-gain seismographs provide data for accurate hypocentral coordinates and first motions for most events. Moreover,a large number of broad-band digital and strong-motion recordings have been collected in the epicentral region, which is surrounded by a network of long-period seismographs, and is 20° to 30° from the Canadian Network high gain, short-period stations. The events are particularly well suited for evaluating the $m_b - M_s$ seismic discriminant since they are in a environment similar to the Nevada Test Site, approximately 150 km to the southeast.

2.0 Summary of the Mammoth Lakes Earthquake Sequence

The Mammoth Lakes earthquake sequence and the geology and geophysics of the Long Valley Caldera with which they are associated, have been discussed in numerous, recent papers [See, for example, the special issue of the Journal of Geophysical Research, November, 1985]. The earthquake sequence began in October, 1978, peaked in May, 1980 with the occurrence of four $M_L > 6$ earthquakes over a two day period, and has continued to the present. These earthquakes are associated with the intersection of the Sierra Nevada frontal fault system and the Long Valley Caldera. The Long Valley Caldera was formed 0.7 million years ago by collapse and subsidence associated with the eruption of the

Bishop tuff (Bailey *et al.*, 1976), and volcanic activity has continued on a reduced scale into the Holocene. The dominant fault of the area is the Hilton Creek fault along which several hundred meters of pure normal fault displacement has occurred since the formation of the Long Valley Caldera (Bailey *et al.*, 1976). Extension of the Hilton Creek fault into the Long Valley Caldera appears to have occurred as recently as 0.3 million years ago, possibly indicating that the caldera had cooled sufficiently by that time to support stresses large enough to generate earthquakes.

Lide and Ryall (1985) discuss the distribution of 344 master event aftershock locations in the weeks following the four $M_L > 6$ events (the time period for the events examined in this study). Most of the earthquakes they located occurred in the Sierrian block, south of the caldera. In map view, they lay in a triangular shaped zone, of which the north boundary is approximately formed by the southern rim of the caldera and of which the east boundary is approximately formed by the Sierran frontal fault system. Three trends can be recognized in the aftershock data: two NNE trends, one of which forms the eastern boundary of the aftershock sequence, and a WNW trend which lies along the southern boundary of the caldera. A cross-section perpendicular to the NNE trends shows the aftershocks in the Sierrian block occur in a triangular shaped zone the base of which dips at about 45° to the east. Thus in the west, events extend down to 4 - 5 kms depth, while in the east they extend down to 11 - 13 kms depth. The $M_L > 6$ events lie near the base of this zone.

3.0 Data

This study utilizes seismograms of those earthquakes whose epicenters are shown in Figure 1 and listed in Table 1. These events comprise only a small fraction of the total number of events which have occurred in the Mammoth Lakes area since the earthquake sequence began in October, 1978. Events selected for study consist of those for which strong-motion or digital local seismograms, long-period regional seismograms, and short-period Canadian Network body-wave magnitudes where avaliable. All events have been located using arrival times from the local stations shown in Figure 1, with additional readings from local stations operated by the University of Nevada and the California Institute of Technology. Vetter (1984) has determined first motion focal mechanisms for many of these earthquakes.

Seismograms used in this study are from the seismograph stations shown in Figure 1 and listed in Table 2. The SMA-1 strong-motion accelerographs were installed by the California Division of Mines and Geology (Turpin, 1980), or by the University of Southern California (Moslem *et al.*, 1983). Digital stations operated by the U.S. Geological Survey and described by Archuleta *et al.* (1982), consist of either force-balance accelerometers or velocity transducers and Sprengnether DR-100 recorders. The SMA-1 analog seismograms were digitized at a sample interval of either 0.025 sec or 0.005 sec; the digital recordings supplied from the U.S. Geological Survey were digitized at an interval of 0.005 sec. All the above stations are denoted by triangles in Figure 1. For events along the southern boundary of the caldera, the SMA-1 and digital seismographs sample a large

fraction of the focal sphere. The radiation pattern of events south of the caldera is not as well sampled.

Figure 1 also shows the locations of the regional long-period stations (denoted by squares) whose seismograms were used to determine surface wave magnitudes. These stations surround the Mammoth Lakes region and, with the exception of the California Institute of Technology station at Pasadena (PAS), belong to the world wide network (WWSSN). Readings from the Canadian Network stations (denoted by stars) were used to determine body wave magnitude. All events in this study have nearly identical paths to the regional and teleseismic stations, so the data are uncontaminated by path effects.

4.0 Data Analysis

4.1 Magnitude Analysis

M_L: Chavez and Priestley (1985) determined M_L for 82 events of the 1980 Mammoth Lakes earthquake sequence (Table 2, column 7) by converting the digital, horizontal component data into equivalent Wood-Anderson seismograms. In determining M_L for these events, they developed and used an attenuation function appropriate to the Great Basin. "True" M_L based on Wood-Anderson amplitude measurements for the main shocks and larger aftershocks of the sequence have been reported by the University of California-Berkeley and by the California Institute of Technology. Chavez and Priestley found that their magnitudes were in close agreement with M_L determined from the Wood-Anderson seismograms recorded in California.

m_b: The *Earthquake Data Reports* of the U.S. Geological Survey report peak-to-peak amplitude, period, and individual station body-wave magnitudes. From this listing we have tabulated the body-wave magnitudes reported for Canadian Network stations at distances greater than 20° from Mammoth Lakes, and from these have determined an average m_b (Table 2, column 8) for 21 earthquakes studied.

M_s: We have determined surface wave magnitude for 34 events of the Mammoth Lakes sequence using amplitude measurements from long-period seismograms at regional distances. M_s (Table 2, column 9) was determined using the definition of Marshall and Basham (1972);

$$M_s = \log A + B(\Delta) + P(T) \qquad (1)$$

where A is one-half the peak-to-peak ground amplitude of the Rayleigh wave with a period T at a distance Δ, $B(\Delta)$ is a correction for the average effects of attenuation, scattering, geometrical spreading and refraction, and $P(T)$ is a correction factor for dispersion which allows measuring the surface wave amplitude at periods other than 20 seconds.

4.2 Body-wave analysis

Nature of the Seismograms at Near Distance: The seismograms analyzed display varying degrees of complexity, ranging from simple pulses to wave trains many seconds long. This variation can be due to source complexity, position of the station on the focal sphere, or to propagation affects. Some of the complex seismograms observed are easily attributable to source complexity since in those cases seimograms with both complex and simple nature have been observed at the same station for nearly co-located events. In other cases, however, both complex and simple seismograms have been observed at different stations for the same event. In these instances, seismograms showing large, simple S-waves often have relatively small P-wave amplitudes, and those with complex S-wave have large P-wave arrivals, indicating that the complexity is related to the position of the station on the focal sphere, i.e., if the S-wave amplitude is large (away from a node), it will exceed the scattered energy and the resulting seismogram will have a simpler character, whereas if the station is near an S-wave node, the scattered energy will predominate and the seismogram will appear to be more complex and have a lower amplitude (Tucker and Brune, 1977). In some cases, it is apparent from the long period oscillations following the S-wave, that earth structure contributes to the complexity of the seismograms. The effects of earth structure on seismic propagation will be discussed in more detail below.

Seismic Spectra: We have determined the seismic spectra for the events indicated in Table 1. We have compared our spectral results to those presented by Archuleta *et al.*, and find good agreement with our results, which also include the analysis of the strong-motion data. Spectral parameters for the smaller events in Table 4 of Archuleta *et al.* are consistent with the spectral parameter determined by Andrews (written communications, 1985). In the discussion below we have used the spectral parameters for small Mammoth Lakes aftershocks reported by Archuleta *et al.* (1982).

Displacement amplitude specta for the events indicated in Table 1 were computed from the locally recorded body-wave data. Time windows were chosen to be long enough to include the entire S-wave arrival, but short enough to minimize the inclusion of surface wave energy. Rather than rotate the data into radial and transverse components, we computed the vector sum of the two horizontal component spectra. The spectra were normalized to a hypocentral distance of 10 km, and plotted as log spectral amplitude (Ω) vs. log frequency (ω) and interpreted in terms of a flat, low-frequency asymptote, Ω_o, a high frequency fall-off with a slope in the range -1 to -3, and the corner frequency (f_c) at which the two trends intersect. In almost all cases, there is a second corner in the data at frequencies between 10 and 16 Hz. Below this frequency the spectra drop off with a slope of -4 to -5. The asymptotes were fit by eye using an interactive computer routine; an example of the fiting is shown in Figure 2. Although simple, the fitting technique used here is felt to be adequate, given other known errors involved in estimating Ω_o and f_c. Where we have events in common, our spectral fits are consistent with those of Andrews (written communication, 1985), who used a more objective technique.

The fits were then corrected for average radiation pattern and converted to full-space spectra by accounting for the free surface effect, using the following equation:

$$\Omega_o(full-space)_{10km} = \frac{\Omega_o(observed)_{10km}}{k\, R_{\vartheta\varphi}} \tag{2}$$

where k is the correction for the free surface SH-wave amplication, and $R_{\vartheta\varphi}$ is the correction for the average radiation pattern. Values of Ω_o and f_c, and their associated errors are given in columns 10 through 13 of Table 2.

Estimation of Data Errors: Where more than one recording was available for an event, errors in Ω_o and f_c due to scatter in the data were estimated by calculating an average spectral value and a standard deviation. The average values of Ω_o, $<\Omega_o>$, were determined by the formula

$$<\Omega_o>_{10km} = antilog\left\{\frac{1}{NS}\sum_{i=1}^{NS}\log\Omega_{0_i}\right\}$$

where Ω_{0_i} is the long-period spectral level at the i^{th} station , and NS is the number of stations recording the event. The standard deviation of the log average value of Ω_o was determined by the formula

$$s.d.\,(\log<\Omega_o>) = \left\{\frac{1}{NS-1}\sum_{i=1}^{NS}\left[\log(\Omega_o) - \log<\Omega_o>\right]^2\right\}^{1/2}.$$

A multiplicative error, $E\,\Omega_o$ factor is then determined from

$$E\,\Omega_o = antilog\left\{s.d.\,(\log<\Omega_o>)\right\}.$$

$<f_c>$ and Ef_c were computed in a similar manner. As pointed out by Archuleta *et al.* (1982), when calculating average values of Ω_o or f_c, it is necessary to compute the averages using the equations in the above forms to give equal weight to each observation. If a simple arithmetical average value is determined it will be biased toward larger values, since the errors associated with Ω_o and f_c are log-normally distributed.

Sources of error in estimating the seismic spectrum: The error bars calculated for the long period level Ω_o and the corner frequency f_c in the above section represent only the variations in Ω_o and f_c due to scatter in the observed recordings. There are, however, a number of sources of systematic error inherent in our estimates of Ω_o and f_c. These arise from both wave propagation and recording effects, as well as the assumptions and procedures made in analysing the data.

The correction of the S-wave amplitude for reflection at the free surface assumes that the waves are horizontally polarized (SH), however since we have

not rotated the data into transverse and radial components, the energy is in general some mixture of SH and SV-motion. Abe (1974) discusses experimental studies of S-wave amplification on reflection and concludes that using $k = 2$ in equation (2) (which we have done) applies approximately to SH-wave signals containing some SV-motion. The station-source configuration shown in Figure 1 indicates that multiple arrivials due to reflection should not be a problem in this study, since the S-waves are recorded at close epicentral distance.

No Q correction was made in determining the spectra. Archuleta *et al.* (1982) found that variations in whole-path Q had a small effect on the measurement of Ω_o for Mammoth Lakes events. More recent studies, however, suggest that near source recordings of the Mammoth Lakes aftershocks (Peppin, 1985: Barker, 1985), and possibly near source recordings in general (Anderson, 1985; Cranswick *et al.*, 1985) are strongly contaminated by variations in the structure very near to the recording site. Archuleta (1985) has analysed data recorded on a borehole seismograph in the epicentral region of the Mammoth Lakes aftershocks, to estimate the effect of the near surface structure on the seismic recording of the data (and consequently on the seismic spectra). In this experiment, recordings were made at three levels in the borehole -- at the surface, just below the sediment-bedrock interface (35 meters depth), and well into the bedrock (166 meters depth). The most obvious difference between the surface and bedrock time series was the increased complexity of the surface recordings compared with those in bedrock. Archuleta found little difference in the spectral levels of the two bedrock recordings, but approximately a four-fold amplitude increase in the data from the surface instrument. This amplication can partially be accounted for by the free surface amplication factor due to reflection (normally taken as a factor of 2 for pure SH-waves), and partially due to the effects of the impedance contrast between the glacial moraine at the surface and the underlying bedrock (approximately a factor of 1.85). Of relavance to the present study, spectral ratios between the surface and bedrock instruments show that the sediment amplification is essentially uniform across the 2.0 to 50.0 Hz band and does not shift f_c.

The effect of amplication due to the impedance contrast between the near surface sediment and the underlying bedrock at the various sites is somewhat more difficult to acess, as there is a variety of sediment types and thickness over the array shown in Figure 1. On the average, the effect of the sediment-bedrock impedance contrast should be approximately a factor of 2, irrespective of the variation of the sediment thickness observed in the Mammoth Lakes region. Thus based on Archuleta's borehold results, the long period spectral levels obtained from routine analysis of the seismic spectra of locally recorded surface data in the Mammoth Lakes region are probably overestimated by a factor which is close to two but not by an order of magnitude or more (Barker, 1985; Peppin, 1985). However, there appear to be only negligible effects of near surface structure on the estimated corner frequencies.

The spectra have been normalized to a hypocentral distance of 10 km. Not all events were located, and in those cases the S-P times were used to determine distance. The hypocentral accuracy of the located events is about ± 3 km

(Cockerham, personal communication) which would cause as much as 30% error in the normalization of any single spectra. Systematic errors in hypocentral location could affect the normalized average spectra, however there is no reason to suspect systematic location errors.

A final source of error inherent in the estimate of Ω_o comes from the assumption of a single, average radiation pattern correction. If sufficient instruments were available, or if the source parameters (including direction and velocity of rupture) were known, this error could be reduced. A value of 0.6 was used for $R_{\vartheta\varphi}$ (Thatcher and Hanks, 1973) in equation 2. At some azimuths, the amplitude could be 1.67 times larger than the amplitude determined assuming this correction, while near a node in the radiation pattern the amplitude could be quite small. Furthermore, if the source dimension is comparable to the wavelength involved, source propagation might distort the radiation pattern by focusing or defocusing energy, thereby changing the apparent corner frequency for different directions and possibly reducing the calculated moment.

4.3 Surface Wave Analysis

Determination Surface Wave Moment: Surface waves provide estimates of Ω_o which sample a lower frequency portion of the seismic spectrum, and which are independent of those obtained from S-wave spectra. We have determined surface wave moments for the earthquakes by fitting the general features of the observed Rayleigh waves recorded at regional distances, with a synthetic surface wave seismograms (*Figure* 3). Parameters needed to calculate the synthetic seismograms are the earth velocity and attenuation structures and the fault parameters of the individual earthquakes. Since the events are located at the western edge of the Great Basin, while most of the seismograph stations are located in western North America, we used the velocity structure determined for the Great Basin from surface wave dispersion measurements (Priestley and Brune, 1978). The Great Basin attenuation model by Patton and Taylor (1984) was used, with a slight lowering of the surficial shear wave Q. The earth model used in making the surface wave calculations is given in Table 3. Since for the majority of events we have studied, we do not have fault-plane solutions, nor do we know the focal depth we determined an average relationship for the Mammoth Lakes area in the following manner. Vetter (1984) has determined fault plane solutions for a large number of events in the Mammoth Lakes area, and found that the mechanisms can generally be subdivided into two groups. The first group consists of earthquakes with strike-slip mechanisms (average plane of strike N14°E, dip 80°ESE, slip N16°E or strike N73°W, dip 80°SSW, slip N76°E) which are most commonly at depths less than 9 km. The second group consists of earthquakes with oblique or normal mechanisms (average planes of strike N03°E, dip 64°E, slip N40°E or strike N50°W, dip 38°SW, and slip N86°W) usually at depths greater than 9 km. Synthetic surface wave seismograms were calculated for both mechanisms, for 2, 5, 8, 11 and 14 km depth. Surface-wave amplitudes were determined from the 10 synthetic records at each station and an average conversion factor determined for both focal mechanisms and all focal depths. The resulting relationship between surface wave magnitude M_S and seismic

moment M_0 for the Mammoth Lakes area is given by the equation

$$\log M_0 = M_S + 19.40(\pm 0.06). \tag{3}$$

Sources of Error: Tucker and Brune (1977) used surface wave spectra to make lower frequency estimates of seismic moment for comparison with moments determined from body waves. They made a careful estimate of the errors involved in estimating the seismic moment from the surface wave spectra. These errors included procedural errors, path structure and attenuation, lateral refraction (multipathing), source finiteness, and uncertainties in fault parameters (depth, dip, strike, and slip vector) in correcting for the radiation pattern. They concluded that these effects could lead to a maximum error in the final result of no more than a factor of 4.

Low-frequency Spectral Level from Surface Waves: Equation (3) allows us to rapidly determine the seismic moment, M_o, from the surface wave amplitude measurements. These surface wave moments were converted to full-space spectral levels (Ω_o) at their observed frequencies for comparison with the spectral levels determined from the, near source body-wave recordings. Using a shear wave speed (β) of 3.5 ks^{-1}, a density (ρ) of 2.9 $kg\ m^{-3}$, 0.6 for the radiation factor ($R_{\vartheta\varphi}$), and the seismic moment determined by fitting the surface waves, the spectral level from the

surface wave moments, normalized to 10 km is given by

$$\Omega_o(full-space)_{10km} = \frac{R_{\vartheta\varphi} M_o}{4\pi\rho\beta^3(10\,km)} = 3.84 \times 10^{-25} M_o \quad . \tag{4}$$

This gives values of Ω_o at surface wave frequencies for comparison with the spectra obtained from the body-wave accelerograms. Values of Ω_o derived from the surface wave moments and the associated error in Ω_o are given in column 14 and 15 of Table 1. The frequency at which the surface waves Ω_o was determined and its associated error are given in column 16 and 17.

5.0 Results

5.1 Comparison of short-period and long-period estimates of seismic moment

Figure 4 is a plot of Ω_o determined from the spectral analysis of the strong-motion and digital data recorded at near distances ($\Delta < 20$ km), and Ω_o determined from surface waves recorded at larger distances ($\Delta > 375$ km). Error bars indicate the scatter in the observations. The reference line through the data is of unit slope and zero intercept. Those points lying above the line have larger local body wave Ω_o relative to the observed surface wave Ω_o, while points below the line have larger surface wave Ω_o compared to the observed local body wave Ω_o. As shown in this figure, most of the events we have studied show no significant differences in Ω_o measured at frequencies near 1 Hz compared to Ω_o measured at frequencies near 0.1 Hz.

Differences in Ω_0 over this band can arise due to partial stress drop (Brune, 1970) or to afterslip on the fault (Hartzell and Brune, 1979). The agreement between the low and high frequency determinations of Ω_0 indicates that the Mammoth Lakes events we have studied are simple, that is they are neither partial stress drop events nor events with a large long-period heave following the breaking of the initial asperity. Thus our data suggest that seismic radiation across the band studied is produced from a simple mechanism, possibly the breaking of a single asperity. This may arise due to a higher overall state of stress in the crust in the vicinity of Mammoth Lakes as suggested by Wyss and Brune (1971); most of the aftershocks we have studied occur in the granitic block where strength and stress may be higher than on the deeper, throughgoing fault plane. Alternatively, the granitic block may be now so brecciated that stress can only be concentrated over planes of limited extent which break as a single unit.

5.2 Relationship between m_b, and M_s

Figure 5 compares the m_b vs. M_s data for the Mammoth Lakes earthquakes to the North American earthquake and explosion data of Marshall and Basham (1972). Magnitudes in that study were determined from seismograms recorded on Canadian Network stations. In our study, Canadian Network data were used to determine m_b, while data from long-period stations in the western U.S. were used to determine M_s. Though it is possible that this might lead to a systematic difference between M_s determined by Marshall and Basham, and the M_s determined for the Mammoth Lakes earthquakes by us, there does not seem to be a strong effect. This is evidenced by the fact that our paths overlap those of Marshall and Basham to a large extent, and the data sets in Figure 5 overlap as well. Neither the Marshall-Basham data nor the Mammoth Lakes earthquakes data have been corrected for depth variations. All Mammoth Lakes events fall within the earthquake population and discriminate from explosions, although some events are offset from the earthquake mean towards the explosion population.

5.3 Magnitude-Moment relationships

Log M_0 *vs.* M_L *relationship*: Figure 6 is a plot of log seismic moment, M_0, derived from the spectra of the near-source digital and strong-motion recordings, vs. M_L values published by Chavez and Priestley (1985). They found that the data are fit by the line

$$\log M_0 = (1.20 \pm 0.05) M_L + (17.49 \pm 0.19) \qquad (1 < M_L < 6)\,, \tag{5}$$

and do not exhibit curvature of the type noted by Bakun (1984) or Hanks and Boore (1984) for other California earthquake sequences.

The log M_0 vs. M_L relationship given in equation (5) differs from that given by Archuleta *et al.*, (1982) which used data primarily in the range $3 \leqq M_L \leqq 5$ with only one event above M_L 5. Our data span the range $1 \leqq M_L \leqq 6$ with seven events above M_L 5. Archuleta *et al.*, (1982) found that the log M_0 vs M_L relationship for

the 40 events for which they had University of California - Berkley M_L determinations was

$$\log M_o = (0.96 \pm 0.06) M_L + (18.14 \pm 0.23) \qquad (2.9 \leq M_L \leq 6.2)$$

but for the larger events with more reliable M_L estimates it was

$$\log M_o = (1.05 \pm 0.08) M_L + (17.76 \pm 0.33) \qquad (3.5 \leq M_L \leq 6.2) .$$

The greater slope in equation (5) is due to the fact that we used larger moments for events with $M_L > 5.0$ than did Archuleta *et al.*, (1982). For example, for the May 27, 1980 event at 14:50, Archuleta *et al.*, (1982) found a seismic moment of 2.33×10^{24} dyne-cm based on two recordings whereas Priestley *et al.*, (1985) obtained a value of 7.24×10^{24} dyne-cm from nine recordings. The slope of equation (5) is less than Archuleta *et al.*, (1982) found for the data of Thatcher and Hanks (1973), but is identical to the relation of Bakun and Lindh (1977) for the Oroville, California earthquake sequence:

$$\log M_o = (1.21 \pm 0.03) M_L + (17.02 \pm 0.07) .$$

Oroville, in the western Sierra Nevada, is located in a structural environment which is more similar to that of Mammoth Lakes than the southern California region studied by Thatcher and Hanks (1973).

In a study of five different source regions (Parkfield, San Juan Bautista, the Sargent fault, Coyote Lake, and the Livermore Valley), Bakun (1984) detected an inflection in the $\log M_o$ vs. M_L plot at about M_L 3. For small events he found the relationship to be

$$\log M_o = 1.26 M_L + 17 \qquad (1.5 \leq M_L \leq 3.5)$$

which is identical to our equation (5) which is based on data in the range $1 \leq M_L \leq 6$. However, for events in the same magnitude range as our data Bakun (1984) found the relationship to be

$$\log M_o = 1.5 M_L + 16 \qquad (3.5 \leq M_L \leq 6.25) .$$

Bakun (1984) and Hanks and Boore (1984) have noted that log M_o vs. M_L plots for California earthquakes exhibit positive curvature when the range of magnitudes considered is sufficently large. Hanks and Boore (1984) computed theoretical log M_o vs. M_L relationship based on the assumption of a constant stress drop of a 100 bars. They thus restricted the spectrum scaling law to be a function of seismic moment alone. Their calculated values are shown by the stars in figure 6. They show only slight curvature for $M_L < 5$ but seismic moment increasing ever more rapidly for larger magnitudes. This phenomenon is not observed in our Mammoth Lakes data, suggesting that assumption of constant stress drop independent of magnitude is not valid for this earthquakes sequence. However, given the small curvature in the theoretical values below

$M_L \approx 5$, together with the scatter in the observations, the data are consistent with constant stress drop for the smaller events, but suggest that the larger events are greater than 100 bars stress drop. This does not necessarily imply that the overall stress drop of the larger events is greater than 100 bars, but that the high frequency radiation giving rise to the observed M_L may be coming from the breaking of a high stress asperity. Alternatively, the moments from the near-in body-wave data may be giving an underestimate of the total seismic moment. Given *et al.* (1982) found from long period teleseismic data that the seismic moment of the 801481450 event was 1.1×10^{25}, a factor of 5 to 10 greater than the estimated moment from the near-in body-wave data.

Log $\mathbf{M_o}$ *vs.* $\mathbf{M_s}$ *relationship*: Equation (3) is the log M_o vs. M_s relationship derived from fitting the observed long-period surface wave seismograms recorded at regional distances, with synthetic surface wave seismograms computed for the Great Basin structure (Priestley and Brune, 1978; Taylor and Patton, 1984). We can compare equation (3) with similar relations established for the western United States. Wyss and Brune (1968) originally established a moment-local magnitude relationship for events less than magnitude 6 in the western U.S. Seismic moments were determined for 272 events which averaged over a wide range of tectonic regions (California, Nevada, Arizona, Utah and Baja California), and were found to be best fit by the curve given by the equation

$$\log M_o = 1.7 M_L + 15.1 \qquad (3 < M_L < 6) .$$

Using the M_s vs. M_L relationship given by Wyss and Brune (1968), this becomes in terms of $M_{S(G)}$ (the surface wave magnitude defined by Gutenberg (1945))

$$\log M_o = M_{S(G)} + 19.2 \qquad (3 < M_S < 6) .$$

This definition can be compared with the relationship derived directly from Gutenberg's (1945) definition of surface wave magnitude. According to that definition, a magnitude 6 earthquake produces a far-field displacement of $100\mu m$ at distance 22° for surface waves of period 20 seconds. In terms of moment Gutenburg's relationship becomes

$$\log M_o = M_{S(G)} + 19.3 .$$

Thus this point represents an average of the numerous observations on which the surface wave magnitude was based. As pointed out by Richter (1958), the scale was adjusted to agree with the local magnitude values of 6 to 7. Tucker and Brune (1977) determined M_o from spectral analysis of regionally recorded surface wave seismograms of the San Fernando aftershock sequence. They also used the Marshall - Basham definition (equation 1) to determine M_s for these events. The values they obtained were related by the equation

$$\log M_o = M_{s(MB)} + 19.3 ,$$

identical to the relationship postulated using the Gutenburg definition of surface wave magnitude. Comparing these various relationships between M_s and log M_o we conclude that the use of the Great Basin velocity and attenuation models (Priestley and Brune, 1978; Patton and Taylor, 1984) has increased the estimated moment of the events by 26% over that determined for the Gutenburg continental model.

6.0 Comparison of magnitude estimates with source spectra

We empirically determined formulae which relate the various types of magnitude estimates to the source spectrum by computing constants, C, which satisfy

$$\log \Omega = M - C$$

where Ω is the spectral amplitude normalized to 10 km at the frequency which the particular magnitude (i.e., M_L, m_b, M_s) was determined for some reference event. We chose the event at 801490516 as our reference since (1) both the source spectrum (from the close-in body-wave seismograms) and the magnitudes are well determined, (2) it is one of the smaller events and consequently the effects of fault finitness are minimized, (3) the frequencies at which m_b and M_s were determined are lower than the corner frequency, and (4) the event is shallow. The relationships which we obtained are:

$$\begin{aligned} \log\Omega &= M_L - 6.25 \ , \\ \log\Omega &= m_b - 5.95 \ , \\ \log\Omega &= M_s - 5.00 \ . \end{aligned} \qquad (5)$$

These values compare well with those found by recasting equations (3) and (4) in terms of the normalized amplitude Ω:

$$\log\Omega_o = M_s - 5.01 \ ,$$

$$\log\Omega_o = 1.2M_L - 6.93 \ .$$

Figure 7 shows the result of applying equation (5) to the magnitude estimates of four representative Mammoth Lakes events, which sample the range of depth and focal mechanism observed. In each plot the source spectrum determined from analysis of the close-in body-wave data is shown by the intersecting heavy lines. Error bars at the intersection indicate the scatter observed in Ω_o and f_c. The other points with error bars are the spectral amplitude values computed from the magnitude estimates. In each case the points are plotted at the mean frequency at which the individual magnitude estimates were made (M_s to the extreme left, M_L to the extreme right, and m_b between them). The error bars for these points also indicate the observed scatter. Figure 7a is for the reference event.

The 801481901 event (Fig. 7b) is similar in magnitude and depth to the reference event. Both events have a similar corner frequency. m_b fall below the corner frequency and on the flat portion of the spectrum; M_L falls above f_c and near the high frequency asymptote. The M_s value falls below the long-period level, but this is not significant considering the error bars on M_s and Ω_0.

The event 801471857 (Fig. 7c) is almost one magnitude unit larger than the reference event 801490516, but is of similar depth. The M_s value for this event falls close to the long-period level while both m_b and M_L are near the high frequency asympote. These latter two measurements were made at frequencies within the error bars f_c.

The event 801471224 (Fig. 7d) occurring at 12.5 km, is the deepest event studied, as well as one of the deepest events of the Mammoth Lakes sequence. For this event, M_L falls near the high frequency asymptote above the corner frequency, while m_b is at a frequency below the corner and approximately a factor of two beneath the long period level. The M_s error bars intersect the long period level although the average value is slightly below, possibly due to the increased source depth.

The corner frequencies of the 801471224 and 801471857 earthquakes are about a factor of 2 lower than 801481901 and 801490516, whereas the corresponding low frequency amplitudes are approximately 10 times higher. Thus the corner frequencies and moment are in agreement with the ω^{-2} model for events of approximately the same stress drop, but with source dimensions different by a factor of 2 (Aki, 1967; Brune, 1970, 1971). The above comparison confirms that the spectral shape inferred from distant measurements of magnitude (M_L, m_b, and M_s), is congruent with the spectral shape observed directly in the near field.

7.0 Comparison of the Mammoth Lakes results with published results for other regions of western North America

Stress drop may vary greatly according to the local tectonic conditions, and consequently a single ampliute parameter such as magnitude may be a poor representation of source conditions. The relationship between the seismic spectra and the parameters M_L, m_b and M_s derived for the Mammoth Lakes earthquakes does not necessarily apply to other regions.

Figure 8 compares the Mammoth Lakes data for moment estimates from near source data vs. M_s, with similar data for two published studies. The line $\log M_o = M_s + 19.4$ determined for the Mammoth Lakes data form the upper bound to the San Fernando aftershock observations of Tucker and Brune (1977). The two events from the Victoria, Baja California, Mexico swarm reported by Munguia and Brune (1984) lie above the line. Only events for which M_s was available could be included. Thus of the 43 events published by Tucker and Brune (1977) for the San Fernando aftershock sequence, Figure 8 only includes 12. The San Fernando events plot in a cloud to the right of the line defined by the Mammoth Lakes events, i.e., they have larger surface wave magnitudes for a given local body-wave moment than do events of the Mammoth Lakes aftershocks. Tucker and Brune found that there were other events which had body-wave

moments of similar magnitude to the events plotted in Figure 8 but for which surface waves at regional distances were too small to determine magnitude. These would presumably be more consistent with the trend of the Mammoth Lakes data. In contrast to the San Fernando events, the Victoria earthquakes fall above the line determined for the Mammoth Lakes events, i.e., they have smaller M_s than would be predicted from their body-wave spectra. Munguia and Brune (1984) have only determined M_s for two of the 43 events they have studied. These events have stress-drops of 930 and 570 bars.

The flat spectra observed for the Mammoth Lakes earthquakes from surface wave frequencies up to the spectral corner determined from the body wave data indicates that the majority of the Mammoth Lakes events studied are simple events. (1985). Tucker and Brune (1977) have suggested that the larger San Fernando earthquakes (those plotted in Figure 8) are partial stress-drop events, indicated by the fact that their surface wave magnitudes are larger than would be predicted based on the body-wave determination of M_o. This results from a rise in the spectrum at frequencies below the body-wave corner frequency. The larger events of the Victoria swarm are high stress drop events (Munguia and Brune, 1984) and have smaller surface wave magnitudes than would be predicted from their body wave spectra.

Hartzell and Brune (1979) have proposed an alternative model for explaining the difference observed in low and high frequency moments. They suggest that for these events, faulting initiates with a rupture over a relatively small area with a rapid dislocation rate. This first phase of rupture accounts for the smaller body-wave ($\approx$ 1 Hz) estimate of moment. If the rupture then continues to expand, but at a much slower dislocation rate, most of the energy will be at surface wave frequencies ($\approx$ 0.1 Hz) and thus account for the larger moment based on low frequency waves. In this case, Figure 8 should be looked at in a different light. Rather than M_s being *over* estimated for a given body-wave moment, the body-wave moment is underestimated for these event. Das and Kostrov (1985) have proposed a similar model to that of Hartzell and Brune (1979), in which such earthquakes consist of the fracture of a single asperity followed by slip on a finite fault. They find that for such a model, the seismic moment is $(R/r)^2$ larger and the corner frequency (r/R) lower (where r is the radius of the asperity, and R is the radius of the circular finite fault) than for a simple dislocation earthquake of the same magnitude. Since the asperity is a one-sided pulse, the envelope of its spectrum must have the same general form as the spectrum of the simple dislocation model; that is its corner frequency is determined by the pulse duration, its moment is determined by the area under the pulse, and it has a high frequency slope of -2. The major difference between the pulse due to an asperity fracture on a finite fault and a simple crack are the anomalously long pulse duration and the anomalously large seismic moment of the former compared to the latter.

We might now speculate as to why differences such as those observed between the Mammoth Lakes and San Fernando sequences arise. Lide and Ryall (1985) have shown that in the weeks following the main shocks of the Mammoth Lakes sequence (the time period for the events of this study), the majority of

the aftershocks were located in the granitic Sierrian block and were distributed in a triangular shaped zone above a steeply dipping plane on which the $M_L > 6$ main shocks possibly occurred. In comparison, a north-south cross-section (perpendicular to the surface rupture) of the San Fernando events analysed by Tucker and Brune (1977) lie in a granitic block above a zone dipping at 33° (Allen *et al.* (1973). In both the case of Mammoth Lakes and San Fernando, the events which exhibit anamolously large surface wave excitation compared to body wave moments are concentrated near the bottom along the dipping zones which may be considered as a through-going fault plane, while events which would be considered as full stress drop or simple dislocation events are concertrated in the shallow crust. These data suggest that partial stress drop events are more common on developed fault systems, whereas full stress drop events are more common in the surrounding country as it readjust to the stress field generated by the movement on the developed fault plane. Alternatively, the granitic blocks above both the Mammoth Lakes and San Fernando main fault plane may be so highly shattered that stress can only be consentrated on planes of limited extent. These "intrablock" earthqukes occurring in the granitic block above the through-going fault at Mammoth Lakes and San Fernando may be higher or full stress drop events whereas the "interblock" events occurring on the through going fault are partial stress drop events or fracture of asperities on finite faults.

8.0 Conclusions

In comparing short period versus long period excitation of events in the California region, Wyss and Brune (1971) found that events occurring to the north of Bishop, California indicated higher apparent stress than events along the San Andreas fault. In this study we have looked in detail at the relative excitation of low (0.05 - 0.125 Hz) and high (0.5 - 10.0 Hz) frequency seismic energy in this region from aftershocks of the 1980 Mammoth Lakes earthquake sequence.

We have compared the long period spectral level Ω_0 computed from body waves recorded on strong-motion and digital instruments at near epicentral distance ($\sim$ 1 Hz) with Ω_0 computed from regionally recorded surface waves ($\sim$ 0.1 Hz) and find these two values to agree within the observational error for almost all events of the Mammoth Lake sequence.

We have compared the body wave magnitude, m_b, and surface wave magnitude, M_s, and find that Mammoth Lakes events discriminate from nuclear explosions occurring at the Nevada Test Site approximately 150 km to the southeast.

Body-wave moment (M_o) has been related to local magnitude (M_L) by the relation

$$\log M_o = (1.2 \pm 0.05) + (17.49 \pm 0.19) \qquad (1 < M_L < 6)$$

and surface wave moment has been related to surface wave magnitude (M_s) by the relation

$$\log M_o = M_s + (19.40 \pm 0.06) \ .$$

M_L, m_b, and M_s for four representative events were compared with the spectral amplitude at their appropriate frequencies. The three shallow events (801471857, 801481901, and 801490516) and the one deep event (801471224) are consistent with the ω^{-2} model. The stress drops of these events are nearly similar but the source dimension of the 801471857 and 801471224 events are nearly twice that of the other two events, which explains their larger moment and greater surface wave excitation.

Acknowledgments

This research was partly suported by the Defense Advanced Research Projects Agency of the Department of Defense and monitored by the Air Force Office of Scientific Research under contract F49620-83-C-0012 (KP), and by the U.S. Geological Survey under Contract 14-08-001-21863 (KP), and by the National Science Foundation under grant CEE-8319620 (JB). R.J. Archuleta supplied digital seismograms collected by the U.S. Geological Survey, A.F. Shakal and B.E. Tucker supplied stong-motion records from the California Strong Motion Instrumentation Program, and J. Anderson supplied strong motion records from the data collected by the University of Southern California - California Institute of Technology. We thank D.E. Chavez for a careful review of the manuscript.

References

Abe, K., Seismic displacement and ground motion near a fault: The Saitama earthquake of September 21, 1931, *J. Geophys. Res.*, *79*, 4393-4399, 1974

Allen, C.R., T.C. Hanks, and J.H. Whitcomb, San Fernando earthquake: Seismological studies and their tectonic implications, in *San Fernando, California earthquake of February 9, 1971*, Vol. III, ed. L.M. Murphy, 13-21, 1973.

Anderson, J., Implication of attenuation for studies of the earthquake source, Fifth Ewing Symposium, May, 1985.

Aki, K., Scaling law of seismic spectrum, *J. Geophys. Res.*, *72*, 1217-1231, 1967.

Aruchuleta, R.J., E. Cranswick, C. Mueller, and P. Spudich, Source parameters of the 1980 Mammoth Lakes, California, earthquake sequence, *J. Geophys. Res.*, *87*, 4595-4607, 1982.

Archeleta, R., Downhold recordings of seismic radiation, Fifth Ewing Symposium, May, 1985.

Bailey, R. A., Dalymple, G. B. and Lanphere, M. A., Volcanism, structure and geochronology of Long Valley caldera, Mono County, California, *J. Geophys. Res.*, *81*, 725-744, 1976.

Barker, J.S., Modeling local structure using aftershocks of the May 1980

Mammoth Lakes earthquakes (abstract), *Earthquake Notes*, *55*, 21, 1985.

Bakun, W. H. Magnitudes and moments of duration, *Bull. Seism. Soc. Amer.*, *74*, 2335-2356, 1984.

Bakun, W.H., and A.G. Lindh, Local magnitudes, seismic moments, and coda duration for earthquakes near Oroville, California, *Bull. Seism. Soc. Am.*, *67*, 615-629, 1977.

Brune, J.N., Tectonic stress and the spectra of seismic shear waves from earthquakes, *J. Geophys. Res.*, *75*, 4997-5009, 1970.

Brune, J.N., Correction, *J. Geophys. Res.*, *76*, 5002, 1971.

Brune, J., A. Espinosa, and J. Oliver, Relative excitation of surface waves by earthquakes and underground explosions in the California-Nevada region, *J. Geophys. Res.*, *68*, 3501-3513, 1963.

Brune, J.N., T.L. Henyey, and R.F. Roy, Heat flow, stress, and rate of slip along the San Adreas fault, California, *J. Geophys. Res.*, *74*, 3821-3827, 1969.

Brune, J.N.,J. Fletcher, F. Vernon, L. Haar, T. Hanks, and J. Berger, Low stress-drop earthquakes in the light of new data from the Anza, California telemetered digital array, Fifth Ewing Symposium, May, 1985.

Chavez, D.E., and K.F. Priestley, M_L observations in the Great Basin and M_o versus M_L relationships for the 1980 Mammoth Lakes, California earthquake sequence, *Bull. Seism. Soc. of Am.*, *75*, 1583-1598, 1985.

Cranswick, E., R. Wetmiller, and J. Boatright, High-frequency observations and source parameters of microearthquakes recorded at hard-rock sites, submitted to *Bull. Seismo. Soc. Am.*

Given, J. W., Wallace T. C., and Kanamori, H., Teleseismic analysis of the 1980 Mammoth Lakes earthquake sequence, *Bull. Seismol. Soc. Am.*, *72*, 1093-1109, 1982.

Gutenburg, B., Amplitudes of surface waves and the magnitudes of shallow earthquakes, *Bull. Seism. Soc. Am.*, *35*, 3-12, 1945.

Hanks, T. C., and D. M. Boore, Moment-magnitude relations in theory and practice, *J. Geophy. Res.*, *89*, 6229-6235, 1984.

Hartzell, S., and J. Brune, Source parameters for the January 1975 Brawley-Imperial Valley earthquake swarm, *Pageoph*, *11*, 333-355, 1979.

Lachenbruck, A.H., and J.H. Sass, Heat flow and energetics of the San Andreas

fault zone, *J. Geophys. Res, 85*, 6185-6222, 1980.

Lide, C.S., and A.S. Ryall, Aftershock distribution related to the controversy regarding mechanisms of the May 1980, Mammoth Lakes, California, earthquakes, *J. Geophys. Res., 90*, 11,151-11,154, 1985.

Marshall, P.D., and P.W. Basham, Discrimination between earthquakes and underground explosions employing an improved M_s scale, *Geophys. J. R. astr. Soc.,28*,431-458, 1972.

Moslem, K., A. Amini, B. Kontic, J. Anderson, and T. Heaton, Accelerograms from the Mammoth Lakes, California earthquake sequence of May - July, 1980 recorded on a temporary array, Rpt No. CE 83-01, Univ. of Southern California, 1983.

Munguia, L., and J.N. Brune, High stress drop events in the Victoria, Baja California, Mexico, earthquake swarm of 1978 March, *Geophys. J. R. astr. Soc., 76*, 725-752, 1984.

Patton, H.J., and S.R. Taylor, Q Structure of the Basin and Range from Surface waves, *J. Geophys. Res., 89*, 6929-6940, 1984.

Peppin, W.A., What *do* spectral corner frequencies mean anyway? (abstract), *Earthquake Notes, 55*, 14, 1985.

Priestley, K.F., and J.N. Brune, Surface waves and the structure of the Great Basin of Nevada and western Utah, *J. Geophys. Res., 83*,2265-2272, 1978.

Priestley, K. F., J. N. Brune, and J. G. Anderson, Surface wave excitation and source mechanisms of the Mammoth Lakes earthquake sequence, *J. Geophys. Res., 90*, 11,177-11,185, 1985.

Richter, C.F., *Elementary seismology*, W.H. Freeman & Co., San Francisco, 768pp, 1958.

Thatcher, W., Regional variations of seismic source parameters in the northern Baja California area, *J. Geophys. Res., 77*, 1549-1565, 1972.

Thatcher, W., and T.C. Hanks, Source parameters of Southern California earthquakes, *J. Geophys. Res., 78*, 8547-8576, 1973.

Tucker, B.E., and J.N. Brune, Source mechanism and $m_b - M_s$ analysis of aftershocks of the San Fernando earthquake, *Geophys. J. R. astr. Soc., 49*, 371-426, 1977.

Turpin, C.D., Strong-motion instrumentation program results from the May, 1980, Mammoth Lakes, California earthquake sequence, *Calif. Div. Mines*

Geol. Spec. Rep., *150*, 75-90, 1980.

Vetter, U.R., Focal mechanisms and crustal stress patterns in western Nevada and eastern California, *Annales Geophysicae*, *2*, 699-710, 1984.

Wyss, M., and J.N. Brune, Seismic moment, stress, and source dimensions for earthquakes in the California - Nevada region, *J. Geophys. Res.*, *73*, 4681-4694, 1968.

Wyss, M., and J. Brune, Regional variations of source properties in Southern California estimated from the ratio of short- to long-period amplitudes, *Bull. Seism. Soc. Am.*, *61*, 1153-1167, 1971.

STATION PARAMETERS			
STATION ID.	NORTH LAT.	WEST LONG.	TYPE
CBR	37.6790	118.8250	USGS digital
CON	37.5900	118.8530	USGS digital
DMP	37.7380	118.8260	USGS digital
FIS	37.6140	118.8300	USGS digital
HCF	37.6420	118.8500	USGS digital
LAK	37.6400	118.7280	USGS digital
LAR	37.6230	118.8900	USGS digital
LKM	37.6970	118.9360	USGS digital
MGE	37.5610	118.7870	USGS digital
PS1	37.5410	118.5890	USGS digital
ROC	37.4960	118.7190	USGS digital
TOM	37.5510	118.6720	USGS digital
TWL	37.6160	119.0060	USGS digital
bn	37.3700	118.3950	CDMG SMA-1
bs	37.4810	118.6020	CDMG SMA-1
cbr	37.6780	118.8100	USC/CIT SMA-1
cc	37.6140	118.8310	CDMG SMA-1
cl	37.5610	118.7430	USC/CIT SMA-1
cvl	37.5950	118.8500	USC/CIT SMA-1
gnc	37.6200	118.8200	USC/CIT SMA-1
lvf	37.5680	118.7490	USC/CIT SMA-1
mci	37.5860	118.7820	USC/CIT SMA-1
mgc	37.5530	118.7940	USC/CIT SMA-1
ALQ	34.9425	[06.4575	WWSSN LP
BRK	37.8733	122.2600	WWSSN LP
COR	44.5857	123.3032	WWSSN LP
DUG	40.1950	112.8133	WWSSN LP
GOL	39.7003	105.3711	WWSSN LP
GSC	35.3017	116.8046	WWSSN LP
JCT	30.4794	99.8022	WWSSN LP
LON	46.7500	121.8100	WWSSN LP
MSO	46.8292	113.9406	WWSSN LP
PAS	34.1483	118.1717	CIT LP
TUC	32.3097	110.7822	WWSSN LP

Thickness	P-wace speed	Q_α	S-wave speed	Q_β
2.5	3.55	56	2.05	25
22.5	6.10	386	3.56	172
10.0	6.70	233	3.85	103
9.0	7.80	112	4.50	50
10.0	7.85	112	4.52	50
10.0	7.90	112	4.54	50
40.0	7.70	72	4.12	32
16.0	7.70	210	4.06	93
20.0	7.70	240	4.05	106

NO.	DAY	TIME	LAT.	LONG.	DEPTH	M_l‡	m_b	M_s	BODY WAVE				SURFACE WAVE			
									$\log\Omega_o$ (cm-sec)	ERR	f_c (Hz)	ERR	$\log\Omega_o$ (cm-sec)	ERR	T (sec)	ERR
1	146	1633	37.62	118.81		6.06	5.85	5.54					0.5288	1.27	15.0	2.74
2	146	1649				6.02	5.50	4.72					-0.3017		10.0•	
3	146	1708					4.30									
4	146	1748	37.51	118.93			3.90	4.00					-1.1148		12.0	
5	146	1834					4.10									
6	146	1944	37.33	118.83	9.9	6.08	5.30	5.61					0.2656	1.73	17.8	1.79
7	146	2023				4.49										
8	146	2035	37.58	118.83	8.4	5.88	4.90	5.19	-0.4842		8.88		-0.0732	2.01	12.0	1.55
9	146	2036				4.10										
10	146	2059					4.40	3.82					-0.3017		11.0	
11	147	0057					4.07	3.58					-1.5768	1.38	10.4	1.22
12	147	0119					4.27	3.63					-1.3743	1.42	11.0	1.25
13	147	0436	37.58	118.80	0.8	4.34		2.83	-2.8097•				-2.1852	2.62	10.3	2.26
14	147	0556					4.00	3.02					-2.0007	1.45	9.9	1.19
15	147	1020	37.60	118.78	4.6	4.42		3.25	-1.1244•				-1.7624	1.24	9.5	2.18
16	147	1039						3.10					-1.9243		10.0	
17	147	1104						2.11					-2.9105		8.0	
18	147	1224	37.53	118.87	12.4	5.67		4.18	-0.3648	1.27	0.83	1.26	-0.8539	1.37	10.9	1.17
19	147	1357				4.69										
20	147	1437						2.79					-2.2115	1.25	10.3	1.60
21	147	1620						3.84					-1.1852	2.06	11.0	1.30
22	147	1857	37.56	118.83	0.2	5.79			-0.3858	2.07	1.05	1.61	-0.6675	1.33	9.8	1.56
23	148	0054				5.35										
24	148	0201	37.50	118.90	6.0	4.12		2.31	-2.0618				-2.7081		8.0	
25	148	0343				3.94										

- 2 -

NO.	DAY	TIME	LAT.	LONG.	DEPTH	M_l‡	m_b	M_s	BODY WAVE $\log\Omega_o$ (cm-sec)	ERR	f_c (Hz)	ERR	SURFACE WAVE $\log\Omega_o$ (cm-sec)	ERR	T (sec)	ERR
26	148	0407				3.88										
27	148	0536				4.47										
28	148	0646						2.79					-2.2396		10.0	
29	148	0909				4.06										
30	148	1327					3.90	2.79					-2.2396	1.39	10.0	1.58
31	148	1450	37.45	118.79	11.7	6.28	5.48	5.45					0.4417	1.18	12.5	2.50
32	148	1610				4.65										
33	148	1709				4.11										
34	148	1901	37.58	118.77	0.1	4.85	4.33	3.43	-1.3246	2.97	3.24	1.69	-1.5832	1.88	10.0	1.12
35	148	1959				4.81										
36	148	2341	37.60	118.90	9.0	3.92		2.30	-2.6524	4.50	7.38	1.58	-2.7167	1.63	9.0	2.12
37	148	2357	37.53	118.88	0.1	4.04		2.41	-2.5277	2.05	3.99	1.30	-2.6028		11.0	
38	149	0402	37.60	118.79	3.0	4.16		2.64	-1.77[illegible]3	3.74	4.77	1.77	-2.3743		12.0	
39	149	0422				4.18			-2.1391†	1.73	1.44	1.38				
40	149	0516	37.58	118.89	2.5	4.81	4.25	3.69	-1.3632	1.97	2.72	1.23	-1.3365	1.88	10.3	1.07
41	149	0548					3.95	3.36					-1.6598	2.02	10.1	1.12
42	149	0613				3.92			-2.7190†	2.31	3.56	2.10				
43	149	1154	37.47	118.81	9.7	4.42			-1.6003†	2.91	1.36	1.80				
44	150	0418				4.09			-2.1226†	2.00	3.96	1.21				
45	150	0555				4.43										
46	150	1518				3.30			-2.8665†	1.89	4.49	1.52				
47	150	1656				3.76										
48	150	1721				4.21			-2.1169†	2.53	2.34	1.50				
49	150	1855				3.44			-2.6364†	1.67	3.22	2.18				
50	151	0119				3.12			-3.3316†	2.08	6.64	1.31				

- 3 -

NO.	DAY	TIME	LAT.	LONG.	DEPTH	M_L‡	m_b	M_s	BODY WAVE $\log\Omega_o$ (cm-sec)	ERR	f_c (Hz)	ERR	SURFACE WAVE $\log\Omega_o$ (cm-sec)	ERR	T (sec)	ERR
51	151	0829				3.21			-3.0052†	1.61	4.62	2.07				
52	151	0752				3.08			-3.5817†	1.34	9.63	1.26				
53	151	1201				4.58										
54	151	1949				3.92			-2.4881†	1.95	3.99	1.98				
55	152	0058	37.54	118.81	0.4	4.46		2.72	-2.3528	2.24	5.29	2.08	-2.3017	1.50	10.2	1.42
56	152	1011	37.58	118.82	3.3	4.35		2.95	-1.6517	3.61	3.91	1.67	-2.0732		11.0	
57	152	1313				3.51			-2.9281†	2.18	6.07	1.67				
58	152	1343				3.24			-2.9469†	1.78	3.08	1.31				
59	152	1516	37.60	118.78	5.8	4.95		3.65	-0.7908	2.50	4.00	1.93	-1.3743	1.50	11.0	1.17
60	152	1520	37.60	118.78	6.1	4.16		2.86	-2.6636	1.87	6.17	1.58	-2.1604		12.5	
61	152	1530				4.15										
62	152	1535	37.60	118.78	4.8	3.48		2.00	-2.8946†	2.53	2.31	1.56	-3.0177		9.0	
63	152	2014				3.39			-3.0835†	2.75	6.61	1.05				
64	152	2315	37.61	118.83	12.9	4.05		2.52					-2.4966	1.81	10.0	2.24
65	153	0317				4.38		1.74					-3.2695		8.0	
66	153	0647	37.47	118.83	7.4	5.08		2.86	-0.8065	3.18	8.52	1.30	-2.1604	1.23	10.0	1.41
67	153	1220				3.45			-2.7328†	2.08	4.02	1.25				
68	153	1727				3.84			-2.4112†	1.78	4.11	1.51				
69	153	2230				3.55			-2.2596†	1.88	1.90	1.70				
70	153	2334				3.22										
71	154	1819				3.69			-2.9830†	1.59	7.94	1.56				
72	154	2034				3.99			-2.1675†	1.80	2.39	1.50				
73	155	0235				3.37			-3.0665†	2.03	5.23	1.59				
74	156	2103				2.65			-3.5986†	1.63	4.77	1.41				
75	157	1540				2.92			-3.9872†	1.98	7.16	1.70				

- 4 -

NO.	DAY	TIME	LAT.	LONG.	DEPTH	M_L‡	m_b	M_s	BODY WAVE				SURFACE WAVE			
									$\log\Omega_o$ (cm-sec)	ERR	f_c (Hz)	ERR	$\log\Omega_o$ (cm-sec)	ERR	T (sec)	ERR
76	157	1941	37.56	118.87	7.4	4.36	-.--	2.44					-2.5706	2.24	9.3	1.76
77	157	2133				1.71			-4.9957†	1.22	6.50	1.78				
78	157	2157				1.96			-4.5735†	2.60	7.64	1.20				
79	157	2301				2.01			-4.7932†	1.04	8.99	1.32				
80	157	2341				3.10			-3.0825†		5.41					
81	158	0451				2.09			-4.0747†	1.00	4.06	1.00				
82	158	0952				3.06			-3.8234†	1.90	9.66	2.77				
83	158	1333				2.88			-2.5784†	1.76	4.98	1.47				
84	158	1626				3.50			-2.9914†	3.24	4.11	2.25				
85	158	1716				3.53			-2.8327†	1.68	3.33	1.77				
86	159	2317				4.04			-2.0835†	2.24	2.34	1.42				
87	160	0625				3.99			-2.5572†	1.83	5.29	1.32				
88	160	2322	37.60	118.90		4.12		2.31	-2.5364	3.32	4.39	1.92	-2.7081		9.0	
89	163	0440	37.55	118.88	8.4	4.48		3.05	-2.0822	3.53	3.98	2.44	-2.0355	1.99	10.9	1.17
90	163	1710	37.63	118.86	5.1	3.73			-2.5670†	1.89	3.92	1.30				
91	164	0529				3.96										
92	164	1022				3.22			-2.8570†	2.40	4.93	2.26				
93	165	1213				3.22			-3.5031†	2.20	8.51	1.59				
94	180	0057							-1.6289•				-2.4067		9.0	
94	180	0058	37.58	118.81	1.3	4.58		2.83	-1.2467	3.32	9.92	1.92	-2.1852	1.29	8.0	1.63
95	187	1158	37.58	118.80	7.2	4.33		3.01					-2.0007	1.55	10.7	1.24

† Archuleta *et al.*, (1982)

• Priestley *et al.*, (1985)

‡ Chavez and Priestley, (1985)

Figure Captions

Figure 1. Location maps showing the events studied and the stations from which seismograms were analysed. In the lower right-hand map, the solid circles denote locations of events, triangles denote location of strong-motion accelerographs, and digital seismographs. The upper left-hand map shows the locations of the long-period seismographs used for the surface wave analysisd (denoted by squares), and Canadian network short-period stations used to determine body-wave magnitude (denoted by stars).

Figure 2. Representative analysis of a short-period digital seismogram. The bracket over the seismogram indicates the S-wave window; the heavy solid lines indicate the long-period and high-frequency asymptotes fit to the spectrum.

Figure 3. Represe· ative fit of computed surface wave seismogram to the observed seismogram for the WWSSN station at Dugway, Utah (DUG).

Figure 4. Comparison of the body-wave and surface-wave long period spectral levels for the events studied. The line is for reference and has unit slope and zero intercept.

Figure 5. Comparison of the body-wave and surface-wave magnitude. The solid dots (earthquakes) and pluses (explosions) are taken from Marshall and Basham (1972); the solid squares are the Mammoth Lakes events from this study. All body-wave magnitudes are from measurements from Canadian Network seismographs. Surface wave magnitudes taken from Marshall and Basham are from Canadian Network long-period seismographs; surface wave magnitudes for the Mammoth Lakes earthquakes are from long-period WWSSN stations in the western United States.

Figure 6. *Log* M_o vs. M_L for earthquakes in the 1980 Mammoth Lakes earthquake sequence. One standard deviation of the mean error bars are given for events with multiple recordings. The line is from equation (4), and the stars are the theoretical values from Hanks and Boore (1984). (After Chavez and Priestley, 1985.)

Figure 7. Comparison of the source spectra and the amplitudes determined from M_L, m_b, M_s at their appropriate frequencies. The error bars assigned to each spectral value represent the estimated standard error of the measurement: (a) 801490516 (event #40), (b) 801481901 (event #34), (c)

801471857 (event #22), (d) 801471224 (event #18).

Figure 8. Comparison of $\log M_o$ vs. M_s for Mammoth Lakes aftershock data, and $\log M_o$ vs. M_s for several other western North American earthquake sequences. The line plotted is from equation (3).

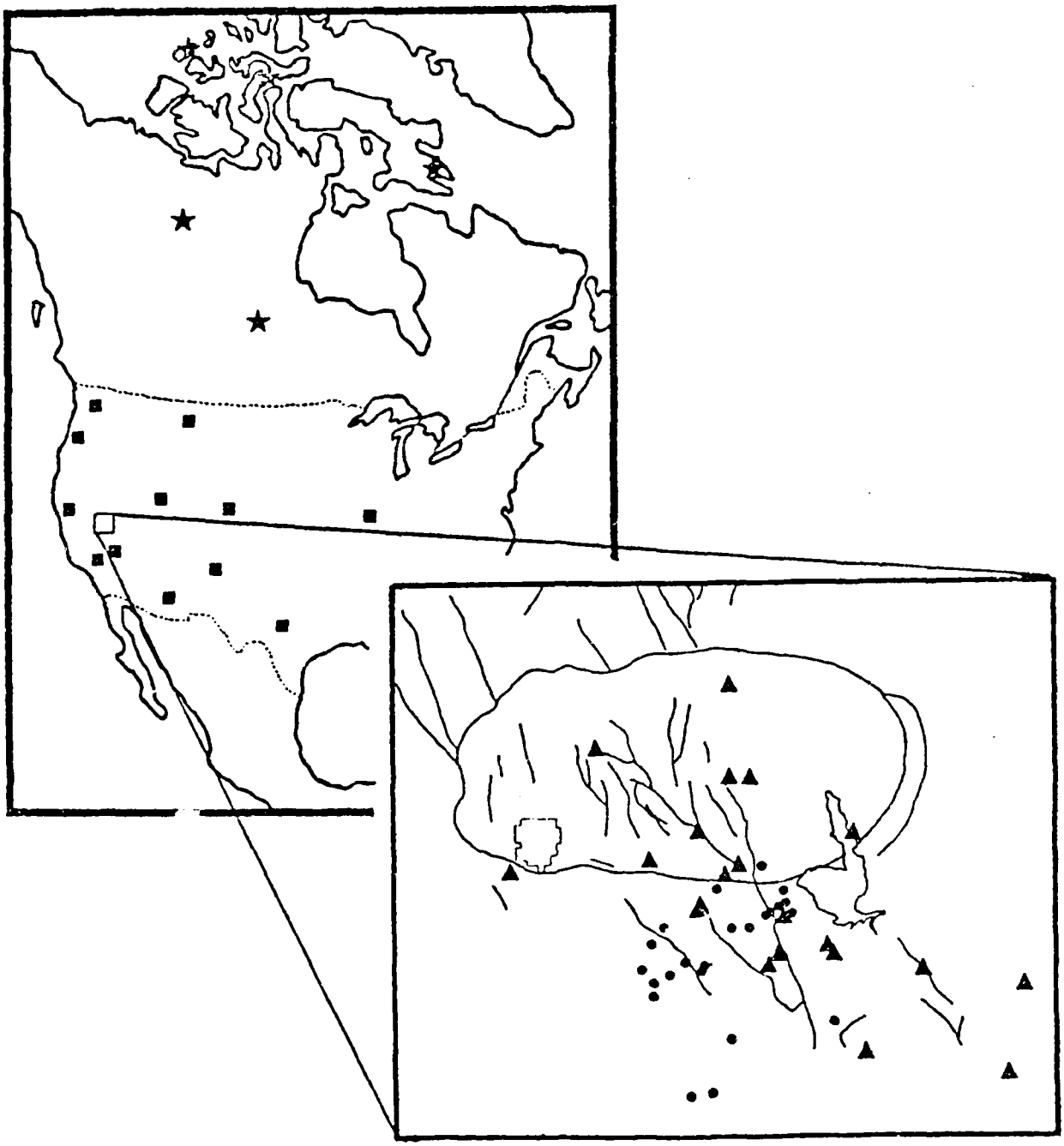

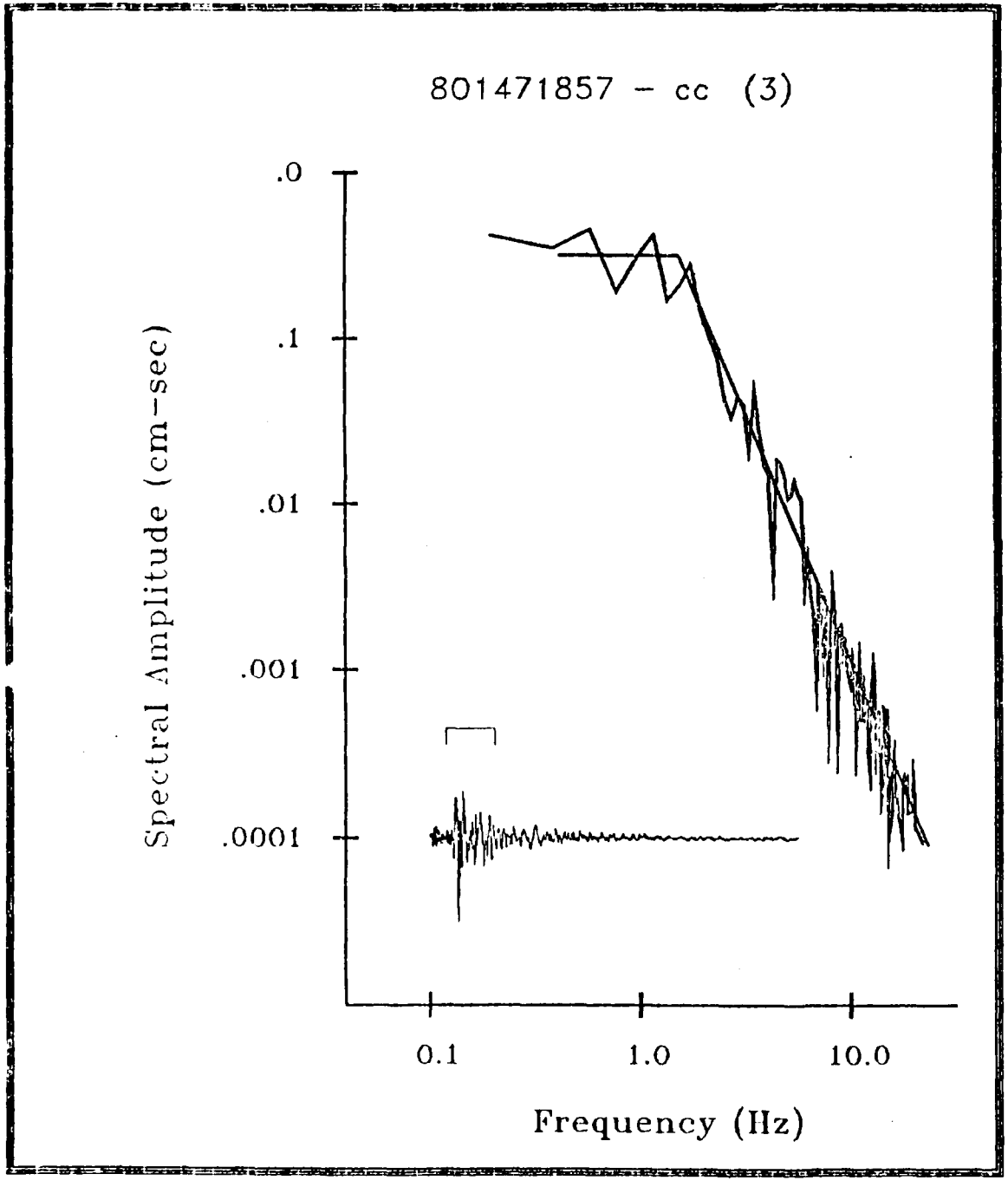
801471857 - cc (3)
.0
.1
.01
.001
.0001
Spectral Amplitude (cm-sec)
0.1
1.0
10.0
Frequency (Hz)

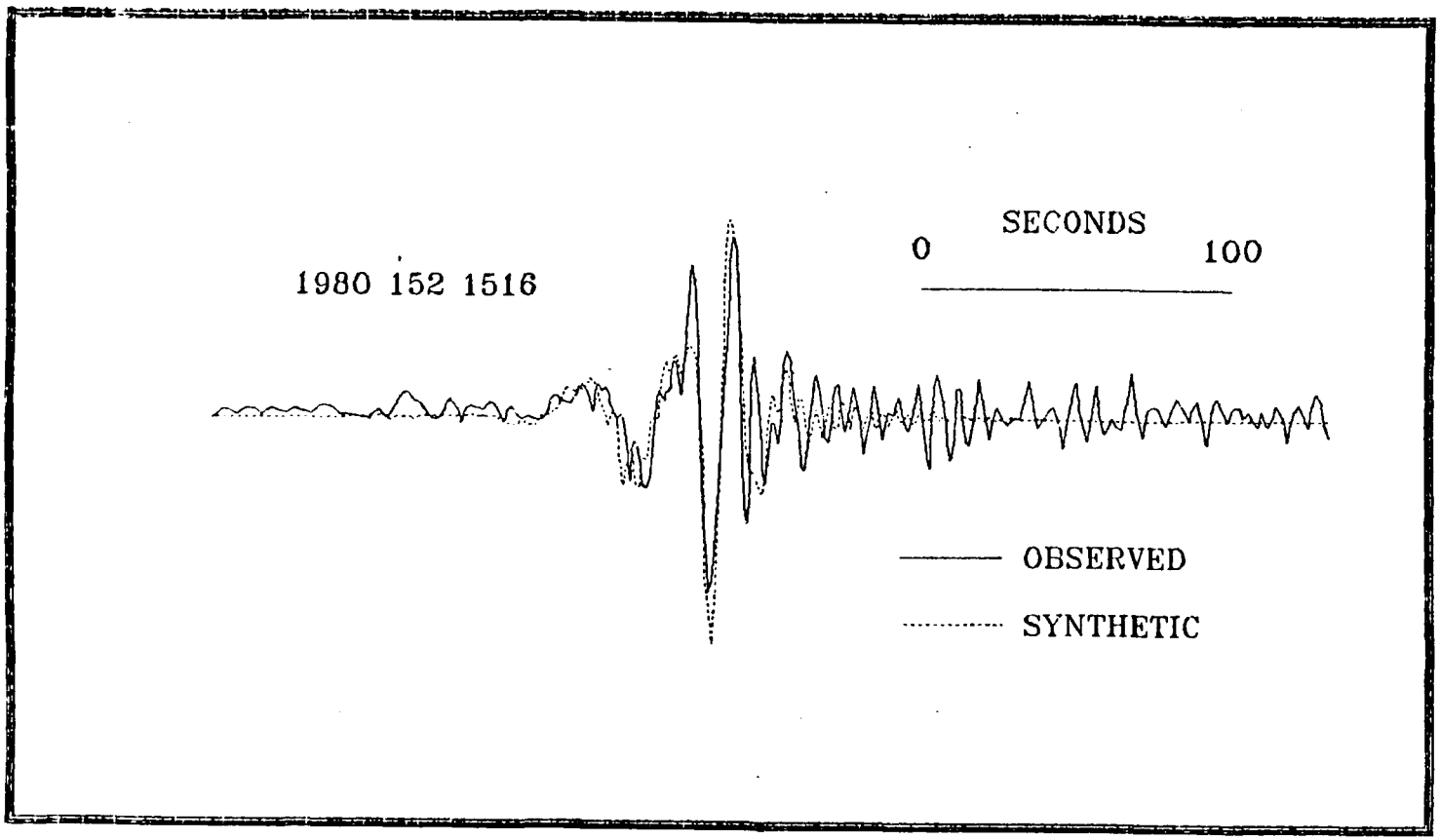
1980 152 1516
SECONDS
0
100
OBSERVED
SYNTHETIC

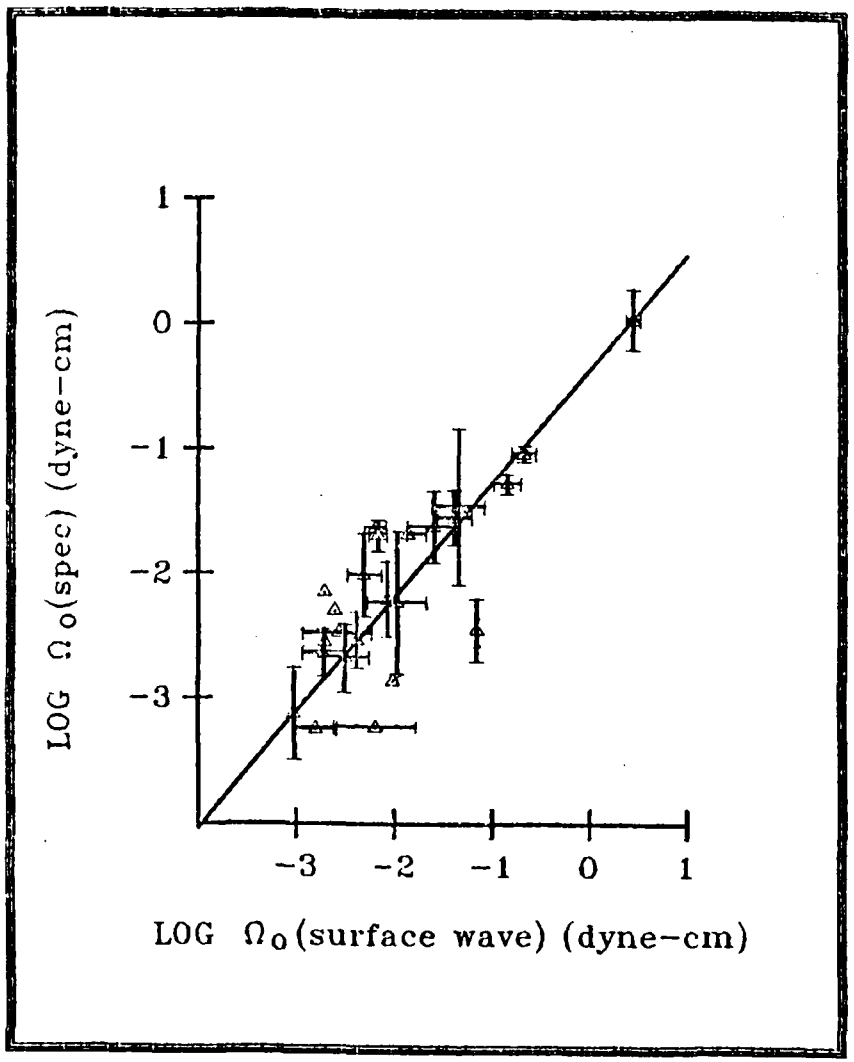
1
0
-1
-2
-3
LOG Ω o(spec) (dyne-cm)
-3
-2
-1
0
1
LOG Ω o(surface wave) (dyne-cm)

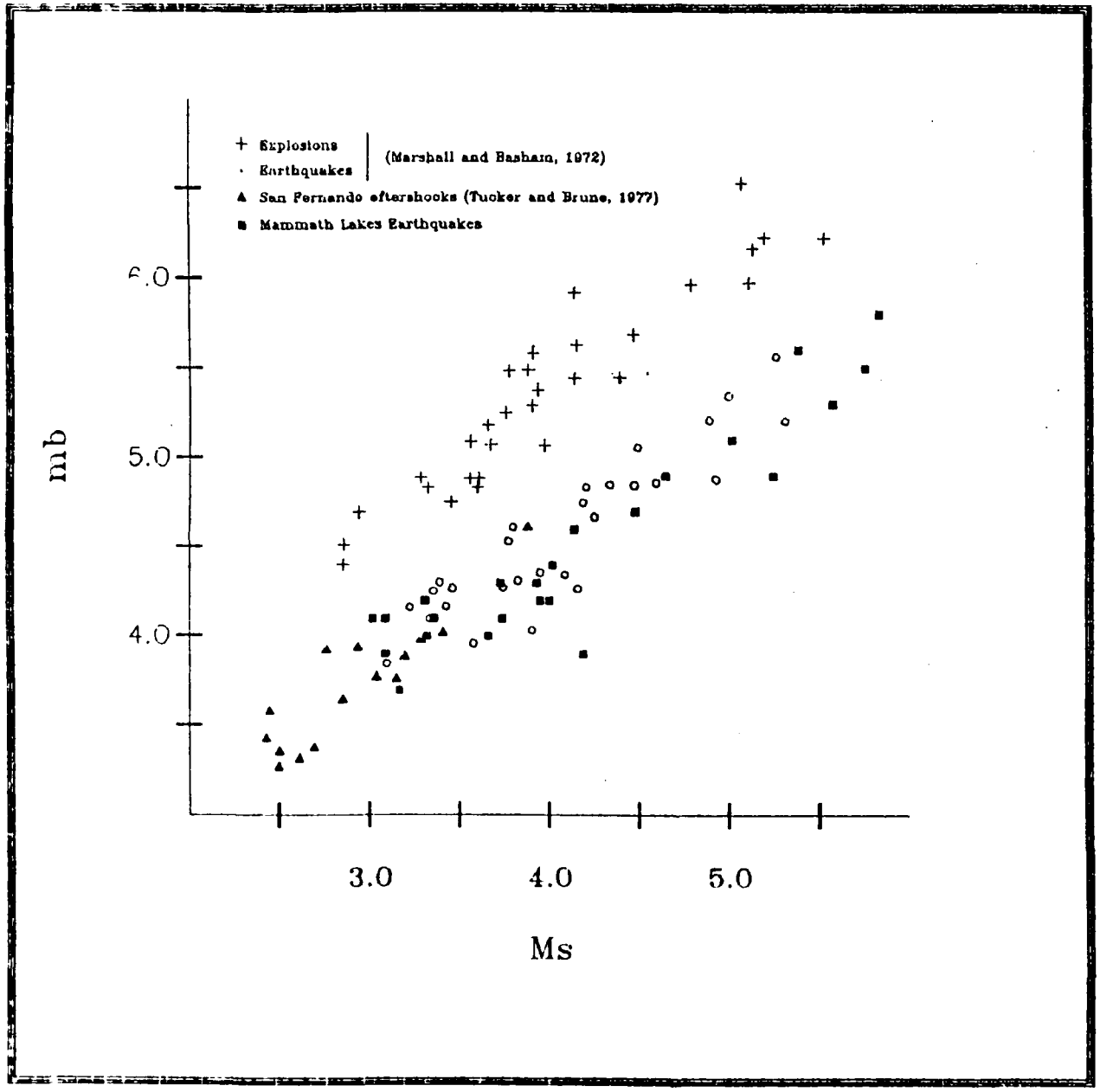
+ Explosions
· Earthquakes
(Marshall and Basham, 1972)
▲ San Fernando aftershocks (Tucker and Brune, 1977)
■ Mammath Lakes Earthquakes
6.0
5.0
4.0
mb
3.0
4.0
5.0
Ms

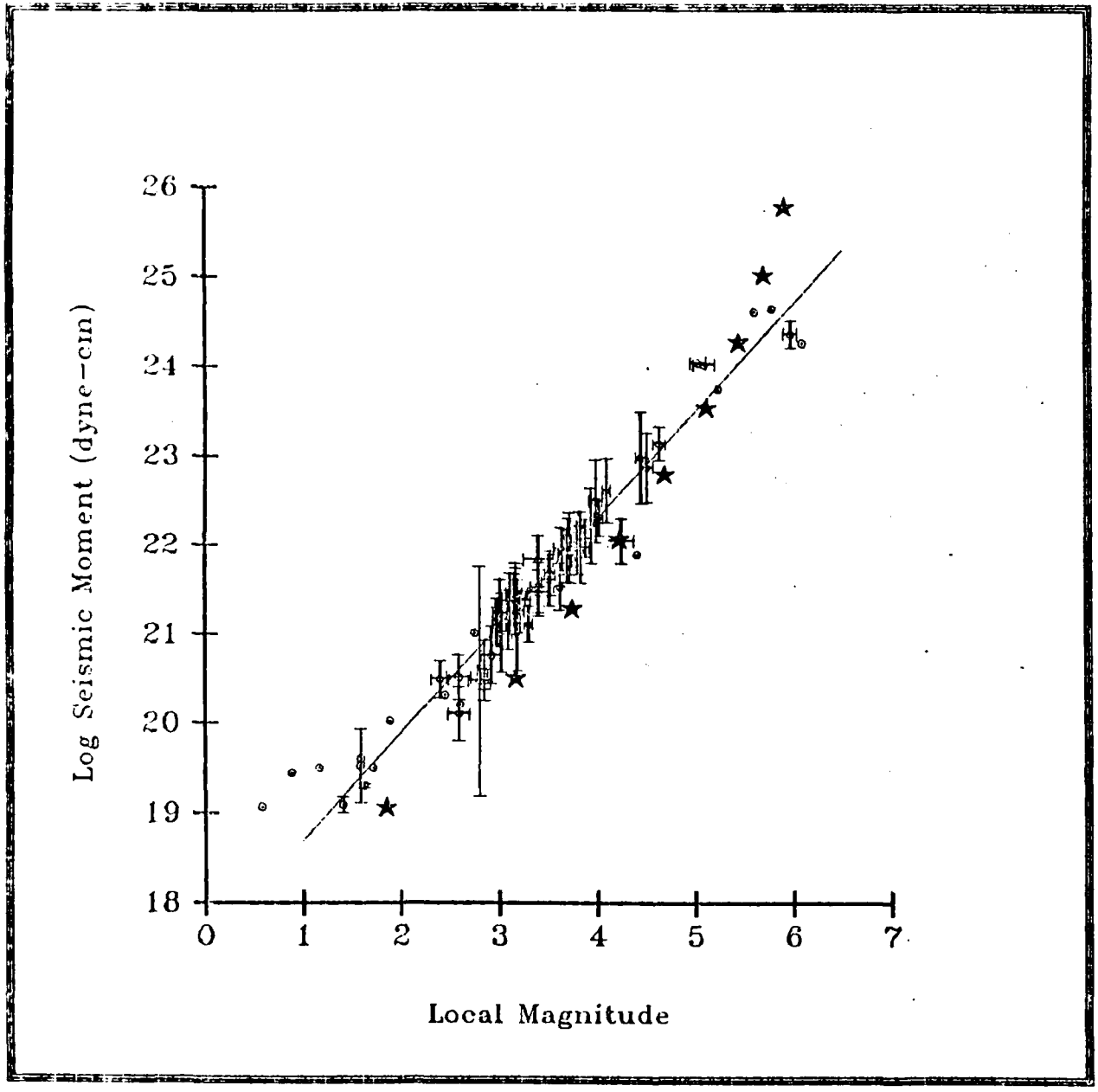
Log Seismic Moment (dyne-cm)
26
25
24
23
22
21
20
19
18
0
1
2
3
4
5
6
7
Local Magnitude

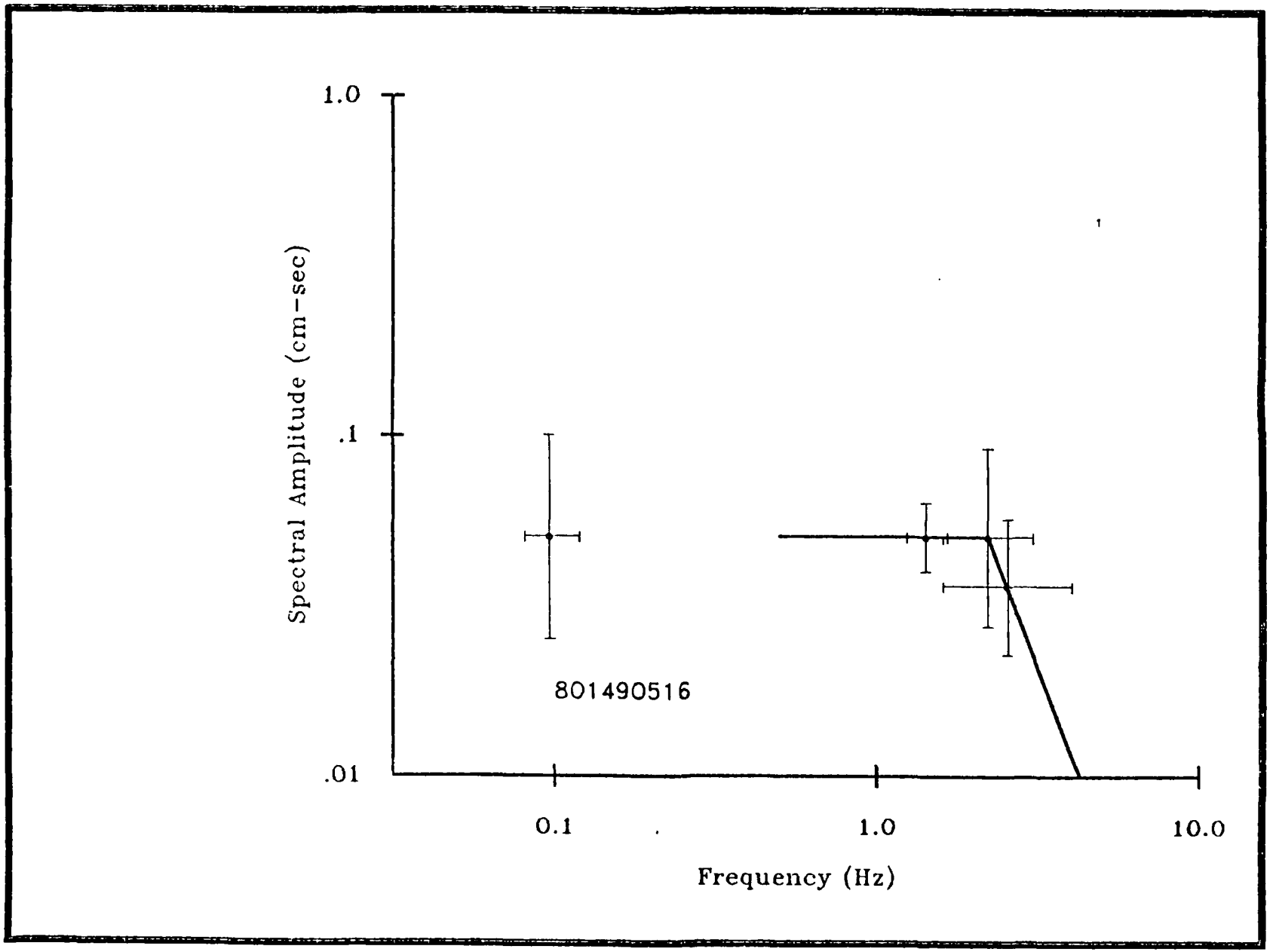
1.0
.1
.01
Spectral Amplitude (cm-sec)
801490516
0.1
1.0
10.0
Frequency (Hz)

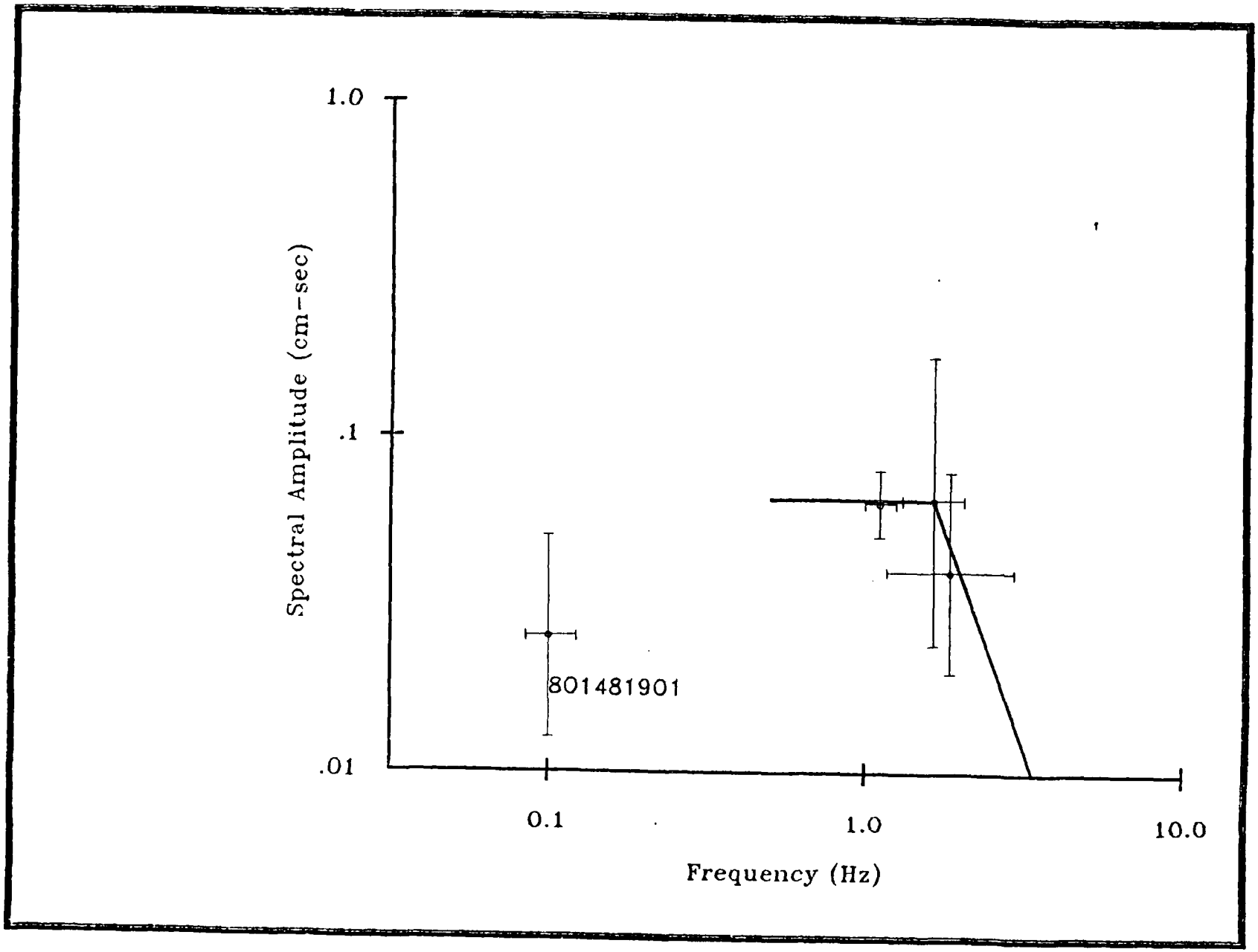
1.0
.1
.01
Spectral Amplitude (cm-sec)
801481901
0.1
1.0
10.0
Frequency (Hz)

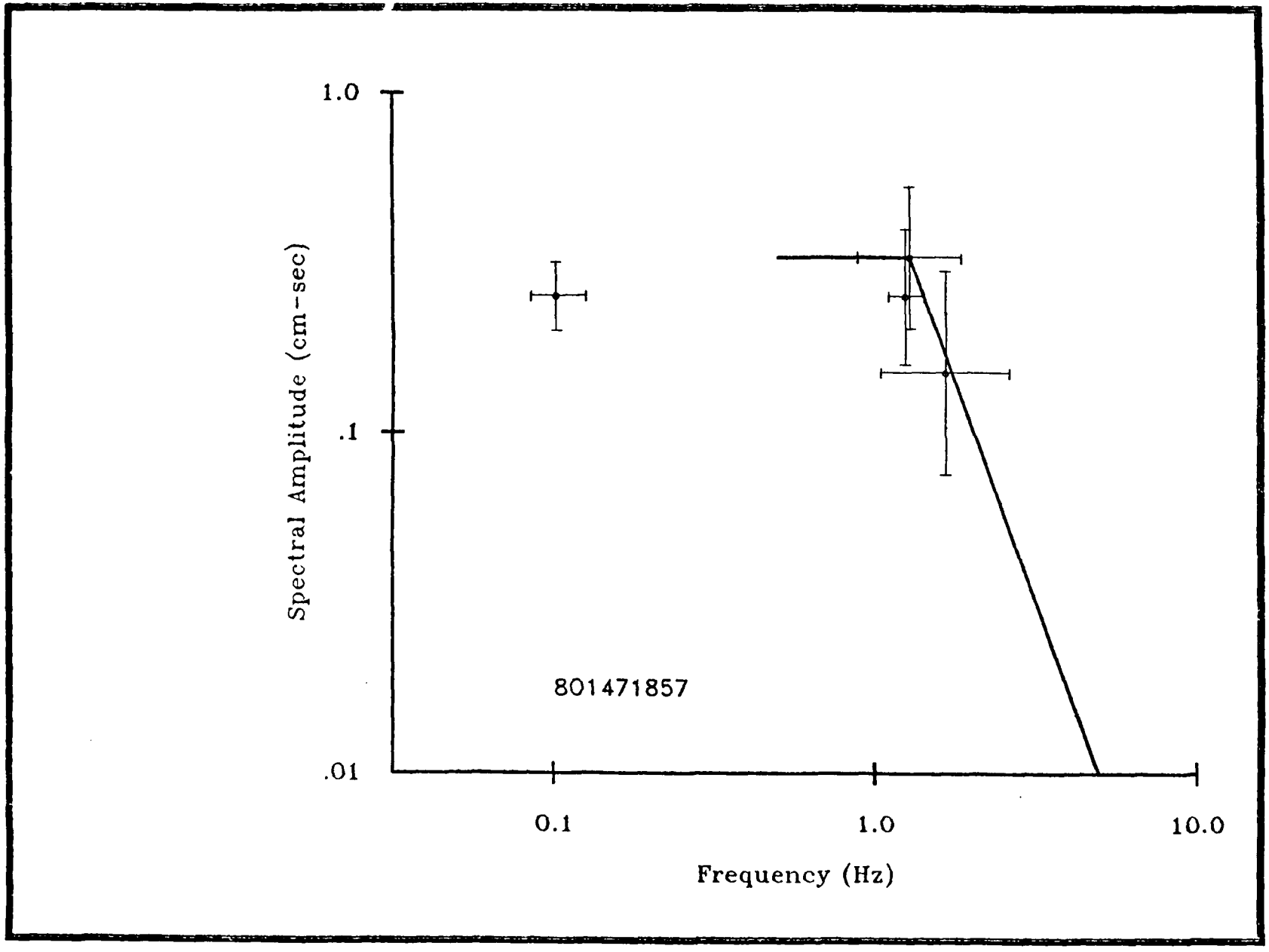
1.0
.1
.01
Spectral Amplitude (cm-sec)
801471857
0.1
1.0
10.0
Frequency (Hz)

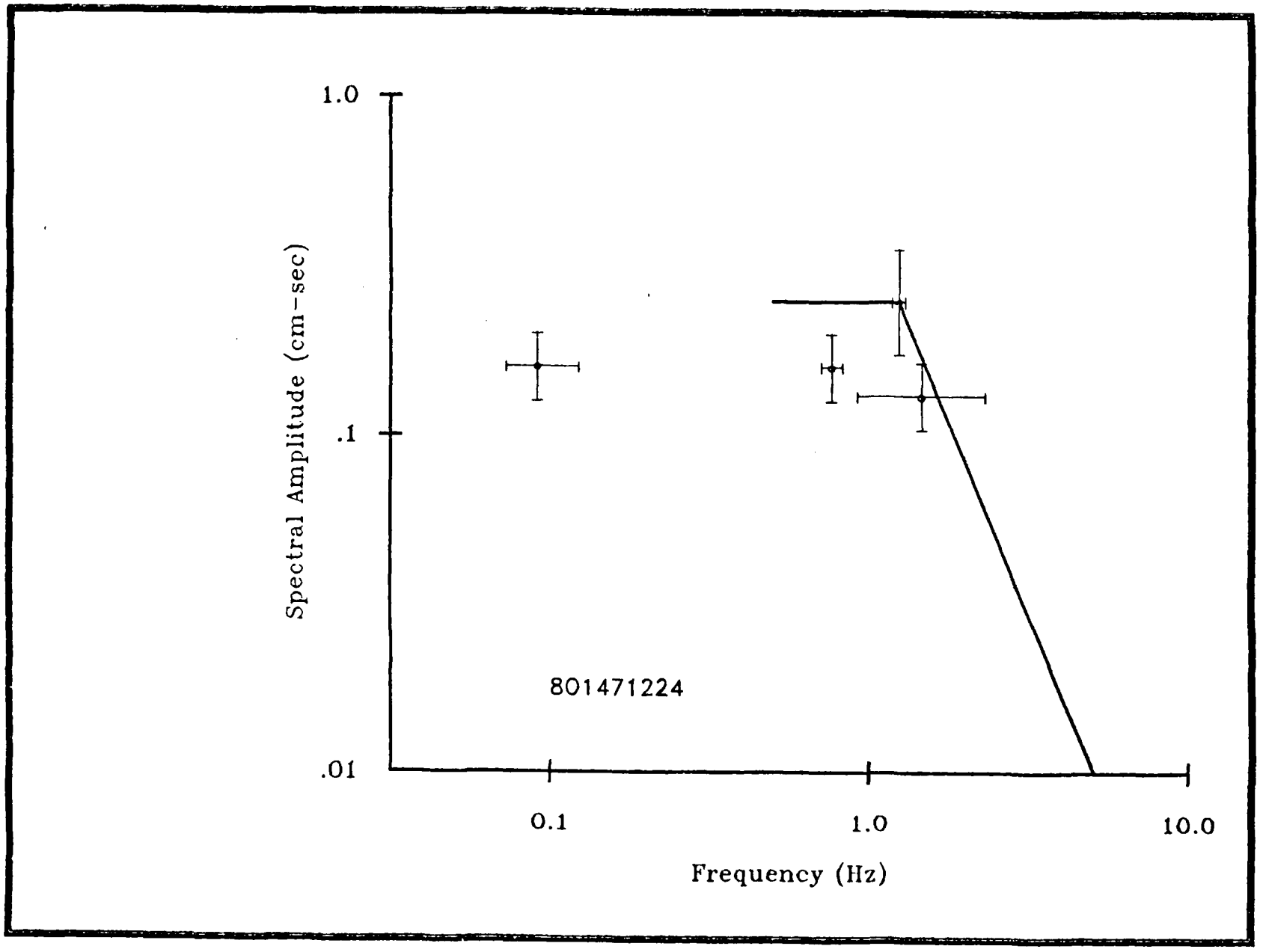
1.0
.1
.01
Spectral Amplitude (cm-sec)
801471224
0.1
1.0
10.0
Frequency (Hz)

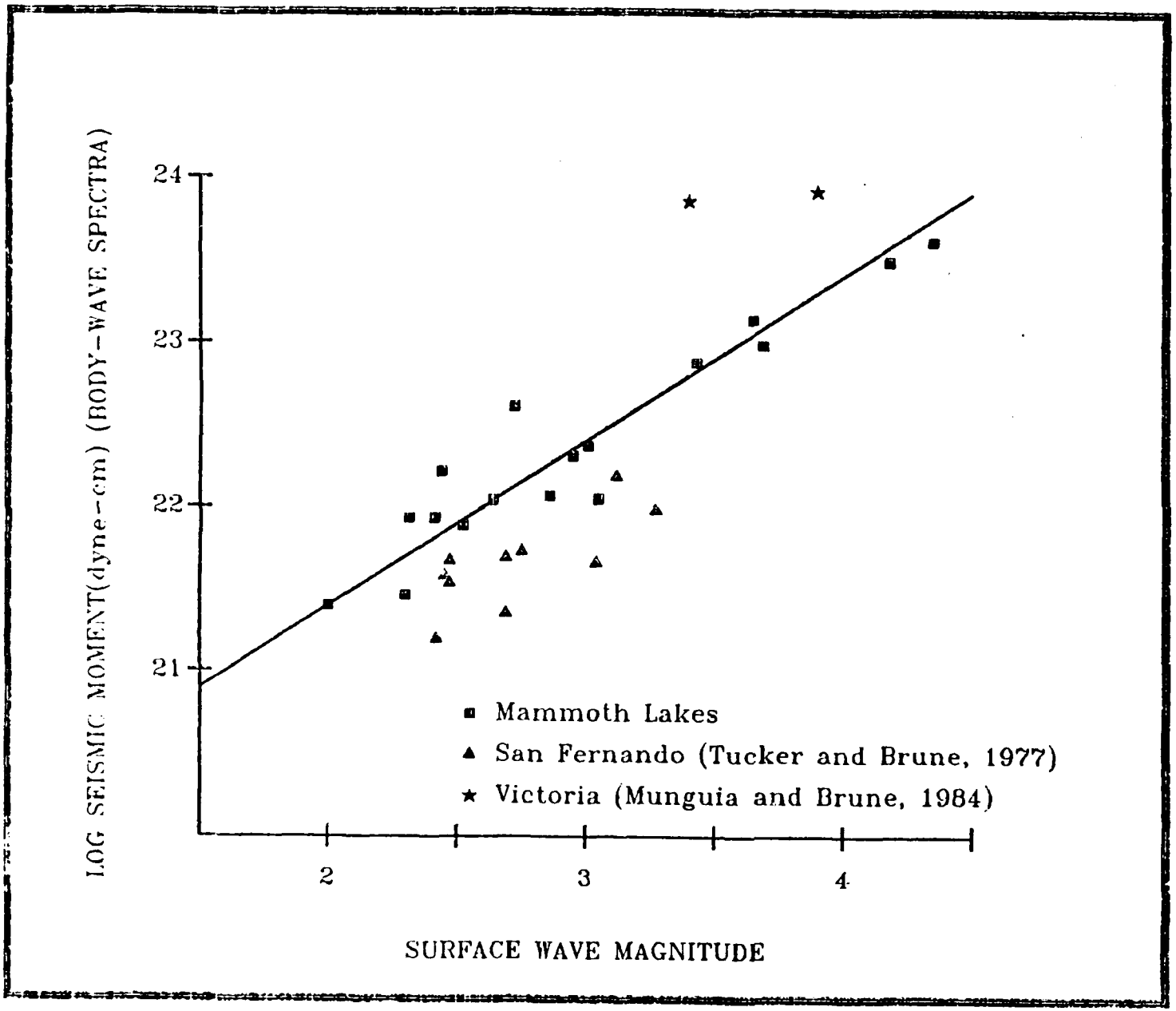
LOG SEISMIC MOMENT(dyne-cm) (BODY-WAVE SPECTRA)
24
23
22
21
2
3
4
SURFACE WAVE MAGNITUDE
Mammoth Lakes
San Fernando (Tucker and Brune, 1977)
Victoria (Munguia and Brune, 1984)

AVERAGE L_g ATTENUATION IN THE GREAT BASIN

David E. Chavez and Keith F. Priestley
Seismological Laboratory, Mackay School of Mines
University of Nevada, Reno, NV 89557

ABSTRACT

We have determined an average, frequency dependent, apparent L_g $Q(f)$ function for Great Basin paths, by measuring the spatial decay of spectral amplitudes. We find that

$$Q(f) = 212f^{0.53} \quad (0.2\,Hz \leq f \leq 4.0\,Hz).$$

This result is in excellent agreement with Singh and Herrmann's (1983) Q model for this same area, based on observations of coda decay.

Introduction

L_g waves are short-period surface waves which propagate in the continental crust with typical group speeds of 3.0 to 3.5 km/sec (Press and Ewing, 1952; Bath, 1954). Knopoff *et al.* (1973) have identified the transverse component of L_g with higher mode Love waves while Panza and Calcagnille (1975) have shown that the vertical-radial component can be identified with higher mode Rayleigh waves.

Currently, most estimates of seismic moment for Great Basin earthquakes have been made using body waves recorded by local networks or fundamental mode surface waves recorded at regional distances. Numerous moderate size earthquakes ($3<M_L<4$) occur in the Great Basin outside of any local network and are too small to be seen at teleseismic distances. They are, however, recorded by stations at regional distances where L_g is almost always a clearly recognized arrival. Street *et al.* (1975) and Herrmann and Kijko (1983) determined empirical formulas which relate the long period asymptote of the L_g spectrum to the seismic moment. They used data from the central and eastern United States where the low attenuation allowed them to neglect any Q effects. There is substantially greater attenuation in the Great Basin however, so a frequency dependent Q model must be obtained in order to correct regional L_g recordings prior to determining the seismic moment.

Nuttli (1973, 1980, 1981, 1984) has used L_g to estimate m_b for earthquakes and explosions, estimate apparent crustal attenuation, discriminate between small earthquakes and explosions, and estimate the yield of nuclear explosions.

In the latter case, he found that if L_g amplitudes are to be used to estimate explosion yields to an accuracy of 30%, then average values of spatial attenuation over large areas (such as the western U.S.) are inadequate. Instead, smaller scale regional estimates must be used in order to account for lateral variations in the attenuation structure.

While L_g has been shown to be a very useful phase for determining a variety of seismological quantities, its utility is diminished in the presence of appreciable attenuation. In an effort to quantify the attenuation affecting L_g propagation for Great Basin paths, we examine recordings of L_g along several paths and measure the spatial decay of spectral amplitudes. The data provide an estimate of the average L_g Q in the Great Basin.

Data and Analysis

The data set for this study consists of regional, digital seismograms for 12 earthquakes in and around the Great Basin recorded at four broad-band seismograph stations operated by the Lawrence Livermore National Laboratory. Figure 1 shows the locations for the earthquakes and seismic stations and the travel paths between them. We selected earthquakes which were recorded by at least three of the four stations and which covered a large range in epicentral distance (ie. no two stations were at a similar distance). As indicated by Figure 1, the travel paths used provide a fair sampling of the Great Basin crust.

The digital seismographs are velocity flat from 0.7 to 10 Hz and operate at a sample rate of 40 samples/second. However, due to memory limitations in the computer used to process the data, we were forced to decimate the data down to a sample rate of 10 samples/second; consequently we have no resolution above 5 Hz. Figure 2 is the magnification curve for the seismograph system used.

A typical set of recordings is plotted in Figure 3, which shows the original (decimated) data and the same data after high-pass filtering by convolving the instrument corrected signal with the response of a WWSSN short-period seismometer. The L_g phase is indicated on the seismograms, and can be seen to be a prominant feature on the short-period record.

We have measured L_g group speeds for 250 regional seismograms with Great Basin paths, including those used in this study. Figure 4 is a histogram of the group speeds obtained, and shows that L_g in the Great Basin typically propagates with a speeds between 3.3 and 3.6 km/sec. The most common speed measured is 3.5 km/sec.

To determine the L_g attenuation, we computed instrument corrected, displacement amplitude spectra of the vertical component L_g phase. We inverted these spectra for the $Q(f)$ function in the following manner. The observed L_g

spectrum is modeled as

$$A(f,R) = \frac{S(f)}{R^{0.5}} e^{\frac{-\pi f t}{Q(f)}} \quad (1)$$

where $A(f,R)$ is the spectral amplitude observed at a distance R, f is frequency, t is the travel time, $S(f)$ is the source term, and Q is the quality factor. This simple model neglects radiation pattern and scattering effects, therefore it provides a measure of the *apparent* rather than the intrinsic Q. Since L_g has been succesfully modeled as surface wave (Knopoff *et al.*, 1973; Panza and Calcagnille, 1975) we have assumed that the frequency domain geometrical spreading scales with the square root of distance. Taking the logarithim (base 10) of both sides of (1) yields

$$\log_{10}A(f,R) + \log_{10}R^{0.5} = \log_{10}S(f) - \left|\frac{1.364 f}{Q(f)}\right| t \quad (2)$$

which is the equation for a straight line, where the source term is the intercept and the Q term controls the slope. Fixing f, we know $A(f,R)$, R, and t for each of the stations and we solve for S and Q using least-squares. By looping over all the frequencies we obtain the source and Q spectra.

We initially determined the travel time for use in equation 2 by taking the travel time to the center of the window which was used to compute the spectrum. However, we found that we obtained larger correlation coefficients overall if we computed the travel time using a speed of 3.5 km/sec. The results presented here were obtained using the latter method, but there is no significant change in the results if the former method is used. This suggests that errors in travel time due to errors in the earthquake locations or origin times do not strongly influence the conclusions presented here.

Since for any given earthquake we are fitting only three or four points at each frequency, the results obtained can be expected to have significant random error. This will be particularly true if the data contain any variations in amplitude due to radiation pattern. We have attempted to compensate for these possible errors by rejecting any results for which the linear correlation coefficient was below 0.8. For several events, this eliminated the data at lower frequencies which were affected by the 6-second microseisms. In general, the data at higher frequencies gave more stable results.

Figure 5a shows all the $Q(f)$ functions obtained with correlation coeffiecients of 0.8 or greater. The average $Q(f)$ function is shown in Figure 5b. A linear least-squares fit to the data in Figure 5b yields

$$Q(f) = 212 f^{0.53} \quad (0.2\,Hz \leq f \leq 1.0\,Hz). \quad (3)$$

Discussion and Conclusions

It is interesting to compare the result obtained above with other published Q functions for the Great Basin. Cheng and Mitchell (1981) used long period L_g waves to estimate a constant Q value of 85. Their data indicate a predominate period of around 5 seconds and so we can consider their Q to be the average crustal value at 0.2 Hz. This is in agrees well with the value of 90, predicted by equation (3).

Our $Q(f)$ function is also in excellent agreement with that found by Singh and Herrmann (1983), who determined regional frequency dependent Q functions for the United States using measurments of coda decay. Their result for the Great Basin in the vicinity of our profile is $Q(f) \approx 200f^{(0.45\pm0.05)}$. Singh and Herrmann were able to relate their observations of coda decay to the L_g spatial attenuation coefficient and concluded that the same attenuation mechanism was responsible for both L_g and coda decay. Our results lend support to this conclusion.

Acknowledgements

We thank H. Patton for making the LLNL data archives available for our use. This research was funded by the Defense Advanced Research Projects Agency of the Department of Defense and monitored by the Air Force Office of Scientific Research under contract F49620-83-C-0012.

References

Bath, M. (1954). The elastic waves L_g and R_g along Euroasiatic paths, *Arkiv. Geofysik.*, **2**, 295-342.

Cheng, C., and B.J. Mitchell, (1981). Crustal Q structure in the United States from multi-mode surface waves, *Bull. Seism. Soc. Am.*, **71**, 161-181.

Herrmann, R.B., and J. Kijko, (1983). Modeling some empirical vertical component L_g relations, *Bull. Seism. Soc. Am.*, **73**, 157-171.

Knopoff, L., F. Schwab, and E. Kausel, (1973). Interpretation of L_g, *Geophys. J. R astr. Soc.*, **33**, 389-404.

Nuttli, O. W., (1973). Seismic wave attenuation and magnitude relations for eastern North America, *J. Geophys. Res.*, **78**, 876-885.

Nuttli, O. W., (1980). The excitation and attenuation of seismic crustal phases in Iran, *Bull. Seism. Soc. Am.*, **70**, 469-485.

Nuttli, O. W., (1981). On the attenuation of L_g waves in western and central Asia and their use as a discriminant between earthquakes and explosions, *Bull. Seism. Soc. Am.*, **71**, 249-261.

Nuttli, O. W., (1984). Methodology of using L_g waves for estimating explosion yield and body-wave magnitude bias between test sites, *in* Nuttli, O. W. and B. J. Mitchell, Attenuation of seismic waves at regional distances, Final Report, Saint Louis University, DARPA Contract F49620-83-C-0015.

Panza G. F., and G. Calcagnille, (1975). L_g, L_1, and R_g from Rayleigh modes, *Geophys. J. R. astr. Soc.*, **40**, 475-487.

Press, F., and M. Ewing (1952). Two slow surface waves across North America, *Bull. Seism. Soc. Am.*, **42**, 219-228.

Singh, S., and R. B. Herrmann, (1983). Regionalization of crustal coda Q in the continental United States, *J. Geophys. Res.*, **88**, 527-538.

Street, R. L., R. B. Herrmann, and O. W. Nuttli (1975). Spectral characteristics of the L_g wave generated by central United States earthquakes, *Geophys. J. R. astr. Soc.*, **41**, 51-63.

Figure captions

Figure 1. Map showing locations of the earthquakes (stars) and recording sites (squares) used in this study and the travel paths between them.

Figure 2. Magnification curve for the seismograph system used.

Figure 3. Examples of typical seismograms recorded at each of the stations. Each record has been individually normalized to the same peak plot amplitude.

Figure 4. Histogram of group speed measurments for 250 recordings of L_g with Great Basin paths.

Figure 5. *a)* Summary of $Q(f)$ functions obtained for each earthquake. Values whose associated linear correlation coefficient was below 0.8 have not been plotted. *b)* Average $Q(f)$ function for the data in *(a)*. One standard deviation error bars are included, as is the least-squares power curve fit to the data (equation 3).

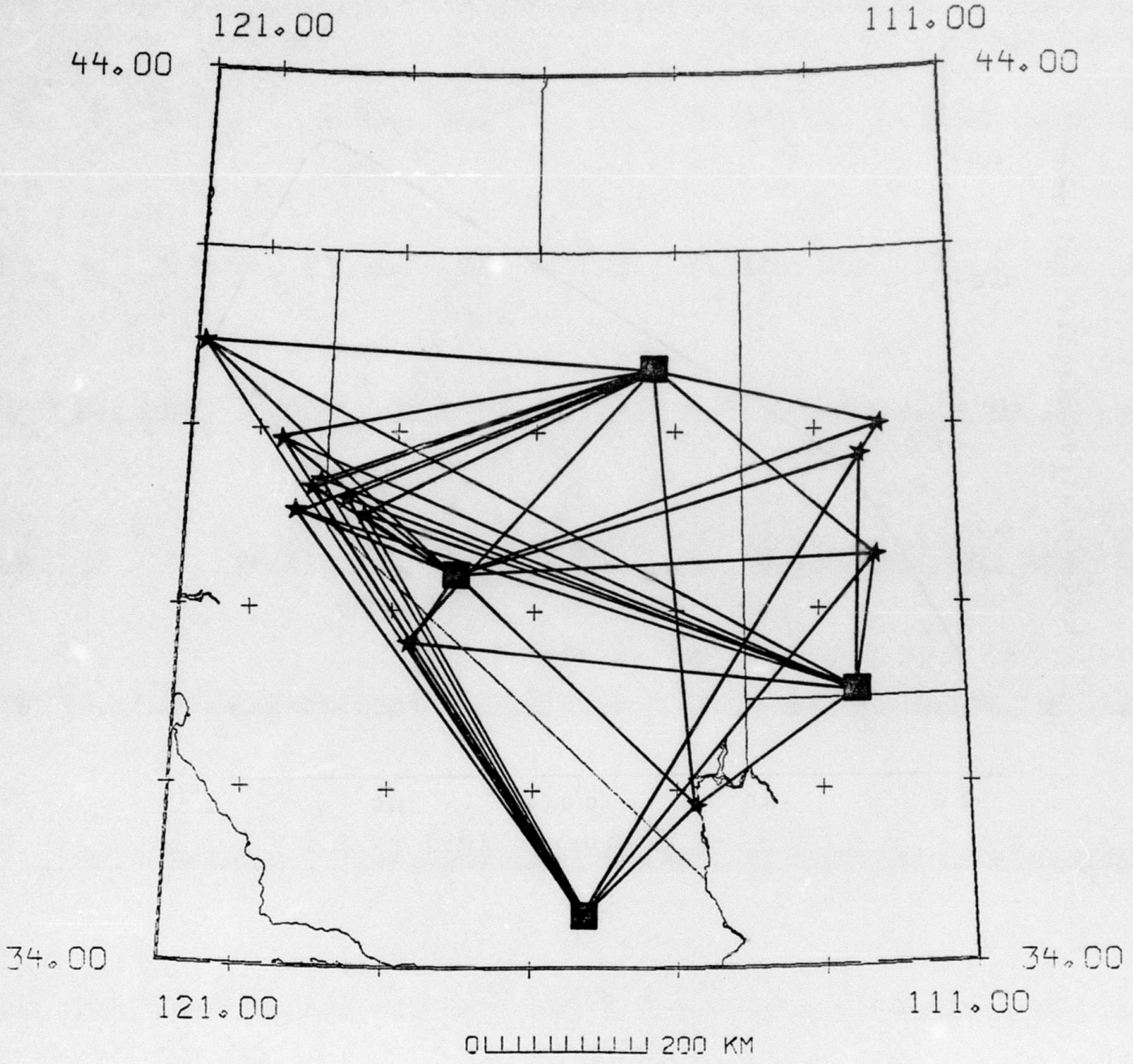

FIGURE 1

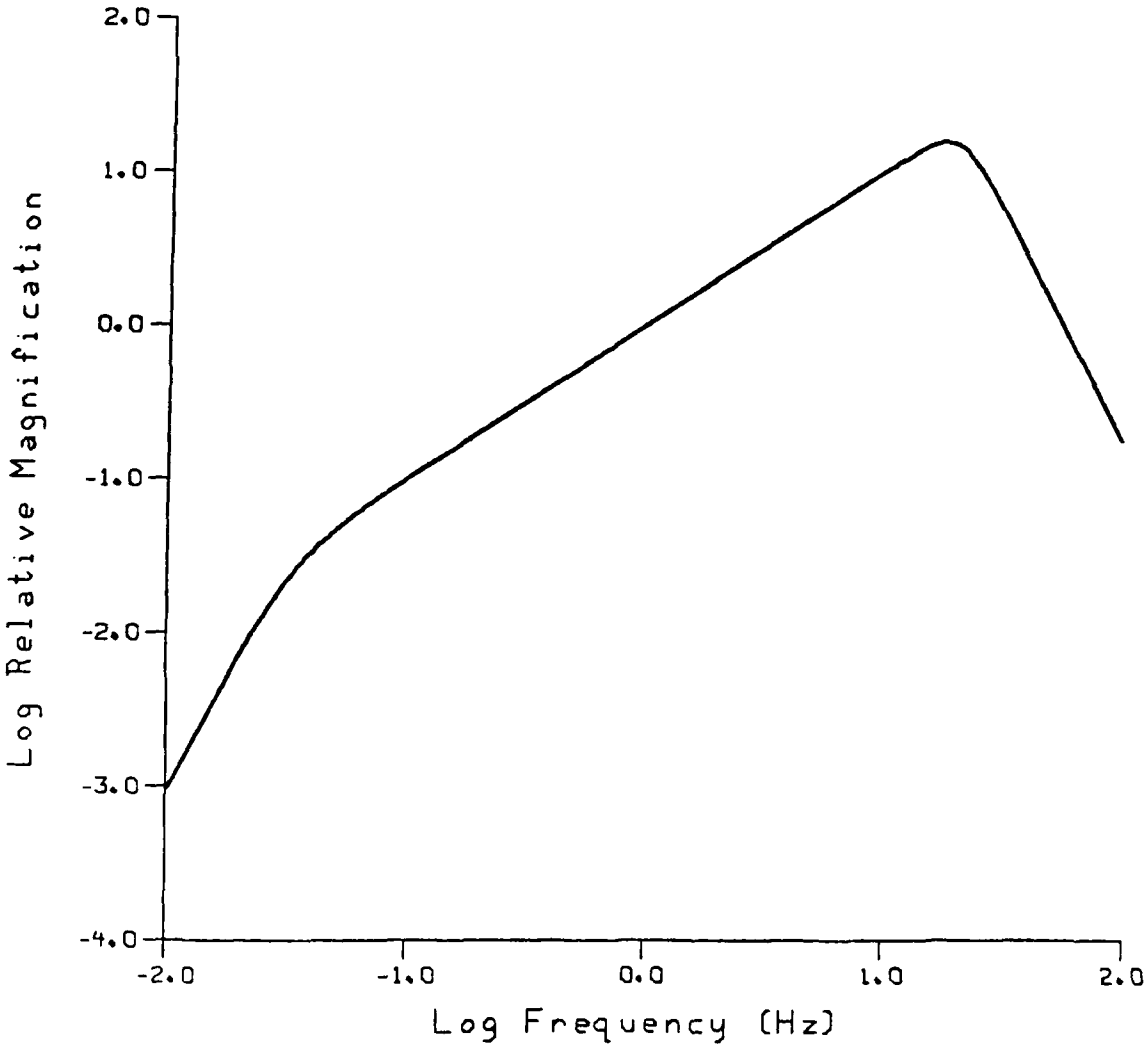
2.0
1.0
0.0
-1.0
-2.0
-3.0
-4.0
Log Relative Magnification
-2.0
-1.0
0.0
1.0
2.0
Log Frequency (Hz)

FIGURE 2

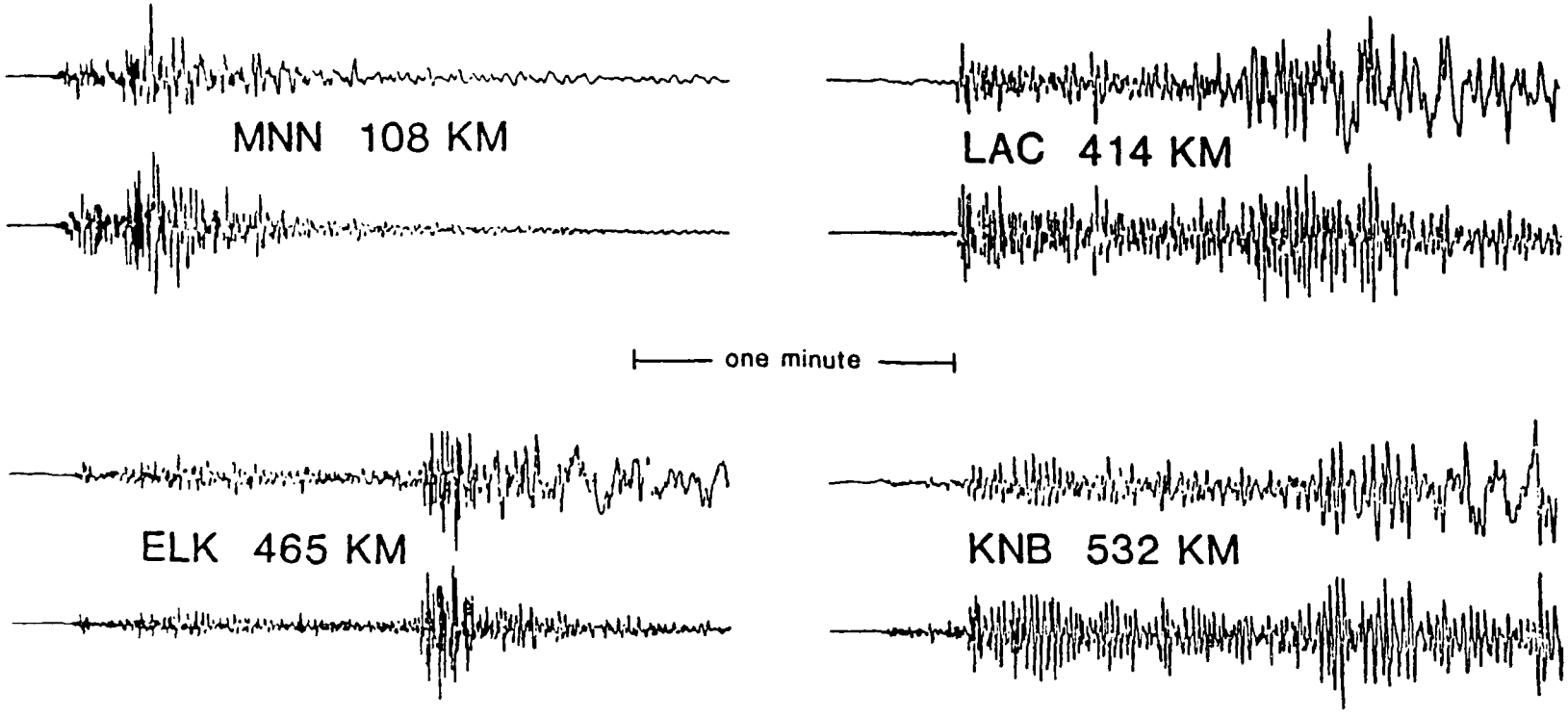

FIGURE 3

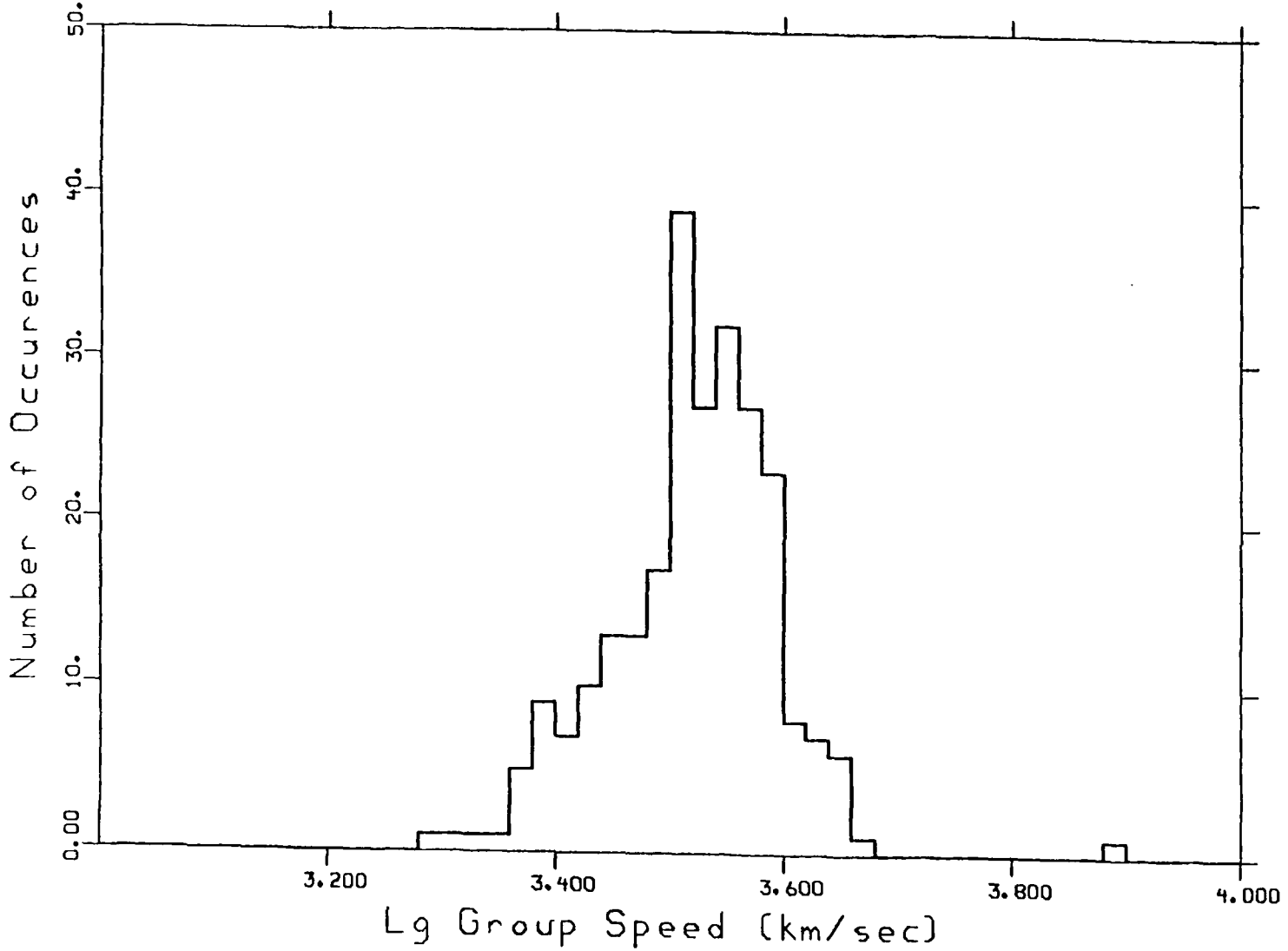
Number of Occurences
50.
40.
30.
20.
10.
0.00
3.200
3.400
3.600
3.800
4.000
Lg Group Speed (km/sec)

FIGURE 4

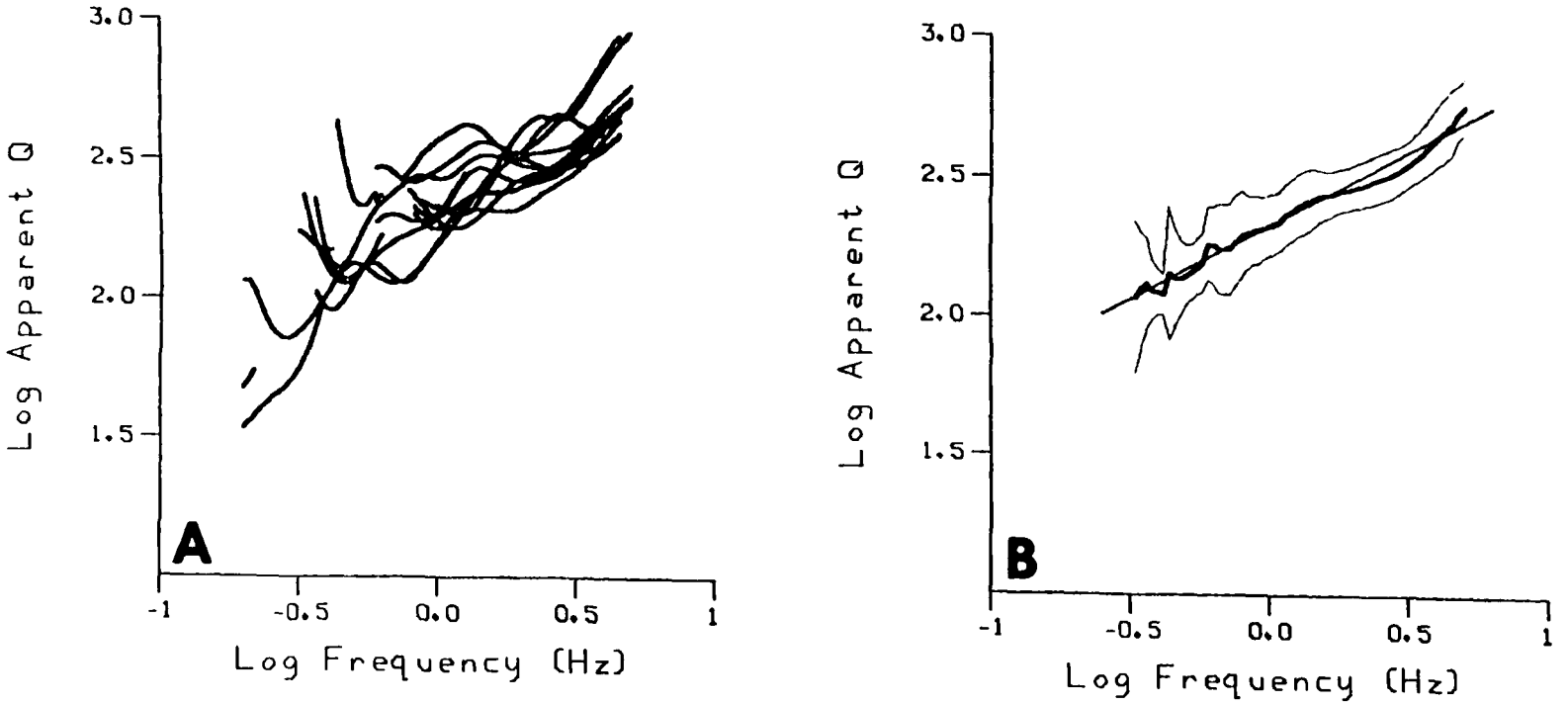
3.0
2.5
2.0
1.5
Log Apparent Q
A
-1
-0.5
0.0
0.5
1
Log Frequency (Hz)
3.0
2.5
2.0
1.5
Log Apparent Q
B
-1
-0.5
0.0
0.5
1
Log Frequency (Hz)

FIGURE 5

Note on mb Bias at Selected Soviet Seismic Stations

Alan S. Ryall

Seismological Laboratory*
University of Nevada
Reno, NV 89557

Introduction

On 25 and 27 May 1980 three M_L 6+ earthquakes occurred in the western Great Basin near Mammoth Lakes, California, about 200 km NW of the Nevada Test Site. As part of our investigation of these earthquakes we requested seismograms from several seismic stations in the Soviet Union, including a station at Semipalatinsk, approximately 100 km NE of the eastern Kazakh test site. This note summarizes m_b determinations for five events on the Soviet records -- the three large Mammoth Lakes events, a smaller (m_b 5.3) Mammoth Lakes shock, plus an earthquake at Tonga (m_b 6.0) that occurred during the time frame of the recordings. The records were searched for eight more events on the ISC list, but none of these were recorded at the Semipalatinsk station and most were not recorded by the other stations. Another strong (m_b 5.4) Mammoth Lakes shock at 16:49 GMT on 25 May and an earthquake in the Kurile Islands (25 May, 23:22 GMT, m_b 4.8) were recorded but not analyzed. Table 1 summarizes information on the events used in this study.

Table 1. List of Events

Date	Time, GMT	Latitude	Longitude	Depth	m_b	M_s
800525	16:33:44.7	37.596 °N	118.830 °W	6.5	6.1	6.1
800525	19:44:51.1	37.547 °N	118.826 °W	5.0	5.6	6.0
800525	20:35:48.5	37.616 °N	118.847 °W	6.1	5.3	5.7
800527	14:50:57.1	37.472 °N	118.807 °W	10.8	5.7	6.0
800527	13:01:37.9	18.610 °S	174.700 °E	55	6.0	4.8

Data

The data included recordings from eight seismic stations on a northeast-trending profile from Kzyl-Agach in the southern part of the Kazakh Fold System to Seymchan in the Northeast Siberian Fold System. Table 2 lists the station coordinates and Figure 1 is a polar projection of Asia showing the station locations. Table 3 gives epicentral distances and azimuths for the five events.

Table 2. Station Locations

Code	Name	Coordinates	Region
BOD	Bodaibo	57 °51'N,114 °11'E	Baikal
ELT	El'tsovka	53 °15'N,86 °16'E	Altai-Sayan
IRK	Irkutsk	52 °16'N,104 °19'E	Baikal
KZL	Kzyl-Agach	45 °25'N,78 °45'E	Kazakhstan
SEI	Seymchan	62 °53'N,152 °26'E	Northeast
SEM	Semipalatinsk	50 °24'N,80 °15'E	Kazakhstan
UST	Ust'-Kan	50 °57'N,84 °45'E	Altai-Sayan
YAK	Yakutsk	62 °01'N,129 °43'N	Yakutiya

* -- Work done at Center for Seismic Studies and partly supported by Science Applications International Corporation.

Table 3. Distance (Δ°) and Azimuth (Θ°) to the Stations										
Sta	05251633		05251944		05252035		05271450		05271301	
	Δ	Θ	Δ	Θ	Δ	Θ	Δ	Θ	Δ	Θ
BOD	75.09	334	75.14	334	75.07	334	75.21	334	95.95	329
ELT	86.95	345	86.99	345	86.92	345	87.07	345	110.06	321
IRK	82.93	335	82.98	335	82.91	335	83.05	335	99.15	322
KZL	95.86	348	95.91	348	95.84	348	95.99	348	114.54	312
SEI	56.77	327	56.82	327	56.75	327	56.89	327	85.23	346
SEM	90.78	348	90.83	348	90.76	348	90.91	348	113.66	318
UST	89.43	345	89.48	345	89.41	345	89.55	345	110.82	318
YAK	66.51	331	66.55	331	66.48	331	66.63	331	91.54	337

Figure 2 is a polar plot of the world centered on a point (81.5° N, 162.0° W) about halfway between the Mammoth Lakes earthquakes and station SEM, showing the epicenter and recording stations. Figure 3 shows the position of the Soviet stations on a lower-hemisphere, equal-area projection of the focal sphere for the three largest Mammoth Lakes earthquakes, together with projections of the fault and auxiliary planes for these events from a study of long-period P- and surface-waves (Given *et al.*, 1982). Based on point-source theory (Keilis-Borok, 1950) and the position of the stations on the focal sphere, P-waves to the Soviet stations should have about 80% of the maximum radiated amplitude.

Figure 4 is a polar projection centered on a point (23.0° N, 147.0° E) about halfway between station SEM and the Tonga earthquake. The Kurile event was in a poor distance range (16-47°) for this study, and and had large scatter in m_b values; it will not be considered in the detailed discussions that follow. For the Tonga earthquake a plot similar to Figure 4 indicates that the Soviet stations are close to the null axis on the fault-plane solution, although the latter is not well-constrained.

Table 4 lists instrument parameters for the 86 recordings that were supplied. Values of the maximum magnification V_m and the period range T_m (corresponding to $V = 0.9\ V_m$) were written on the records. For station KZL the period range T_m was not supplied and the range given in the table was taken from the Soviet publication *Earthquakes in the USSR in 1980* (Akademiya Nauk SSSR. 983). For station BOD the values of V_m marked on the recordings -- "2900" for the NS component and "2700" for the Z and EW -- appeared to be an order of magnitude too low, and the magnification (52,000) for that station was also taken from *Earthquakes in the USSR in 1980.* Use of the larger magnification for BOD is supported by Shishkevish (1974) who lists V_m as 45,000-49,000 for this station in 1970.

For this study only vertical-component recordings from SKM-3 seismographs were used. The SKM-3 system consists of a seismometer and galvanometer with instrument constants designed to produce magnification of ground motion in the range 30,000-100,000 over the period range 0.3-1.5 seconds. According to Aranovich *et al.* (1974) a complete system consists of two SGKM-3 (horizontal) and one SVKM-3 (vertical) seismometers, three GK-VIIM galvanometers and a PS-3M drum recorder. The latter registers the light beams from the three galvanometers on a 29-cm wide by 90-cm long photographic recording. Time marks from a chronometer are printed once per minute. Drum speed was 60 mm/minute for all of the SKM-3 records used in this study except KZL, which recorded at 120 mm/minute. Figure 5 shows relative amplitude response for the eight stations, determined from equations given by Aranovich *et al.* Note that the Soviet short-period seismographs peak at somewhat lower frequency (*ca.* 1 Hz) than systems commonly used in the US, and that for some stations (*i.e.*, SEM and IRK in this study) the system gain is reduced by about a factor of ten at 10 Hz.

Seismometer and galvanometer constants (period, damping) for stations BOD, IRK and SEM were taken from Shishkevish (1974), and the resulting response was checked to insure that the range of T_m was the same as that indicated on the recordings. For ELT the constants given by Shishkevish were modified to give the appropriate upper limit of T_m, and the same constants were used for UST. For YAK Shishkevish lists instrument constants only for the horizontal-component seismographs, and these give a different range of T_m than that specified on the records. For KZL and SEI Shishkevish does not list instrument constants. As a result, for KZL, SEI and YAK various combinations of instrument constants were tried, based on tables of standard setups given by Aranovich *et al.*, until response curves matched the range of T_m marked on the records.

Except for the SKM recordings at station KZL and the long-period recordings at UST all of the records were 12 hours long. The KZL record has twice the time resolution of the other short-period stations and appears to be changed three times a day; the SKD record for UST for 25 May was 24 hours long. Unfortunately the records of primary interest to this analysis -- from station SEM -- were changed at different times than those at other stations and overlap with the latter for only two six-hour periods.

Table 4. Data Received for 25 and 27 May 1980

Sta	Inst	Comp	V_m	T_m
BOD	SKM-3	NS,Z,EW	52,000	0.2 - 1.2
ELT	SKM-3	NS,Z,EW	50,000	0.2 - 1.4
	SKM-3	EW	5,000	0.2 - 1.4
IRK	SKM-3	NS	17,500	1.1 - 1.6
	SKM-3	Z	17,240	1.1 - 1.6
	SKM-3	EW	17,430	1.1 - 1.6
	SKD	NS,Z,EW	1,200	0.2 - 20
KZL	SKM-3	NS	40,900	0.08 - 1.6
	SKM-3	Z	41,500	0.08 - 1.6
	SKM-3	EW	40,600	0.08 - 1.6
	SKM-3	EW	1,050	0.08 - 1.2
SEI	SKM-3	NS,Z,EW	44,600	0.2 - 1.2
	SKD	NS,Z,EW	1,050	0.2 - 20
SEM	SKM-3	NS,EW	30,050	0.84 - 1.5
	SKM-3	Z	28,400	0.8 - 1.5
	SK	NS,EW	1,700	0.41 - 10.9
	SK	Z	1,100	0.5 - 11
UST	SKM-3	NS,Z,EW	50,000	0.2 - 1.4
	SKM-3	E-W	5,000	0.2 - 1.4
	SKD	NS,Z,EW	1,000	0.2 - 22
YAK	SKM-3	Z	18,800	0.3 - 1.3
	SKM-3	NS	37,600	0.8 - 1.4
	SKM-3	EW	36,800	0.8 - 1.4
	SK-KPCh	NS	140	0.3 - 11
	SK	NS	2,130	0.4 - 11
	SK	Z	680	0.4 - 9.0
	SK	EW	1,930	0.4 - 11

Record Quality. Copies of the records were on 35 mm film of poor-to-good quality. For many of the short-period records the contrast between the trace and the background was poor, and attempts to make enlargements of the waveforms using a reader-printer were not successful. As a result the records had to be projected on a viewing screen and traced by hand; the tracings were then digitized for computer analysis.

Quality of the KZL records was especially poor, and the P-waveform for only one event was traced for that station.

Timing. Two or three time corrections were marked on each of the records, usually corresponding to the beginning and end of the recording period. Clock corrections changed at most stations by less than a second per day. A few records were mislabeled as to sense of the time correction, and in one case the time corrections at the two ends of a recording period were interchanged on different records of the same station. The largest clock drift was 0.5 second/hour for the SEM station, but this rate was constant. Tracings of the P-waves were enlarged such that the average time scale was about 270 mm/minute. Station KZL had a drum speed twice that of the other stations, so the enlarged traces were viewed at a scale of 540 mm/min. For most of the events the beginning of the P-wave (PKP for stations at $\Delta \geqslant 110^\circ$) was identified on records of one of the better stations (SEI, YAK, BOD) and the same point was marked and timed on traces for the other stations by overlaying the recordings.

Traveltime residuals were calculated for the Mammoth Lakes earthquakes using hypocentral coordinates and origin times determined by the University of Nevada from local network recordings and traveltimes calculated from the Herrin *et al.* (1968) tables. The Soviet stations had average delays of 0.5-2.2 seconds for the Mammoth Lakes events, relative to the Herrin tables. These delays are not considered to be meaningful for the present study, since the larger earthquakes of this sequence appear to have been multiple events, initiated by small ruptures that recorded at regional stations but not at teleseismic distance ranges (*e.g.*, Given *et al.*, 1982). On the other hand, traveltime residuals for individual stations relative to the average delays for all the stations (Table 5) are fairly consistent for the Mammoth Lakes and Tonga earthquakes. Note that the two stations north of Lake Baikal (BOD, IRK) have early arrivals for waves travelling southwest across the Siberian platform from the Mammoth Lakes events, but are late for paths from Tonga that cross the Baikal graben. Station SEM has small traveltime residuals that average to almost zero.

Table 5. Relative P-wave Residuals, Seconds

Sta	251633	251944	252035	271450	271301	Average
BOD	-1.0	-0.3	-1.2	-0.8	+0.5	-0.6±0.7
ELT				-1.0	-1.5	-1.3±0.4
IRK	-0.7	-0.9	-0.3	-0.9	+0.2	-0.5±0.5
KZL	0.0					0.0
SEI	+0.8	+0.5	+0.6	+1.4	+0.8	+0.8±0.3
SEM	+0.5	-0.5	-0.2	+0.5	+0.5	+0.2±0.5
UST	+0.5	-0.5	-0.2	+0.5	-0.7	-0.1±0.6
YAK	0.0	+0.6	-0.1	+0.6	-0.0	+0.2±0.4

Magnitude Determination

Figure 6 shows an example of the digitized P-waves for the first large Mammoth Lakes event, at 16h 33m on 25 May 1980. All traces are from SVK-M3 instruments, and are normalized; up on the traces corresponds to ground motion up. With the exception of KZL most of the recordings had good signal-to-noise ratios. Stations YAK and BOD appear to have higher frequency content than some of the other stations, including SEM, but this could be a result of differences in instrument response. P-wave spectra for this event, corrected for instrument response, have peaks at about 0.5 and 0.7 Hz; for station BOD the peaks are about equal in amplitude, but for the other stations the amplitude at 0.7 Hz is less than half that at 0.5 Hz. In general the character of the P-wave at the

various stations is similar, consisting of a small first arrival followed 6 seconds later by a larger phase. The time interval between these phases is too consistent for the second arrival to be PcP, since for the distance range of the Soviet stations t(PcP-P) should vary from 60 seconds to zero. The second phase could be another earthquake, but this is unlikely because all of the Mammoth Lakes events have a large second arrival at the Soviet stations. A more likely explanation is that the phase includes the reflected waves pP and and sP. Based on the known crustal structure in the Mammoth Lakes area, a pP-P time of 6 seconds would be consistent with focal depth of about 16 km, and for that depth the sP-P time would be about 8 seconds. For the second and third Mammoth Lakes earthquakes in Table 1, measured X-P times 4.9 and 2.5 seconds would be consistent with focal depths of about 13 and 6.5 km, respectively, if these arrivals were pP. The fourth Mammoth Lakes event has a complex P-signature and the timing of the second phase is not consistent from one station to another.

Magnitude was determined from computer plots of the digitized P-waves using the standard formula

$$m_b = \log_{10} \frac{A}{T} + B(\Delta),$$

where A is the amplitude of vertical ground motion in nanometers and T is the period corresponding to amplitude A. From the range in m_b values given in the *Bulletin of the International Seismological Centre*, it appears that some observatories measured the amplitude of the initial P-wave for the Mammoth Lakes events, while others measured the amplitude of the second phase. The IASPEI Commission on Practice Concerning Amplitude and Period Measurement recommended in 1979 that "the P wave amplitude measured should be that of the maximum trace deflection, usually within the first 25 seconds of the first onset or before the arrival of the next clear phase." Other workers have recommended measuring A and T within the first few cycles (Zavadil, 1980) or even within the first 3/4 cycle (the "b" amplitude) of the P-wave (Eisenhauer, 1980). Because of the discrepency between maximum amplitude in the P-coda and amplitude of the P onset, we determined m_b for the Mammoth Lakes earthquakes from the maximum amplitude in the first two cycles and from the maximum amplitude in the first 12 seconds -- in both cases taken as one-half the peak-to-peak amplitude. The resulting individual and average m_b values are listed in Tables 6 and 7, together with magnitudes determined by the International Seismological Centre (ISC) and Moscow (MOS), and deviations δm_b from the ISC values.

A third set of magnitudes was determined from measurements of A and T on traces produced by deconvolving the instrument response from the digitized recordings. The deconvolution was accomplished using a program written by W. Peppin to calculate the complex transfer function of a seismograph, given the period and damping of the seismometer and galvanometer, together with the maximum magnification of the system and the period at which the maximum magnification occurs. The records were tapered and bandpass-filtered (0.25-8.0 Hz) before deconvolution, and filtered again (0.1-5.0 Hz bandpass) after deconvolution. Figure 7 gives examples of the P-waves for the first large Mammoth Lakes earthquake after correction for instrument response and filtering. For these records m_b was determined only using the maximum amplitude in the large phase following the initial P-wave. Magnitudes and residuals are listed in Table 8.

Table 6. Magnitudes and Residuals, Uncorrrected Data, First Two Cycles

	05251633		05251944		05252035		05271450		Average
Sta	m_b	δm_b	m_b	δm_b	m_b	δm_b	m_b	δm_b	δm_b
BOD	5.47	-.63	4.97	-.63	4.96	-.34	5.34	-.36	-.49±.16
ELT*							5.78	+.08	+.08±.0
IRK	5.53	-.57	4.98	-.62	4.84	-.46	5.76	+.06	-.40±.31
KZL*	5.58	-.52							-.52±.0
SEI	5.67	-.43	5.17	-.43	5.09	-.21	5.54	-.16	-.31±.14
SEM	5.72	-.38	4.73	-.87	4.89	-.41	5.80	+.10	-.39±.40
UST	5.42	-.68	4.68	-.92	4.92	-.38	5.69	-.01	-.50±.39
YAK	6.16	+.06	5.21	-.39	5.48	+.18	6.38	+.68	+.13±.44
Avg	5.66		4.96		5.03		5.75		
ISC	6.1		5.6		5.3		5.7		
MOS	6.3		5.7		5.5		5.9		

Table 7. Magnitudes and Residuals, Uncorrrected Data, First 12 Seconds

	05251633		05251944		05252035		05271450		Average
Sta	m_b	δm_b	m_b	δm_b	m_b	δm_b	m_b	δm_b	δm_b
BOD	6.04	-.06	5.76	+.16	5.46	+.16	5.66	-.04	+.06±.12
ELT*							5.59	-.11	-.31±.0
IRK	6.16	+.06	5.66	+.06	5.40	+.10	5.58	-.12	+.03±.10
KZL*	6.04	-.06							-.06±.0
SEI	6.48	+.38	5.81	+.21	5.62	+.32	6.03	+.33	+.31±.07
SEM	6.34	+.24	5.63	+.03	5.48	+.18	5.76	+.06	+.13±.10
UST	6.18	+.08	5.52	-.08	5.22	-.08	5.71	+.01	-.02±.08
YAK	6.60	+.50	6.10	+.50	5.90	+.60	6.04	+.34	+.49±.11
Avg	6.30		5.75		5.51		5.80		
ISC	6.1		5.6		5.3		5.7		
MOS	6.3		5.7		5.5		5.9		

Table 8. Magnitudes and Residuals, Corrrected Data, First 12 Seconds

	05251633		05251944		05252035		05271450		Average
Sta	m_b	δm_b	m_b	δm_b	m_b	δm_b	m_b	δm_b	δm_b
BOD	6.12	+.02	5.65	+.05	5.50	+.20	5.70	+.00	+.07±.09
ELT*							5.77	+.07	+.07±.0
IRK	6.20	+.10	5.61	+.01	5.38	+.08	5.64	-.06	+.03±.07
KZL*	6.24	+.14							+.14±.0
SEI	6.47	+.37	5.98	+.38	5.76	+.46	6.00	+.30	+.38±.07
SEM	6.32	+.22	5.71	+.11	5.53	+.23	5.80	+.10	+.17±.07
UST	6.13	+.03	5.60	+.00	5.41	+.11	5.64	-.06	+.02±.07
YAK	6.74	+.64	6.22	+.62	6.10	+.80	6.35	+.65	+.68±.08
Avg	6.33		5.80		5.61		5.86		
ISC	6.1		5.6		5.3		5.7		
MOS	6.3		5.7		5.5		5.9		

* -- ELT and KZL not used in determining average m_b values.

For the Tonga earthquake, values of m_b were determined from the maximum amplitude in the P-wave, from traces uncorrected and corrected for instrument response. Four of the stations for this event were beyond 100° and distance corrections were taken from a curve developed by Ringdal (1985).

Table 9. Magnitudes and Residuals for Tonga Event

	Uncorrected Data		Corrected Data	
Sta	m_b	δm_b	m_b	δm_b
BOD	5.85	-.14	6.12	+.12
ELT	6.09	+.09	6.22	+.22
IRK	5.38	-.62	5.42	-.58
SEI	6.19	+.19	6.17	+.17
SEM	6.07	+.07	6.06	+.06
UST	5.79	-.21	5.78	-.22
YAK	6.16	+.16	6.15	+.15
Avg	5.93		5.99	
ISC	6.0		6.0	
MOS	5.9		5.9	

Discussion

In this study we have determined magnitude m_b for five earthquakes on 25 and 27 May 1980, from recordings at eight Soviet seismic stations on a 4,300 km-long profile from eastern Kazakh to eastern Siberia. In general, our average magnitudes for the Mammoth Lakes earthquakes (Tables 7 and 8) are about 0.2 m_b unit higher than those determined by the ISC, but for the Tonga event our m_b is close to the ISC value. As might be expected our values are also about the same as magnitudes attributed to Moscow in the ISC *Bulletin*. For the data uncorrected for instrument response our average values differ from the Moscow m_b's by 0.00±0.06 unit; for the corrected data our values are higher than the Moscow m_b's by 0.06±0.06. Magnitudes determined from A and T measured in the first two cycles of the P-wave for the Mammoth Lakes earthquakes (Table 6) averaged 0.33 and 0.50 m_b unit smaller than the ISC and Moscow values, respectively.

The largest positive m_b residuals were for station YAK (average δm_b = 0.33 for the uncorrected data in Tables 7 and 9; 0.42 for the corrected data in Tables 8 and 9). Yakutsk is located on the central Siberian platform in an area where, according to Potap'ev *et al.* (1974), the depth to crystalline basement is shallow, 0 5-1.0 km. About 10 km west of Yakutsk a major north-south fault offsets basement rocks, with the western side downdropped by about 4 km. P-wave velocities in the crust are high, 6.2-6.4 km/sec (Vol'vovsky, 1973), the crust is about 40 km thick, and the P_n velocity is about 8.0 km/sec (Vol'vovsky and Vol'vovsky, 1975; Ryall *et al.*, 1980).

The largest negative m_b residuals were observed for station IRK for the Tonga event (-0.62 uncorrected, -0.58 corrected), for which the raypath crosses the southern part of the Baikal rift zone in a WNW direction. The rift zone is characterized by complex geologic structure, including deep crustal inhomogeneities and velocity anomalies in areas of recent rifting. Within the rift zone P-wave velocity in the crust increases from 5.8 km/sec near the surface to 6.4 km/sec at the crust/mantle interface, crustal thickness is 34-36 km, and the P_n velocity is 7.7-7.8 km/sec (Puzyrev *et al.*, 1975; Ryall *et al.*, 1980). Puzyrev *et al.* (1977) attribute the low P_n velocity to partial melting of upper mantle material, and compare the Baikal region with the East African rift system, the Rhine graben and the Basin and Range province. It is interesting that IRK, which is located on the southern edge of the central Siberian platform just north of the Baikal

rift, has smaller values of δm_b (+0.03±0.10 uncorrected, +0.03±0.07 corrected) for the Mammoth Lakes earthquakes, for which the P-waves approach the station in a SSW direction across the platform and do not appear to be affected by the structure of the rift zone. According to Puzyrev *et al.* (1977) the platform is characterized by uniform layering, with distinct reflecting horizons at depths of 18-21 and 23-27 km, crustal thickness of about 40 km, and "normal" P_n velocity of about 8.1 km/sec.

The m_b residuals for station SEM are intermediate between IRK and YAK. SEM is near the Irtysh River, on the boundary between the west Siberian platform to the north and the Kazakh fold system to the south. In this area the crustal thickness is about 45 km, P_n velocity is 8.2-8.4 km/sec, and P-velocity in the crust is high (Vol'vovsky and Vol'vovsky, 1975). The station is in the Zaysan fold belt, which is relatively simple in terms of stratigraphy and structure. Sediments, principally of Carboniferous age, contain thick limestone deposits and lesser amounts of interbedded volcanics. Folding and faulting are relatively minor in this area, compared with more extensive folding, faulting and intrusion in the Chingiz-Tarbagatai geanticlinal zone to the southwest, in which the eastern Kazakh test site is located (Peyve and Mossakovsky, 1982). For the Mammoth Lakes earthquakes δm_b for this station is +0.13±0.10 for the uncorrected data (Table 7) and +0.17±0.07 for the corrected data (Table 8). For the Tonga earthquake it is +0.07 for the uncorrected, +0.06 for the corrected data. As noted above, SEM is near a maximum on the radiation pattern for the Mammoth Lakes earthquakes, and near the null axis for the Tonga event.

Several published works treat magnitude residuals for stations of the Soviet network, and provide for a comparison with our results (Table 10). First, in a study of magnitude and global network detection capability Ringdal (1985) recomputed m_b for about 70,000 earthquakes, using A and T values given in the ISC *Bulletin* and a maximum-likelihood estimation technique (Ringdal, 1976). In another study, North (1976) calculated mean station magnitude bias from m_b values given in the ISC *Bulletin* for nearly 40,000 events from 1964 to 1973. The biases were computed for the "best" (in terms of events reported) 72 stations with respect to the mean magnitude of observations reported by this set of stations, with the requirement that an event be reported by more than 15 of these stations before a bias was calculated.

In work by Soviet authors Vanek *et al.* (1978, 1980) determined magnitude *corrections* (Δm_b) for 32 reference stations of the Unified System of Seismic Observations (ESSN) of the Soviet Union, following a recommendation of the KAPG Conference at Prague in 1972 to create a uniform system for determining magnitude for the Eurasian continent. The station corrections were determined separately for phases PV, PV_S and PH – respectively the P-wave recorded on vertical mid-band, vertical short-period and horizontal mid-band seismographs. Calculations were also made separately for five different source regions around the USSR – Alaska, Japan, the Phillipines, Asia and the Mediterranean. The number of earthquakes in each source region was not given in the 1980 paper, but in the earlier work it ranged from 35 events for Asia and the Mediterranean to 93 events for Japan. The corrections were with respect to one of the reference stations, OBN, selected at least in part for its bias toward large m_b values. Based on a comparison of Δm_b values for the various source regions the reference stations are grouped according to the number of corrections needed for the different source regions. Thus, a station for which Δm_b was the same for all five source regions was classed as a reference station of the *I Kind*, a station with the same correction for four of the five source regions would be a station of the *II Kind, etc.* Of interest to our study, station SEM has the same PV_S correction for all of the source regions, Δm_b = +0.32, making it a station of the *I Kind* and indicating that it has a δm_b *bias* of -0.32 relative to station OBN. Standard deviations are not given by Vanek *et al.* (1980) but in the earlier work they average ±0.05 m_b unit. For comparison with magnitude bias given by other authors, we reversed the sign of Δm_b and increased all of the resulting values by 0.39 --

Ringdal's (1985) bias for station OBN, which Vanek *et al.* use as a base station.

Table 10. Comparison of Station Residuals and δm_b (OB2-NV)

Sta	Ringdal	North	Vanek*	δm_b[1]	δm_b[2]	$\delta m_b (OB2-NV)$[3]
BKR	+0.38±0.33		+0.30			-0.44
BOD	-0.02±0.34			-0.05	+0.10	-0.11
CLL	+0.16±0.26	+0.20±0.32	+0.09			-0.25
ELT	+0.15±0.34			-0.01	+0.15	-0.20
FRU	+0.35±0.33		+0.36			-0.46
ILT	+0.08±0.32		+0.03			-0.16
IRK	-0.03±0.31			-0.30	-0.28	+0.10
KHC	+0.03±0.26	+0.10±0.26	+0.08			-0.17
KHE	+0.37±0.31		+0.31			-0.44
KRA	+0.32±0.29	+0.22±0.29	+0.22			-0.35
KZL				-0.06	+0.14	-0.14
MOX	+0.07±0.25	+0.02±0.27	+0.01			-0.13
OBN	+0.39±0.33		+0.39			-0.49
PET	+0.24±0.36		+0.35			-0.40
PRU		+0.04±0.24	-0.06			-0.09
SEI				+0.25	+0.28	-0.37
SEM			+0.07	+0.10	+0.12	-0.20
TIK	+0.03±0.37		+0.00			-0.12
UST				-0.12	-0.10	+0.01
YAK	+0.43±0.34			+0.33	+0.42	-0.49
YSS	+0.20±0.41		+0.02			-0.21
ZAK	-0.11±0.33		-0.03			-0.03

* -- Given by authors as Δm_b corrections relative to base station OBN. Sign reversed and all values increased by 0.39 for comparison with Ringdal (1985).

1 -- Mean of δm_b for Tonga earthquake plus average δm_b for four Mammoth Lakes events from Table 7. Uncorrected data.

2 -- Mean of δm_b for Tonga earthquake plus average δm_b for four Mammoth Lakes events from Table 8. Corrected data.

3 -- Average residual (-0.10±0.35) for OB2-NV with respect to ISC *Bulletin* minus average station residual.

With a couple of exceptions the station residuals listed in Table 10 from the work of Ringdal (1985), North (1976) and Vanek *et al.* (1978, 1980) agree to within a few hundredths of a unit of m_b. Our station residuals are based on a very limited data set and show more scatter when compared to those of the other authors. However, they are in general agreement with the published values, and two of the stations -- SEM and YAK have values of δm_b that are in excellent agreement with those of Vanek *et al.* and Ringdal, respectively.

As a final step we computed the m_b bias between a granite site at the Nevada Test Site and the Soviet stations listed in Table 10. In this calculation we used A and T measurements listed by Der *et al.* (1978) for 83 seismic events for the period September 1976 to March 1977, recorded by a digital seismic system (SDCS) at station OB2-NV (Climax stock at north end of Yucca Valley on NTS). In the Der *et al.* report, the A

values are peak-to-peak amplitudes in nanometers, and magnitudes are computed using distance corrections of Veith and Clawson (1972). For consistency with the work by Ringdal (1985) and North (1976), magnitudes were recomputed using the Gutenberg and Richter (1956) corrections and dividing the peak-to-peak amplitudes by two to obtain zero-to-peak amplitudes. Residuals for the 83 events were calculated as $\delta m_b = m_b(OB2-NV) - m_b(ISC)$, and these were averaged to obtain an average δm_b of -0.09±0.39. Five values that fell outside the 2σ limits ($-0.87 \leqslant \delta m_b \leqslant 0.69$) were dropped and the average δm_b recalculated to obtain -0.10±0.35. This number represents the average bias of the OB2-NV site with respect to network-averaged m_b values listed in the ISC *Bulletin*. To determine the bias of OB2-NV with respect to the Soviet stations, the average residuals in Table 10 for those stations were subtracted from -0.10. The resulting bias values are listed in the right-hand column of Table 10.

Of particular interest to questions of yield verification, the m_b bias of the NTS granite site with respect to station SEM at Semipalatinsk is -0.20, with a range of -0.17 to -0.22. The smaller of these figures (-0.17) is based on the study by Vanek *et al.* (1980), and the larger (-0.20, -0.22) are from our measurements of Soviet records of the Mammoth Lakes and Tonga earthquakes. It should be noted that the bias values in Table 10 represent only the bias due to attenuation in the upper mantle and crust under the respective seismic stations; they do not include other effects such as differences in coupling for explosions at the two test sites, effects due to tectonic release, or those related to focusing and defocusing of seismic waves in the vicinity of a given explosion. The reader should also be reminded that the Semipalatinsk station is about 100 km from the East Kazakh test site, and that, according to Peyve and Mossakovsky (1982), crustal rocks under the test site have been subjected to greater folding, faulting and intrusion than those under the seismic station.

Acknowledgements

Most of this work was done while the author was working as a visiting scientist at the Center for Seismic Studies, Arlington, VA, and was partly supported by Science Applications International Corporation. The research was also partly done at the University of Nevada, Reno, NV, with support from the Defense Advanced Research Projects Agency under contract number F49620-83-C-0012, monitored by the Air Force Office of Scientific Research.

References

Akademiya Nauk SSSR (1983). *Zemletryaseniya v SSSR v 1980 godu* (Earthquakes in the USSR in 1980), Nauka Press, Moscow.

Aranovich, Z.I., Ed. and others (1974). *Apparatura i metodika seismometricheskikh nablyudenii v SSSR* (Apparatus and method of seismic observations in the USSR), Nauka Press, Moscow, 240 pp.

Der, Z.A., M. S. Dawkins, T.W. McElfresh, J.H. Goncz, C.E. Gray and M.D. Gillispie (1978). *A Comparison of Teleseismic P Wave Amplitudes and Spectra Observed at Selected Basin and Range Sites and in Eastern North America, Phase 1 Final Report - Volume 2*, Teledyne Geotech Rept. SDAC-TR-77-7, 223 pp.

Eisenhauer, T.D. (1981). Body wave magnitude definitions, in *A Technical Assessment of Seismic Yield Estimation, DARPA-NMR-81-01*, 3 pp.

Given, J.W., T.C. Wallace and H. Kanamori (1982). Teleseismic analysis of the 1980 Mammoth Lakes earthquake sequence, *Bull. Seism. Soc. Am.*, *4*, 1093-1109.

Gutenberg, B. and C.F. Richter (1956). Magnitude and energy of earthquakes, *Ann. Geof., 9*, 1-15.

Keylis-Borok, V.I. (1950). On the question of determining the dynamic parameters of the focus, *Trudy Geofiz. Inst., Akad. Nauk SSSR, 9*, 3-19.

Peyve, A.V. and A.A. Mossakovsky (1982), Ed., and others. *Tektonika Kazakhstana* (Tectonics of Kazakhstan, explanatory report for the Tectonic Map of Eastern Kazakh), Nauka Press, Moscow, 139 pp.

Potap'ev, S., G. Babayan and I. Podvarkova (1974). *Regional Geophysical Investigations in Almost Inaccessible Regions*, Nauka Press, Novosibirsk.

Puzyrev, N., S. Krylov, B. Mishen'kin, Z. Mishen'kina, G. Petrik and V. Seleznev (1977). *The Structure of the Earth's Crust and Upper Mantle According to Data of Seismic Investigations*, Naukova Dumka Press, Kiev, USSR.

Ringdal, F. (1985). *Study of Magnitudes, Seismicity and Earthquake Detectability Using a Global Network*, Center for Seismic Studies Rept., in press.

Ryall, A.S., V.C. Fryklund and M. Mirkovitch (1980). *DSS Data and Regional Monitoring (Application to the Central Siberian Platform)*, R&D Associates Rept. RDA-TR-194206-001, 73 pp.

Shishkevish, C. (1974). *Soviet Seismographic Stations and Seismic Instruments, Part I*, Rand Corp. Rept. R-1204-ARPA, 200 pp.

Vanek, J. and 32 others (1978). Station corrections for longitudinal waves in the Homogeneous Magnitude System of the Eurasian continent, *Akad. Nauk SSSR, Izvestiya Earth Physics, 14*, Amer. Geophys. Un., 169-178.

Vanek, J., N.V. Kondorskaya, I.V. Federova and L. Khristoskov (1980). Optimization of amplitude curves for longitudinal seismic waves for purposes of development of a uniform magnitude system for seismic observations on the Eurasian continent, *Doklady Akad. Nauk SSSR, 250*, 834-838, transl. by Scripta Publ. Co.

Vol'vovsky, I.S. (1973). *Seismic Studies of the Earth's Crust in the USSR*, transl. by Addis Translations International, 289 pp.

Vol'vovsky, I.S. and B.S. Vol'vovsky (1975). *Cross-Sections of the Earth's Crust in the Territory of the USSR, Plotted from Deep Seismic Soundings*, transl. by Addis Translations International, 268 pp.

Zavadil, R.J. (1981). Definitions and estimates of body wave magnitude, in *A Technical Assessment of Seismic Yield Estimation, DARPA-NMR-81-01*, 4 pp.

Figure Captions

Figure 1. Polar projection of Eurasia showing stations used in this study. Radius of map is 40°.

Figure 2. Polar projection showing location of Mammoth Lakes earthquakes (solid circle) and stations used in study (triangles). Radius of map is 52°.

Figure 3. Fault-plane solutions for three of the largest Mammoth Lakes earthquakes (from Given *et al.*, 1982). Lower-hemisphere, equal-area projection. Solid circles – location of raypath to Soviet stations used in study.

Figure 4. Polar projection showing location of Tonga earthquake (solid circle) and stations used in study (triangles). Radius of map is 60°.

Figure 5. Response curves for SVK-M3 short-period vertical instruments for stations used in this study.

Figure 6. P-waves digitized from Soviet recordings for the Mammoth Lakes earthquake on 25 May 1980 at 16:33 GMT.

Figure 7. P-waves corrected for instrument response for the 25 May 1980, 16:33 GMT, earthquake.

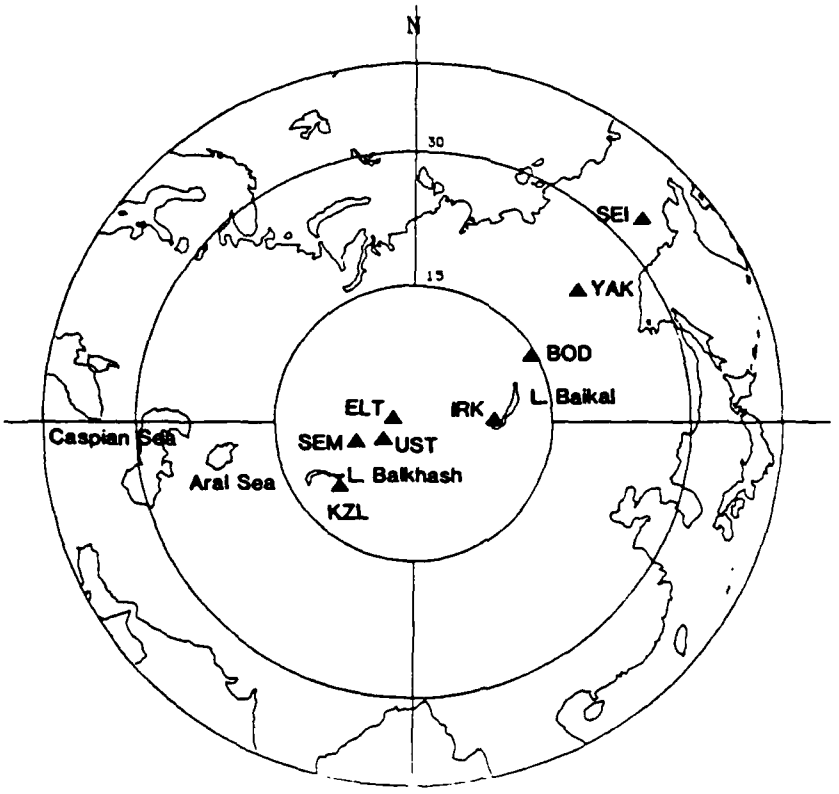

Figure 1

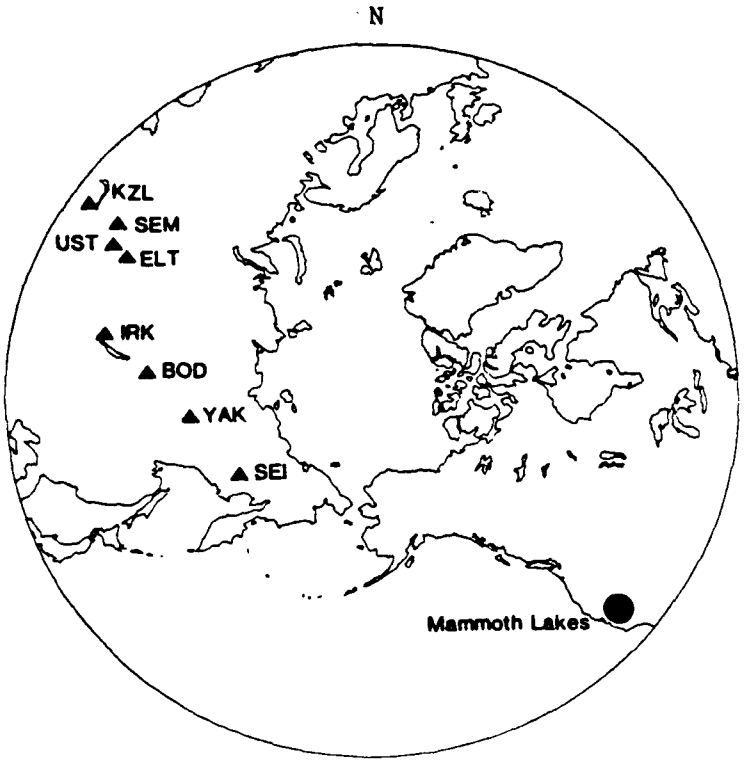

Figure 2

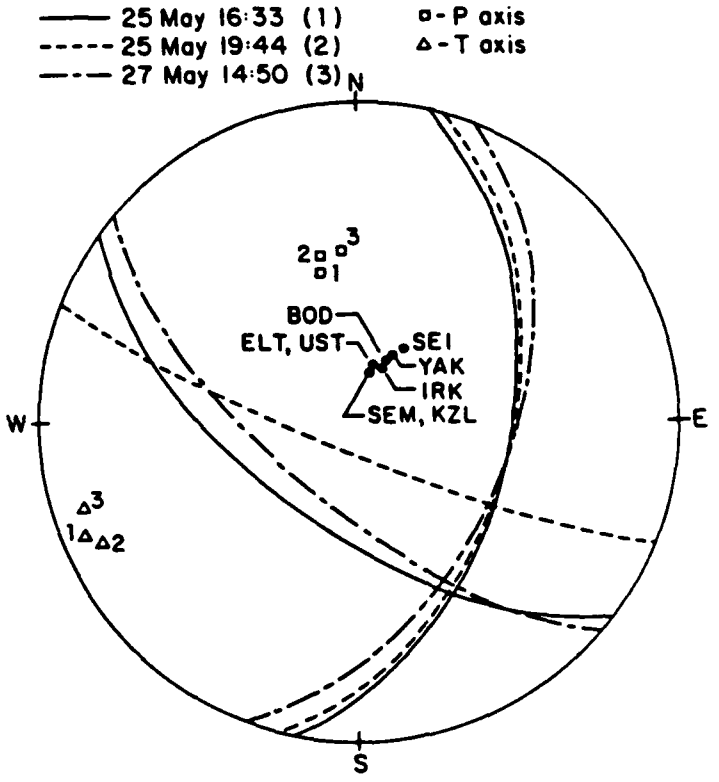

Figure 3

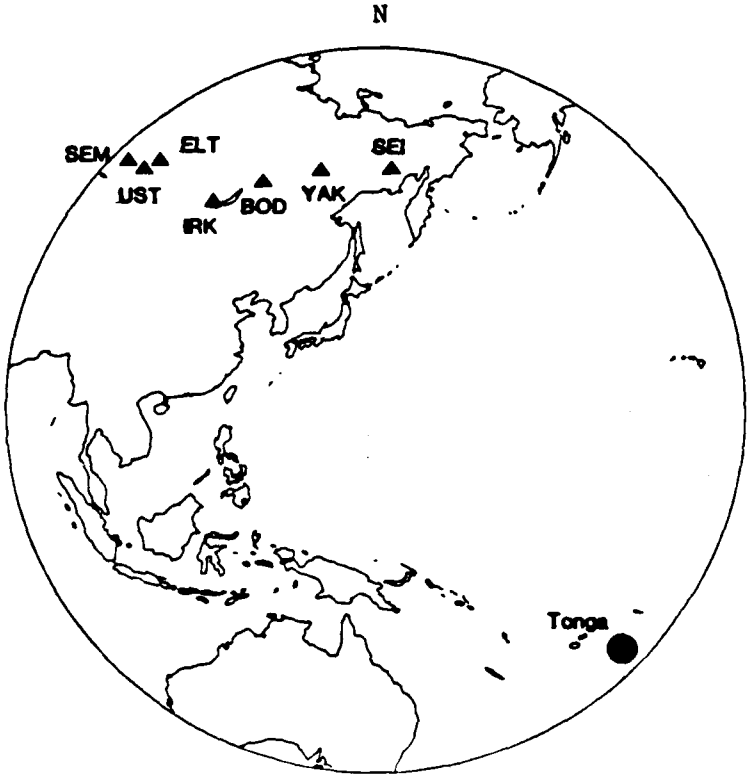

Figure 4

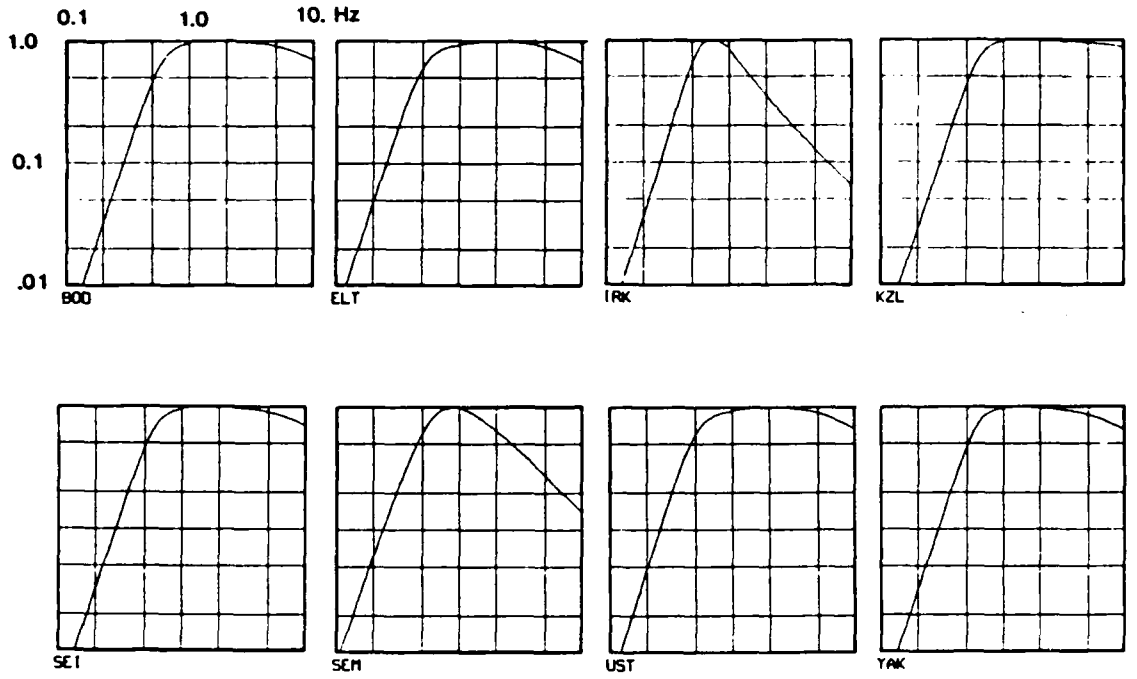

Figure 5

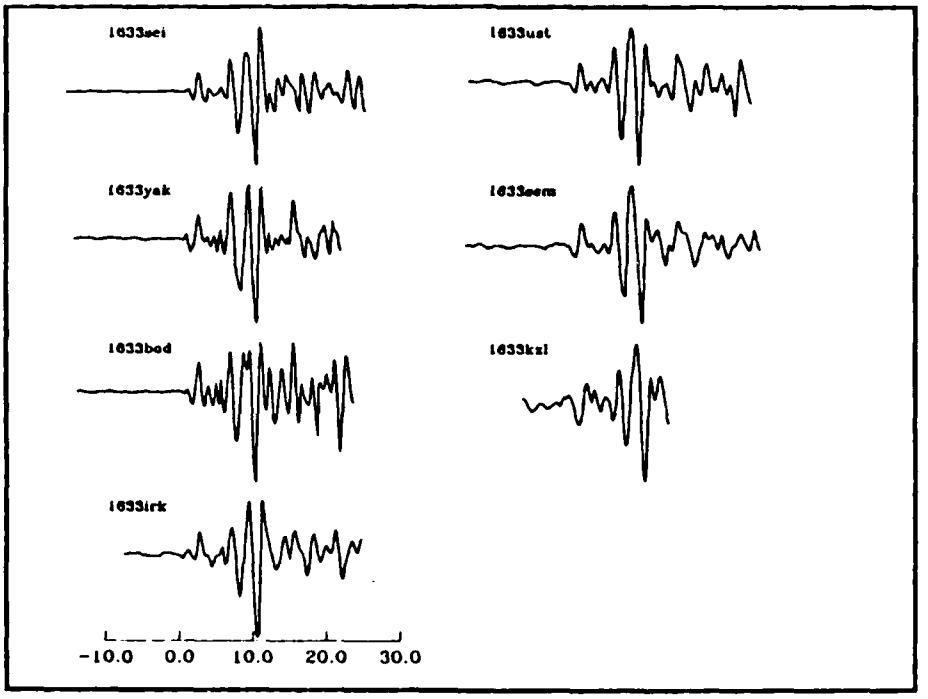

Figure 6

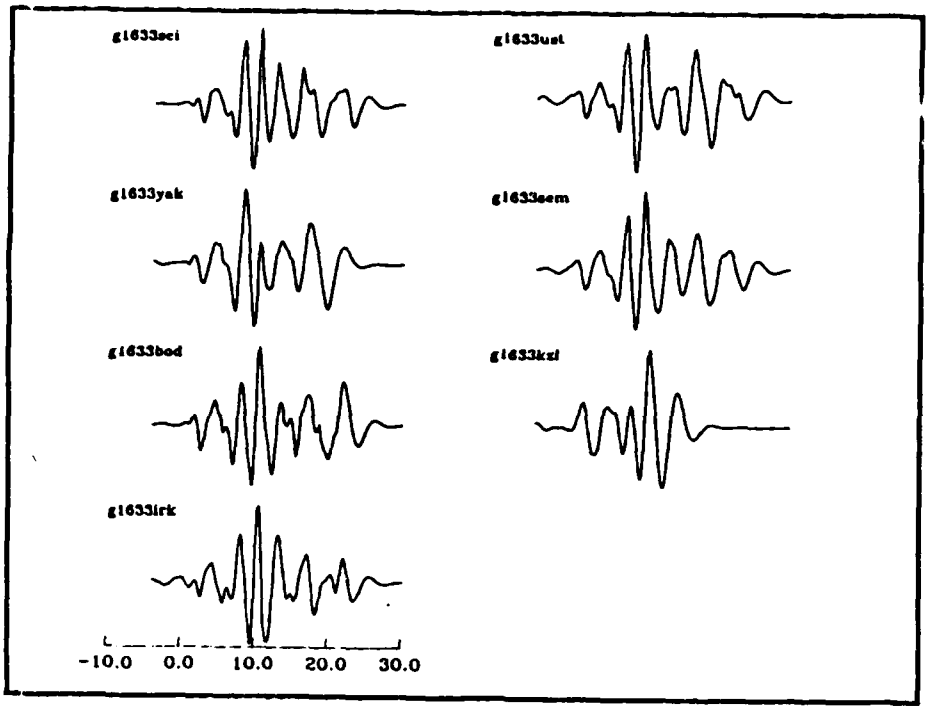
g1633oci
g1633ust
g1633yak
g1633oem
g1633bod
g1633kzl
g1633irk
-10.0
0.0
10.0
20.0
30.0

Figure 7

CRUSTAL STRUCTURE IN THE VICINITY OF YUCCA MOUNTAIN, NEVADA

Azmi Ismail and Keith F. Priestley
Seismological Laboratory, Mackay School of Mines
University of Nevada, Reno, NV 89557

ABSTRACT

We have interpreted data from two seismic refraction profiles recorded by the U.S. Geological Survey in the vicinity of the proposed Nuclear Waste Repository at Yucca Mountain in southern Nevada. The first shot consists of two profiles, the longer of which has 33 recordings of a nuclear explosion at the Nevada Test Site and extends from 45 to 110 km and the other has 26 recordings extending 50 to 90 km from the shot point. The second consists of 71 recordings of a chemical explosion near Beatty, Nevada, and extends ≈70 km, east-west across Yucca Mountain. Gravity and well log data are used to correct the refraction travel-time data for delays due to lateral variations in near-surface structure. The travel-times for the two profiles were combined, reparameterized in terms of delay time and ray parameter, and inverted for average, extermal velocity-depth bounds for the region. These show a steep gradient in the shallow crust (depth less than 5 km) with speeds increasing from ≈4.5ks^{-1} to 6.2 ks^{-1} and a shallow gradient below 5 km where speeds increase from ≈6.2ks^{-1} to 6.5 ks^{-1} at 25 km. A specific velocity-depth model consistent with the extremal bounds has been found by two-dimensional ray tracing. The structure of the upper crust is highly variable with the Paleozoic basement varying between the surface and 3.5 km depth. A thick, low-speed section is indicated by large delays across the Crater Flat-Prospector Pass caldera complex. A prominent arrival 1.5 to 2.0 seconds after the initial P-wave time, observed in the distance range 48 to 65 km, is interpreted as a mid-crustal boundary at 13 to 17 km depth. The profiles are of insufficient length to see P_n, however a prominent arrival 3 to 4 seconds after P_g, observed at distances greater than 80 km, is interpreted as P_mP from the Moho at approximately 35 km depth.

Introduction

Since 1978 the U.S. Geological Survey has conducted a series of seismic refraction experiments to elucidate the shallow crustal structure in the vicinity of Yucca Mountain, on the western boundary of the Nevada Test Site (NTS) (Hoffman and Mooney, 1984). The purpose of these experiments is to aid in site evaluation for the proposed nuclear waste repository at Yucca Mountain. However, much of the data collected is suitable for delineating deeper crustal structure in the vicinity of NTS. We have obtained the digital data from the U.S.

Geological Survey and have embarked on a program of interpretation of the data in terms of the deeper crustal structure. Figure 1 shows the location of the refraction profiles. To date, our analysis have been confined to two profiles, those from shot point 3 , a nuclear explosion on Pahute Mesa, and shot point 4, a chemical explosion near Beatty, Nevada. Data from shot point 3 was collected along two profiles. The first profile (3A) is along the axis of Yucca Mountain, in the distance range of 40 to 110 km, and the second profile (3B) is across the Crater Flats Caldera Complex with a distance range of 50 to 90 km. Data from shot point 4 was collected along a 70 km, east trending profile from near Beatty, across Bare Mountain, Yucca Mountain, to Skull Mountain on the NTS. All the seismograms are vertical component velocity records, digitized at 200 samples per second.

Data Analysis

Figure 2 is record sections of the data recorded along the profiles 3A and 3B. These record sections have been normalized. Delays of the order 0.3 to 0.5 seconds are observed in the profile 3A at distances of approximately 45 to 60 km. A reflective phase is identified at distances between 80 to 110 km and is interpretated as reflections from the Moho (P_mP). The record section for profile 3B shows delays of 0.4 to 0.5 seconds in the distance range of 52 to 60 km. These can be attributed to the large amount of volcanic tuffs and sediments in the caldera complex, which erupted approximately 10 m.y. ago (Carr, 1984). Figure 3 is a record section of the data collected along the profile from shot point 4. At distances between 48 to 65 km, the first arrivals are attenuated and emergent, however, there is a strong reflected phase 1.5 to 2.0 seconds after the first arrival coming in at these distances. This phase is identified as reflections from an intra-crustal boundary. The length of this profile is insufficiently long to observe any P_n arrivals. The average error in picking arrival times for profiles 3A and 3B are, 0.01 seconds, and 0.08 seconds, with maximum errors of 0.02 and 0.18 seconds at distances of 70 km and 109 km, respectively. Profile 4 has an average timing error of 0.03 seconds with maximum of 0.11 seconds at 47 km.

The travel-time data for these profiles have been corrected for the near surface delays using the delay times from the shallow structure interpretation of Hoffman and Mooney (1984), and inferences of the near surface structure from gravity data (Healey *et al.*, 1978). The two data sets from shot points 3 and 4 were combined, and reparameterized in terms of the delay time, τ and the ray parameter, p. There are several advantages of reparameterizing the travel-time data in this manner. One is that the $\tau(p)$ function and the earth structure are linearly related, allowing the application of linear-inverse theory to invert the

$\tau(p)$ data in order to construct and evaluate consistent earth models. Another advantage is that the $\tau(p)$ function, which is a single value, monotonically decreasing function, will show a discontinuous in the presence of a low-velocity zone. The $\tau(p)$ data, along with time-distance, cross-over and triplication constraints, were inverted for bounds on the velocity structure using the procedures outlined by Garmany *et al.*, 1979, Orcutt *et al.*, 1980, and Orcutt, 1980. The latter constraints tend to smooth the inversion of velocity-depth function. The resulting bounds on the velocity depth function are shown in Figure 4. These bounds indicate a steep gradient in the shallow crust for depths less than 5 km. The speed corresponding to this depth is approximately 4.5 ks^{-1} to 6.2 ks^{-1}. At deeper depths, the velocity gradient shallows to speeds which increase from 6.2 ks^{-1} to 6.5 ks^{-1} at 25 km deep. The velocity-depth bounds of Figure 4 contain all the possible models compatible with the travel-time data, but do not in themselves represent the actual velocity-depth function. To develope a specific velocity-depth model, we used an average velocity-depth function as a starting model, and a two-dimensional ray tracing routine. (McMechan and Mooney, 1980). By fitting the observed travel-time data to the calculated travel-times based on the specific velocity-depth model, we have constructed a preliminary model which is consistent with the velocity-depth bounds (Figure 5).

We have derived a preliminary earth model using the delay time method which is consistent with the Paleozoic basement that varies from surface outcrops to depths of 3.5 km. Large delays observed over the Crater Flats Caldera Complex is explained by a 3 to 4 km thick, low-speed section, underlying the complex. We have interpreted the reflected phase in seen in profile 4 as an intra-crustal boundary whose depth ranges from 13 to 17 km. From the profiles 3A and 3B, we estimate the depth to the Moho to be approximately 35 km. Our model is further constrained using gravity data. Figure 6 shows the results of gravity modeling with our model. Our analysis suggests the following density versus speed relationship: a density of 2.7 g/cc corresponds to speeds of 6.1 ks^{-1} and higher, a density of 2.5 g/cc corresponds to speeds of 4.0 ks^{-1} to 5.7 ks^{-1}, a density of 2.45 g/cc corresponds to speeds of 3 ks^{-1} to 4.5 ks^{-1}, and a density of 2.1 g/cc corresponds to speeds of 2.0 ks^{-1} to 3.1 ks^{-1}. We have also incorporated well log data in our gravity modeling which constrains the surface layer at Yucca Mountain (Spengler and Rosenbaum, 1980).

Discussion and Conclusion

Our preliminary model correlates well with that obtained by Hoffman and Mooney (1984), derived by trial and error fitting of the observed travel times. Our data indicate that the deeper layers are not very well constrained, however.

We combined data from profiles 3A, 3B, and 4 for our inversion. Combination of these data results in relatively high scattering which affects the τ analysis. Better resolution of the near surface structure would allow us to reduce this scatter. We have relatively good control for the lateral structure in the east-west line, however most of the scattering effects can be attributed to the near-surface lateral variations between shot point 3 and its closest station, 45 km away. We have no control on the shallow structures at this distance. The shallowest structure we can define is approximately 5 to 6 km deep, based on the velocity structure of profile 4. Since the line passes through Timber Mountain caldera, we estimate that there exist a thick, low-speed section in Timber Mountain.

The high speeds seen in the Crater Flats area suggest that the caldera contains a high density fill. This is not implausable, considering that highly welded tuffs are known to exist there.

References

Carr, W.J., 1984, Regional structure setting of Yucca Mountain, southwestern Nevada, and late Cenozoic rates of tectonic activity in part of the southwestern Great Basin, Nevada and California. *U.S. Geological Survey, Open-File Report 84-854*, 109 pp.

Garmany, J., Orcutt, J.A., and R.L. Parker, 1979, Travel-time inversion: a geometrical approach. *J. Geophys. Res.* **84**, 3615-3622.

Healey, D.L., Wahl, R.R., Currey, F.E., and W.E. Stephens, 1978, Bouguer gravity map of Nevada-Death Valley Sheet, *Nevada Bureau of Mines and Geology, Map 69*.

Hoffman, L.R. and W.D. Mooney, 1984, A seismic study of Yucca Mountain and vicinity, southern Nevada; data report and preliminary results. *U.S. Geological Survey, Open-File Report 83-588*, 50 pp.

McMechan, G.A. and Mooney, W.D., 1980, Asymptotic ray theory and synthetic seismograms for laterally varying structures: theory and application to the Imperial Valley, California. *Bull. Seism. Soc. Am.* **70**, 2021-2035

Orcutt, J.A., MacKenzie, K., and McClain, J., 1980, The role of X(p) constraints in linear, extremal inversion of explosion profile data. *Bull. Seism. Soc. Am.*

70, 2103-2116.

Orcutt, J.A., 1980, Joint linear, extremal inversion of seismic kinematic data. *J. Geophys. Res.* **85**, 2549-2660.

Spengler, R.W. and Rosenbaum, J.G., 1980, Preliminary interpretation of geologic results obtained from boreholes UE25a-4, -5, -6, and -7, Yucca Mountain, Nevada Test Site. *U.S. Geological Survey, Open-File Report 80-929*, 33 pp.

Figure Captions

Figure 1. Map showing the locations of Shot points 3 and 4 (closed circle), and station locations (open triangles).

Figure 2. Record section for profiles 3A and 3B.

Figure 3. Record section of profile 4

Figure 4. Extremal velocity-depth bounds for profiles 3A, 3B, and 4.

Figure 5. Two-dimensional ray tracing of the specific velocity-depth model that is consistent with the velocity depth bounds in Figure 4.

Figure 6. Comparison of observed and calculated gravity data for the model in Figure 5.

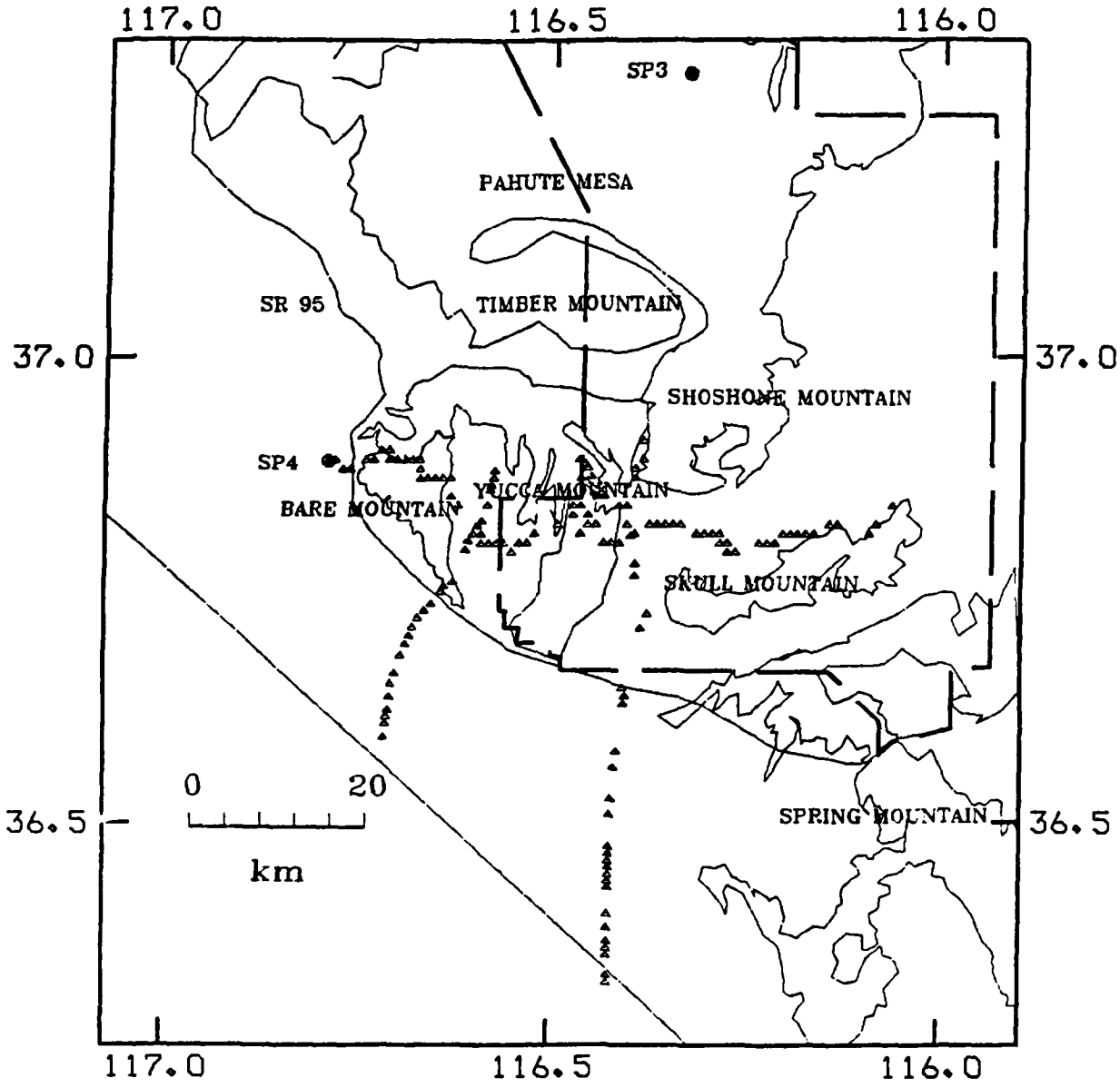
117.0
116.5
116.0
SP3
PAHUTE MESA
SR 95
TIMBER MOUNTAIN
37.0
37.0
SHOSHONE MOUNTAIN
SP4
YUCCA MOUNTAIN
BARE MOUNTAIN
SKULL MOUNTAIN
0
20
36.5
SPRING MOUNTAIN
36.5
km
117.0
116.5
116.0

Figure 1

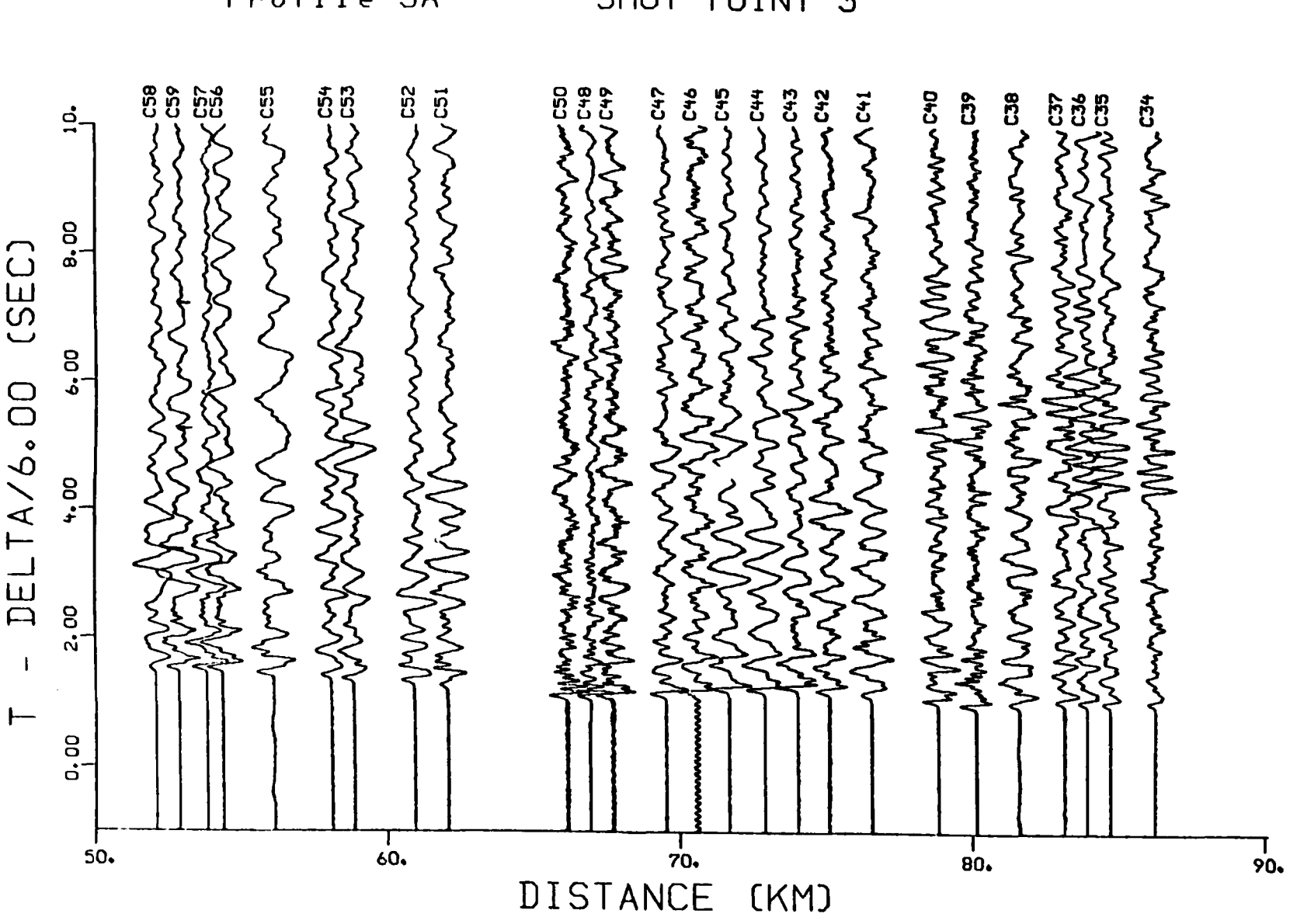
Profile 3A
SHOT POINT 3
C58
C59
C57
C56
C55
C54
C53
C52
C51
C50
C48
C49
C47
C46
C45
C44
C43
C42
C41
C40
C39
C38
C37
C36
C35
C34
T - DELTA/6.00 (SEC)
0.00
2.00
4.00
6.00
8.00
10.
50.
60.
70.
80.
90.
DISTANCE (KM)

Figure 2

Profile 3B SHOT POINT 3

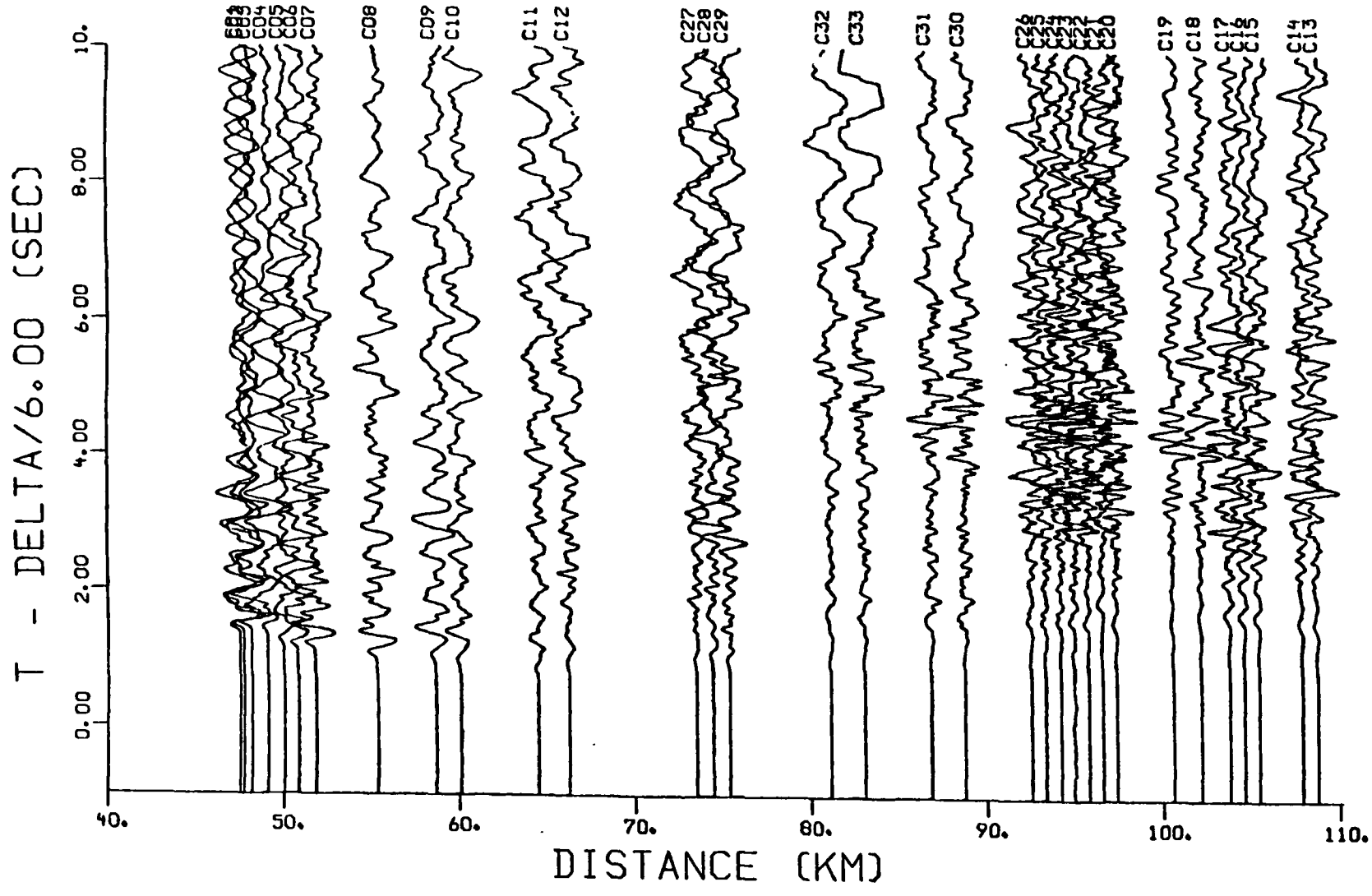

Profile 4 SHOT POINT 4

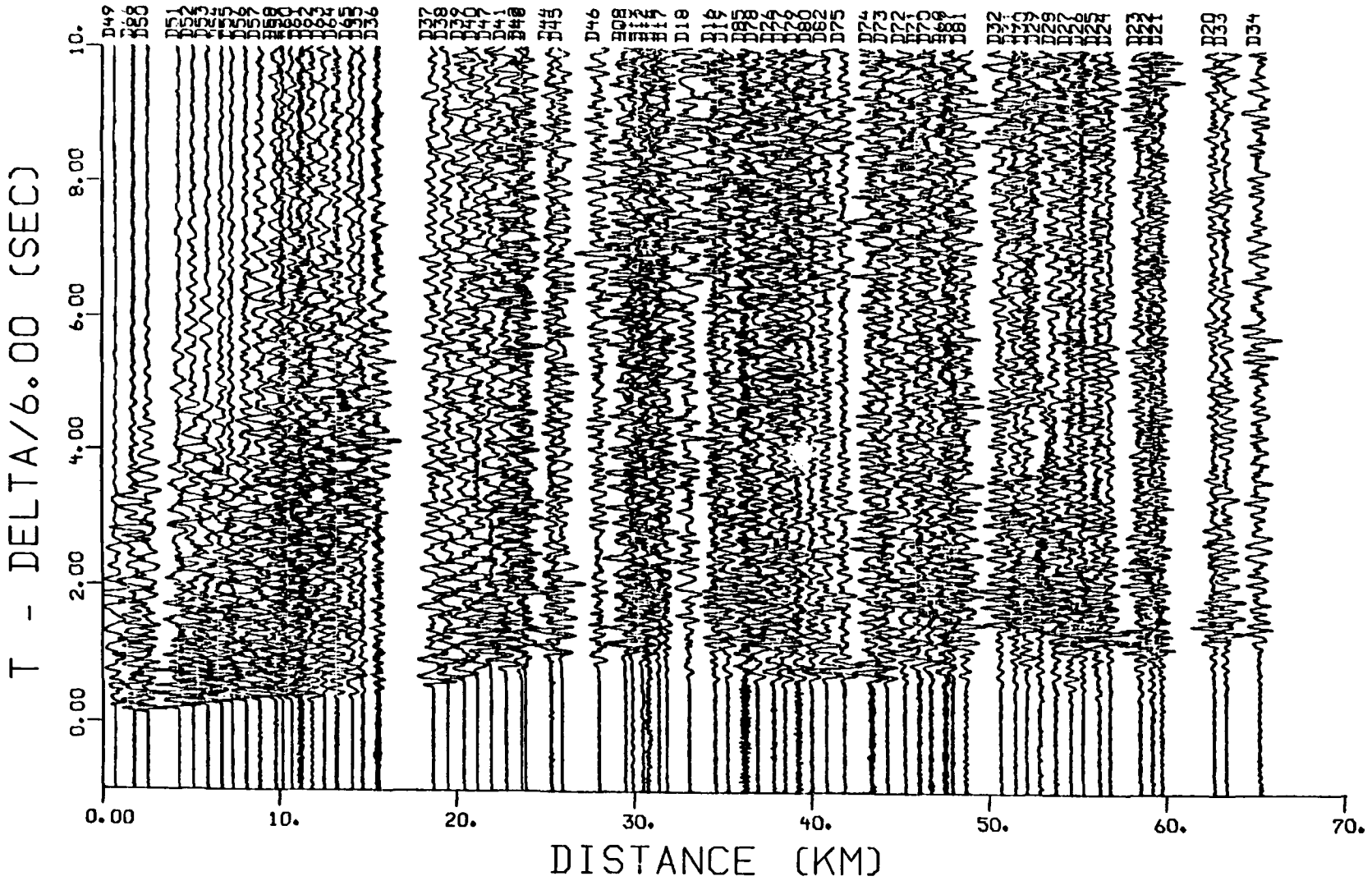

Figure 3

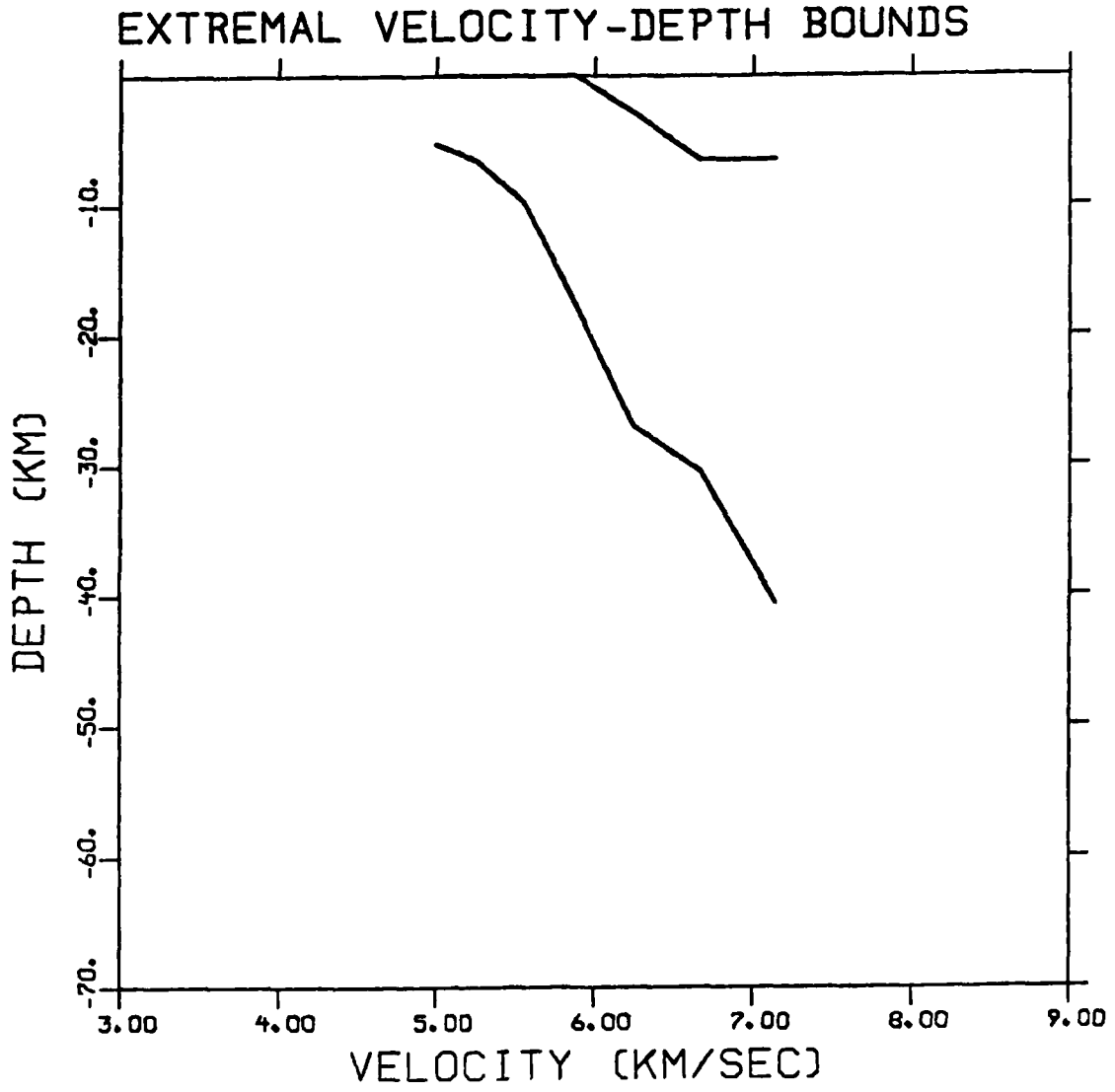
EXTREMAL VELOCITY-DEPTH BOUNDS
DEPTH (KM)
-10.
-20.
-30.
-40.
-50.
-60.
-70.
3.00
4.00
5.00
6.00
7.00
8.00
9.00
VELOCITY (KM/SEC)

Figure 4

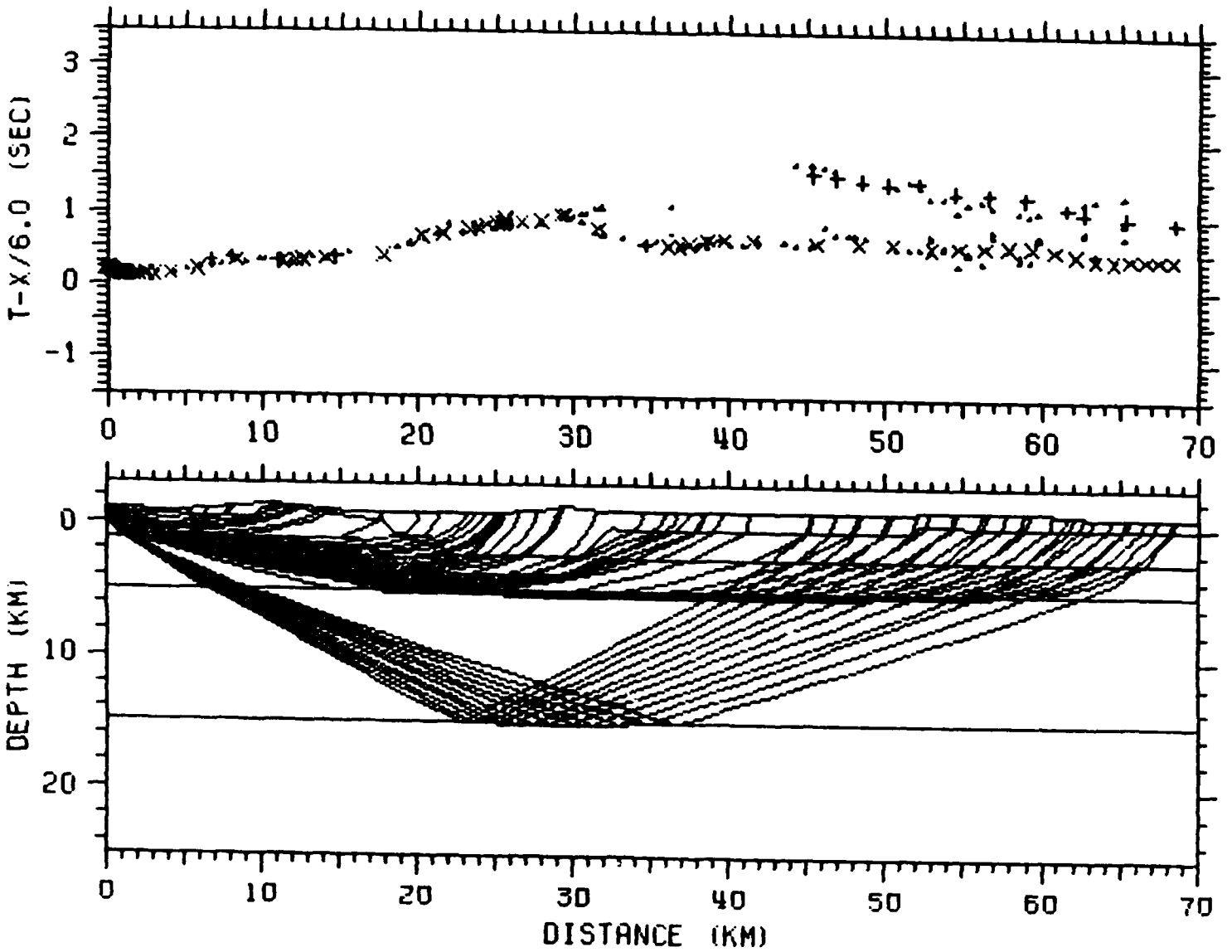

Figure 5

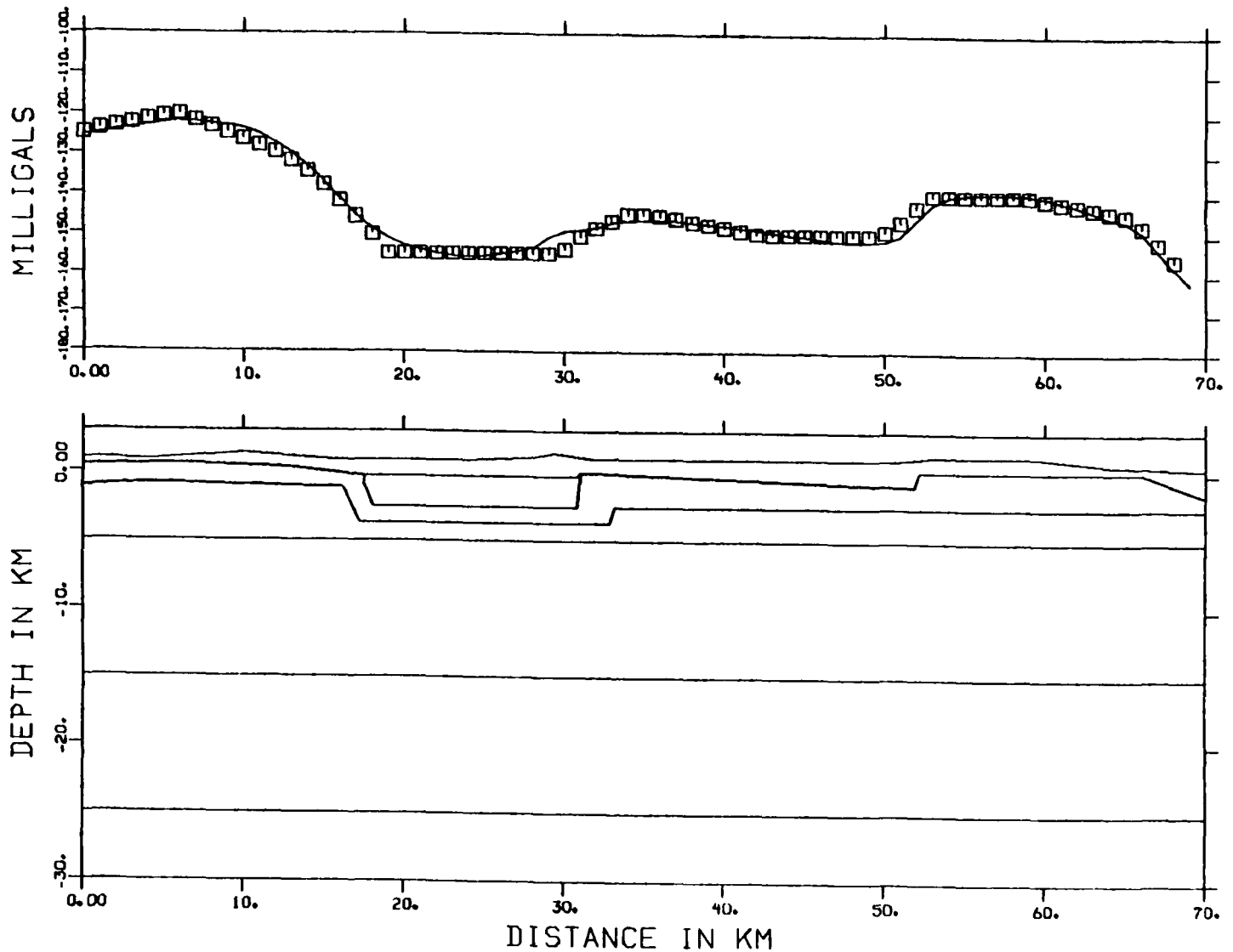
MILLIGALS
-100.
-110.
-120.
-130.
-140.
-150.
-160.
-170.
-180.
0.00
10.
20.
30.
40.
50.
60.
70.
DEPTH IN KM
0.00
-10.
-20.
-30.
0.00
10.
20.
30.
40.
50.
60.
70.
DISTANCE IN KM

Figure 6